ADVANCED MODELLING AND CONTROL FOR DEMAND SIDE MANAGEMENT IMPLEMENTATION IN SMART GRID

MAI WEIJIE

Ph.D

The Hong Kong Polytechnic University

2017

The Hong Kong Polytechnic University

Department of Electrical Engineering

ADVANCED MODELLING AND CONTROL FOR DEMAND SIDE MANAGEMENT IMPLEMENTATION IN SMART GRID

MAI WEIJIE

A thesis submitted in partial fulfillment of the requirements

for the Degree of Doctor of Philosophy

October 2016

CERTIFICATE OF ORIGINALITY

I hereby declare that this thesis is my own work and that, to the best of my knowledge and belief, it reproduces no material previously published or written, nor material that has been accepted for the award of any other degree or diploma, except where due acknowledgement has been made in the text.

_____(Signed)

_____MAI Weijie_____(Name of student)

Abstract

In order to increase the utilization of renewable energy sources and to reduce the need of generator-provided ancillary services and inefficient peaking generation, electricity consumers are progressively transforming into active participants in power system operations via various demand side management programs. Flexible load response is expected to be utilized to achieve lower grid operating costs, increased system reliability and improved energy efficiency, by modulating power consumption in response to various supply conditions, such as high market price, peak demand, overloading, regulation signal, etc.

However, the effects of changing the load profiles on the system performances need to be identified and assessed before implementation, so as to determine the optimal control strategy to maximize the network benefits. Besides, although some demand responsive loads can participate in demand side management schemes by simple connection and disconnection, some require more sophisticated control algorithms because physical constraints of load devices and consumer behavior need to be taken into account.

This thesis firstly proposes a novel hourly electric load of a building based on radial basis function neural network and validate the high accuracy using real building data under various weather conditions.

Next, the most updated statistic information on load composition in residential and commercial load sectors in UK is used to develop the aggregate load models with time-varying model coefficients using a component-based load aggregation methodology, which is able to represent the temporal variations due to the time-varying load composition caused by normal consumer behavior or demand side management actions. Then a general methodology is presented to model DSM scenarios to assess the corresponding impacts on the network

performances, using the wet load in residential sector as an example. In addition, a conservation voltage reduction optimization problem based on the developed time-varying exponential load models is formulated to demonstrate the importance of accurate load modelling in the VVO analysis. Furthermore, the problem of the optimal locations for demand side management deployment is studied by formulating a Optimal Power Flow problem to minimize the amount of load needed (i.e. minimize the number of affected customers) to participate in DSM scheme to relieve an upstream network contingency.

There are various demand manageable loads which require more advanced control algorithms in order to play a significant role in demand side management, such as thermostatically controlled loads. In order to allow more heating, ventilation and air-conditioning (HVAC) system loads to participate in supply-demand balancing and ancillary service market, this thesis introduces a mathematical R-C thermodynamic model of building that can accurately capture the temperature dynamics which is strongly related to the power consumption of HVAC systems. Economic model predictive controllers are then proposed to effectively and optimally modify the power consumption of HVAC systems to reduce the peak load and increase energy efficiency by minimizing the electricity costs while maintaining the temperature within satisfactory levels. Lastly, this work proposes a novel contract framework between buildings, building aggregator and utility that can maximize and reward the flexible power reserve provided by aggregate HVAC loads, and under this developed contract framework, an optimal building aggregator that can aggregate the HVAC loads to declare the power flexibility to the utility for providing fast regulating power is proposed, and dispatch the load according to the power regulation signal from utility in the real-time scheduling stage.

Acknowledgement

Firstly, I would like to express my sincere appreciation to my chief supervisor, Prof. C. Y. Chung, for his endless support, constant guidance and constructive suggestions throughout these years. His patience, enthusiasm, expertise knowledge and innovative thinking have significantly inspired me. Without him, this work would not have been possible.

In addition, I greatly appreciate Dr. Mehdi Maasoumy from The University of California at Berkeley for his patient explanation and inspiring discussion on the R-C thermal network modeling of building, and Dr. Adam Collin from The University of Edinburgh for his insightful discussion and providing a considerable amount of various data used in the process of developing aggregate load models.

My sincere thanks also go to all of my friends and colleagues at the Computational Intelligence Applications Research Laboratory, who have been a real pleasure both to socialize and work with.

A very special acknowledgement goes to my family for constantly believing, encouraging and supporting me.

Last but not least, I also greatly appreciate the support from Hong Kong PhD Fellowship Scheme awarded by The Hong Kong Research Grants Council.

Table of Contents

Abstract ..... **I**

Acknowledgement ..... **III**

Table of Contents ..... **IIV**

Lists of Figures, Tables and Abbreviations ..... **IX**

Chapter 1

Introduction **1**

1.1 Background of Research 1

1.2 Motivations and Objectives 2

1.3 Primary Contributions 6

1.4 Thesis Layout 8

1.5 List of Publications 10

Chapter 2

Literature Review **12**

2.1 Overview of Demand Side Management 12

2.2 Overview of Load Modelling 15

2.2.1 ZIP/Polynomial Load Model 15

2.2.2 Exponential Load Model 16

2.2.3 Identification of Load Model Coefficients 16

2.3 Optimal Power Flow 18

2.4 Voltage Var Optimization 18

2.5 Energy-Efficient Buildings 20

Chapter 3

Electrical Load Forecasting for Buildings Based on Radial Basis Function Neural Network 22

3.1 Introduction 22

3.2 Proposed Load Forecasting Model 24

3.2.1 Justification of Choosing RBFNN 24

3.2.2 Theory of RBFNN 25

3.2.3 Hourly Electric Load Forecasting Model based on RBFNN 26

3.2.4 Performance Evaluation of Forecasting Model 29

3.3 Case Study and Discussion 30

3.4 Chapter Summary 34

Chapter 4

Aggregate Load Models with Time-varying Model Coefficients based on Component-based Load Aggregation Methodology 36

4.1 Introduction 36

4.2 Overview of Aggregate Load Modeling Approach 38

4.3 Example: Aggregate Residential Load Model 40

4.3.1 Load Demand Curves 41

4.3.2 Load Composition 41

4.3.3 Converting Load Types into Load Categories 44

4.3.4 Generic Models 51

4.3.5 Aggregating Generic Models to Form LV Aggregate Load Model 53

4.4 Network Aggregation 56

4.5 Example: Aggregate Commercial Load Model 57

4.6 Chapter Summary 64

Chapter 5

Applications of Time-varying Aggregate Load Models in Active Distribution Systems 66

5.1 Modelling of Demand Side Management 66

5.1.1 Description of Devised DSM Scenarios 67

5.1.2 Impacts of DSM on LV Aggregation Load Model 70

5.1.3 Impacts of Devised DSM Scenarios on Power Flow 72

5.2 Conservation Voltage Reduction With Time-varying Exponential Load Models 77

5.2.1 Problem Formulation for CVR 78

5.2.2 Solution Methodology 80

5.2.3 Test System Setting for Case Study 81

5.2.4 Impacts of Time-varying Coefficients on CVR Dispatch 83

5.2.5 Effectiveness of Proposed CVR 88

5.3 Evaluation of the ability of DMLs at Various Locations to Benefit Power Network by OPF Analysis 92

5.3.1 Problem Formulation of DSM-based OPF 93

5.3.2 Case Study 1 94

5.3.3 Case Study 2 97

5.4 Chapter Summary 99

Chapter 6

Mathematical R-C Thermodynamic Model of Smart Commercial Buildings 101

6.1 Introduction 101

6.2 Fundamental Principles of Thermodynamic Model for Building 101

6.2.1 Heat Transfer 102

6.2.1.1 Heat Conduction 102

6.2.1.2 Heat Convection 103
6.2.1.3 Heat Radiation 103
6.2.2 Heat Storage 104
6.3 Configuration and Operating Principle of HVAC System 105
6.4 Equivalent Circuit of Thermal Network 106
6.4.1 Thermal Resistance and Thermal Potential 106
6.4.2 Thermal Capacitance 107
6.4.3 Illustration Example 108
6.5 Thermodynamic Model for the Whole Building 109
6.5.1 Assumptions for the Model Development 109
6.5.2 Model for a Single Building 112
6.5.3 Linearization of Nonlinear Thermodynamic Model 115
6.5.4 Parameters Identification and Model Validation 116
6.5.5 Aggregation of Thermodynamic Building Model 121
6.6 Chapter Summary 122

Chapter 7

Design of Model Predictive Controller Based on Thermodynamic Building Model for Demand Side Management in Smart Grid 123

7.1 MPC for Energy Efficiency Improvement and Peak Load Reduction 123
7.1.1 Classical Control Methodologies for HVAC 124
7.1.2 Overview of Model Predictive Control 125
7.1.3 HVAC Power Consumption Models 126
7.1.4 Economic MPC for Flexible HVAC Power Consumption 128
7.1.5 Case Studies and Simulation Results 130
7.1.5.1 Original Existing Controller 131
7.1.5.2 Model Predictive Controller 132

7.2 MPC of Aggregating Commercial Buildings for Providing Flexible Power Reserve 136
7.2.1 Feasibility 139
7.2.2 Building-Aggregator-Grid (BAG) Contract Framework 142
7.2.3 Robust Optimal MPC Control for Flexibility Determination 146
7.2.4 Simulation and Results Discussion 147
7.2.4.1 Simulation Set-up and Base Case 147
7.2.4.2 Simulation of Reserve Determination Stage 150
7.2.4.3 Simulation of Real-time Scheduling Stage 153
7.2.4.4 Simulation with No Reward Incentives 157
7.3 Chapter Summary 158

Chapter 8

Conclusion 159

8.1 Summary 159
8.2 Future Work 161

Reference 163

Lists of Figures, Tables and Abbreviations

List of Figures

Fig. 1.1	Transitions from conventional power system to future smart grid	2
Fig. 3.1	General structure RBF neural network	25
Fig. 3.2	Proposed hourly electric load forecasting model based on RBFNN	27
Fig. 3.3	(a) Actual hourly load vs. Predicted hourly load (by RBFNN) (Validation - Scenario A 04/03/2013 – 10/03/2013); (b) Comparison between actual and model predicted hourly load (by RBFNN) for Scenario A	31
Fig. 3.4	(a) Actual hourly load vs. Predicted hourly load (by RBFNN) (Validation - Scenario B 18/05/2013 – 26/05/2013); (b) Comparison between actual and model predicted hourly load (by RBFNN) for Scenario B	32
Fig. 3.5	(a) Actual hourly load vs. Predicted hourly load (by RBFNN) (Validation - Scenario C 30/06/2013 – 07/07/2013), (b) Comparison between actual and model predicted hourly load (by RBFNN) for Scenario C	32
Fig. 3.6	(a) Actual hourly load vs. Predicted hourly load (by MLPNN) (Validation - Scenario A 04/03/2013 – 10/03/2013), (b) Comparison between actual and model predicted hourly load (by MLPNN) for Scenario A	33
Fig. 4.1	Overview of the component-based load aggregation methodology	40

Fig. 4.2	Minimum, average and maximum loading conditions of typical aggregate daily active power demand curves for residential load	41
Fig. 4.3	Residential load decomposition into load types for maximum loading condition	43
Fig. 4.4	Residential load decomposition into load types for minimum loading condition	43
Fig. 4.5	Residential load decomposition into load types for average loading condition	44
Fig. 4.6	Classification of load categories	45
Fig. 4.7	Converting lighting load type demand into load categories with generic models	45
Fig. 4.8	Converting wet load type demand into load categories with generic models	47
Fig. 4.9	Converting cooking load type demand into load categories with generic models	47
Fig. 4.10	Converting CE load type demand into load categories with generic models	48
Fig. 4.11	Converting ICT load type demand into load categories with generic models	49
Fig. 4.12	Residential load decomposition into load categories for maximum loading condition	50
Fig. 4.13	Residential load decomposition into load categories for minimum loading condition	50
Fig. 4.14	Residential load decomposition into load categories for average loading condition	51
Fig. 4.15	General equivalent-circuit model of nonlinear loads	51
Fig. 4.16	Load Aggregation Process based on component-based method	54

Fig. 4.17	Variation of model coefficient in aggregate exponential LV residential load model for active power	55
Fig. 4.18	Variation of model coefficient in aggregate exponential LV residential load model for reactive power	56
Fig. 4.19	Minimum, average and maximum loading conditions of typical aggregate daily active power demand curves for commercial load	58
Fig. 4.20	Commercial load decomposition into load types for maximum loading condition	59
Fig. 4.21	Commercial load decomposition into load types for minimum loading condition	60
Fig. 4.22	Commercial load decomposition into load types for average loading condition	60
Fig. 4.23	Commercial load decomposition into load categories for maximum loading condition	61
Fig. 4.24	Commercial load decomposition into load categories for minimum loading condition	62
Fig. 4.25	Commercial load decomposition into load categories for average loading condition	62
Fig. 4.26	Variation of model coefficient in aggregate exponential LV commercial load model for active power	63
Fig. 4.27	Variation of model coefficient in aggregate exponential LV commercial load model for reactive power	64
Fig. 5.1	Load type decomposition for base case scenario	68
Fig. 5.2	Load type decomposition for DSM1 scenario	69
Fig. 5.3	Load type decomposition for DSM2 scenario	69
Fig. 5.4	Impacts of considered DSM schemes on active power load curves	70
Fig. 5.5	Impacts of considered DSM schemes on reactive power load	70

curves
Fig. 5.6 Effects of considered DSM scenarios on Z_Q of aggregate load model 72
Fig. 5.7 Effects of considered DSM scenarios on n_p of aggregate load model 72
Fig. 5.8 Effects of considered DSM scenarios on n_q of aggregate load model 73
Fig. 5.9 Modified IEEE-33 nodes network 74
Fig. 5.10 Injected active power from the main grid 75
Fig. 5.11 Voltage Profile at Bus 18 76
Fig. 5.12 P_0 and Q_0 for residential loads 82
Fig. 5.13 P_0 and Q_0 for commercial loads 82
Fig. 5.14 Time-varying exponential coefficients for load models 83
Fig. 5.15 CVR Dispatch results of using Load Model 1 84
Fig. 5.16 CVR Dispatch results of using Load Model 2 84
Fig. 5.17 CVR Dispatch results of using Load Model 3 85
Fig. 5.18 CVR Dispatch results of using Load Model 4 85
Fig. 5.19 Voltage profiles at Bus 18 when using different load models 86
Fig. 5.20 Voltage profile at Bus 33 when using different load models 86
Fig. 5.21 Total active power demand when using different load models 87
Fig. 5.22 Total active power loss when using different load models 88
Fig. 5.23 Total active power injected from main power grid when using different load models 88
Fig. 5.24 Voltage profiles at Bus 18 for different scenarios 89
Fig. 5.25 Voltage profiles at Bus 33 for different scenarios 90
Fig. 5.26 Total active power demand for different scenarios 90
Fig. 5.27 Active power loss for different scenarios 91
Fig. 5.28 Injected active power from main power grid for different 91

scenarios

Fig. 5.29 Radial distribution network for case study 95

Fig. 5.30 Effective reserve offered by residential wet load at GSP 98

Fig. 6.1 Illustration of heat conduction 102

Fig. 6.2 Illustration of heat convection 103

Fig. 6.3 Illustration of heat radiation 104

Fig. 6.4 Commercial building HVAC system schematic 105

Fig. 6.5 Illustration of heat transfer though a plane wall and schematic of its corresponding equivalent thermal circuit 106

Fig. 6.6 Thermal circuit network representing a peripheral wall with a window 108

Fig. 6.7 Schematic of three-zones building 110

Fig. 6.8 Thermal network for Zone 1 and its surrounding walls 111

Fig. 6.9 Outside air temperature 118

Fig. 6.10 Measured supply air temperature of HVAC system 119

Fig. 6.11 Measured air mass flow of HVAC system 119

Fig. 6.12 Comparison between measured and simulated zone temperature 120

Fig. 6.13 Absolute error (simulated zone temperature minus measured zone temperature) 120

Fig. 7.1 Relationship between fan power consumption and air volume flow rate 127

Fig. 7.2 Flowchart of proposed economic model predictive controller 129

Fig. 7.3 (a) Supply air temperature of air handling unit; (b) Outdoor air temperature 130

Fig. 7.4 (a) Measured indoor temperature using the original controller; (b) HVAC fan power consumption using the original controller 131

Fig. 7.5 Time-of-Use electricity price for Case 1 and Case 2 132

Fig. 7.6	Results of Case 1 using the proposed MPC controller: (a) Simulated indoor temperature; (b) HVAC fan power consumption	134
Fig. 7.7	Results of Case 2 using the proposed MPC controller: (a) Simulated indoor temperature; (b) HVAC fan power consumption	134
Fig. 7.8	Day-ahead electricity price for Case 3	135
Fig. 7.9	Results of Case 3 using the proposed MPC controller: (a) Simulated indoor temperature; (b) HVAC fan power consumption	136
Fig. 7.10	Manipulation of the power consumption of supply fan	140
Fig. 7.11	Temperatures of 15 randomly selected rooms in the experiments	141
Fig. 7.12	The proposed architecture for BAG contractual framework schematic	143
Fig. 7.13	(a) Supply air temperature of air handling unit; (b) Outdoor air temperature	149
Fig. 7.14	(a) measured indoor temperature using the original controller; (b) HVAC fan power consumption using the original controller	149
Fig. 7.15	Electricity price and flexibility reward rates for simulation	150
Fig. 7.16	Results of Reserve Determination Stage	152
Fig. 7.17	Results of Reserve Scheduling Stage with minutely ancillary signal	154
Fig. 7.18	Results of Reserve Scheduling Stage with hourly ancillary signal	155
Fig. 7.19	Results of Reserve Determination Stage without reward rates	156
Fig. 7.20	Comparison of declared flexibility with and without reward incentives	157

List of Tables

Table 3.1	Statistical Analysis Results of Proposed Load Forecasting Model	34
Table 4.1	Generic values for equivalent circuit model of CFL	52
Table 4.2	Generic values for equivalent circuit model of PE no-PFC	52
Table 4.3	Generic values for equivalent circuit model of PE p-PFC	52
Table 4.4	Load model coefficients of linear loads at residential sector	53
Table 4.5	Load model coefficients of linear loads at commercial sector	63
Table 5.1	Node Types for Modified IEEE-33 Nodes network	75
Table 5.2	Nomenclature for CVR problem formulation	80
Table 5.3	Description of four different scenarios	89
Table 5.4	Nomenclature for DSM-based OPF	94
Table 5.5	Load sectors mix at each bus	95
Table 5.6	The required amount of load to be curtailed to clear the upstream contingency at each bus using different load models	96
Table 6.1	Nomenclature for illustration example	109
Table 6.2	Nomenclature for R-C Thermodynamic Model of Building	111
Table 6.3	Results of parameter identification for Example Zone 1	117
Table 7.1	Nomenclature for BAG contractual framework	142

List of Abbreviations

AMI	Advanced Metering Infrastructure
ANN	Artificial Neural Network
AS	Ancillary Services
AHU	Air Handing Unit
BAG	Building-Aggregator-Grid
BEMS	Building Energy Management System
CB	Commercial Building
CCL	Constant Current Load
CIL	Constant Impedance Load
CFL	Compact Fluorescent Lamps
CPL	Constant Power Load
CSR	Capacitor start - Capacitor run
CT	Constant Torque
CVR	Conservation Voltage Reduction
DER	Distributed Energy Resource
DF	Downward Flexibility
DFR	Downward Flexibility Reward Rate
DG	Distribution Generation
DHW	Domestic Hot Water
DML	Demand Manageable Load
DMS	Distribution Management System
DR	Demand Response
DSA	Distribution System Automation
DSM	Demand Side Management
DW	Dish Washers
EV	Electric vehicle

GIL	General Incandescent Lamps
HVAC	Heating Ventilation Air-conditioning system
ICT	Information and Communication Technologies
ISO	Independent system operator
LFL	Linear fluorescent lamp
LV	Low-Voltage
LOO	Leave-one-out
MAPE	Mean Absolute Percentage Error
MBE	Mean Bias Error
MLP	Multi-Layer Perceptron
MPC	Model Predictive Control
MV	Medium-Voltage
OLTC	On-Load Tap Changer
OPF	Optimal Power Flow
PE a-PFC	Power electronics loads with active power factor correction
PE no-PFC	Power electronics loads with no power factor correction
PE p-PFC	Power electronics loads with passive power factor correction
PSO	Particle Swarm Optimization
QT	Quadratic Torque
RB	Residential Building
RBFNN	Radial Basis Function Neural Network
RES	Renewable Energy Sources
RMSE	Root Mean Square Error
RSIR	Resistor start - Inductor run
SF	Supply Fan
SMPS	Switch-mode power supply
SPIM	Single-Phase Induction Motor
TCL	Thermostatically Controlled Load
TD	Tumble-Dryers

UF	Upward Flexibility
UFR	Upward Flexibility Reward Rate
VAV	Variable Air Volume
VD	Voltage Dependent
VFD	Variable Frequency Drives
VVO	Voltage Var Optimization
WD	Washer-Dryers
WM	Washing Machines

Chapter 1

Introduction

1.1 Background of Research

The proliferation of variable renewable energy sources (RES) together with increased flexible demand and advanced energy storage technology has significant impacts on the methods of operation and planning in distribution networks. Due to the recent progress of information and communication technologies (ICT), a great amount of advanced applications involving these resources are expected to be enabled, which has raised great attentions from various stakeholders, e.g. regulatory bodies, research institutions, distribution companies, consultants, equipment manufacturers, etc.

There are many potential changes in generation, demand and network infrastructure due to the transition from conventional power system to smart grid, as depicted in Fig. 1.1. For example, electricity will progressively be generated closer to consumers that are characterized by higher levels of responsiveness. Besides, bi-directional power flows will be resulted from the connection of considerable volumes of renewable distribution generations (DG) to the distribution networks. In addition, because of the need of greater observability for end-users, advanced metering infrastructures (AMI) are adopted to allow the responsive loads from single or aggregated customers to help managing transmission and distribution systems. Although it is widely recognized that these modernization of existing networks will be critical to enable the low-carbon and energy-efficient power system worldwide, huge challenges will be

created for the system operation and the delivery of cost-effective, reliable and high-quality power supply [1].

Variable RES imposes extra requirements for network operators to efficiently manage network congestions and preserve adequate capacities and reserves. It is acknowledged in [2, 3] that the system flexibility provided by the demand side will be crucial to effectively mitigate the RES variation and operate the future power networks with high penetration of RES. In fact, the increased penetration of renewable-based DGs and system-wide deployment of demand side management (DSM) are identified as two key features of future power networks [4-6].

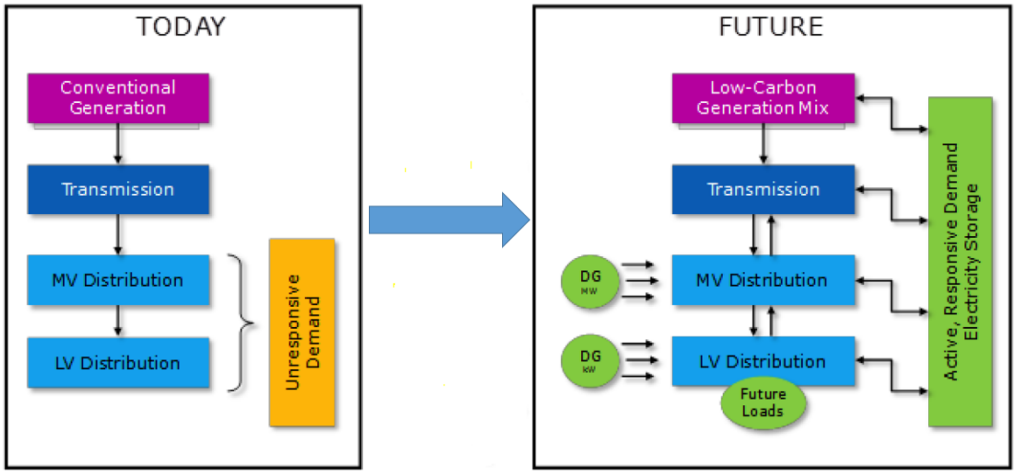

Fig. 1.1 Transitions from conventional power system to future smart grid

1.2 Motivations and Objectives

Active distribution network can be defined as a distribution network where a combination of distributed energy resources (DERs) including generators, energy storage systems and loads, each having some degree of responsibility for system support, can be controlled by distribution system operators in a coordinated way to manage electricity flows using a flexible network topology.

Recently, the authors in [7] has done a survey to investigate the state-of-the-art and identify which improvements are required for the active distribution network, it revealed that, 90% of the utilities which participated in the survey, still use the traditional network planning methods, besides, little or no consideration is given to DG or demand side integration in the development of load forecast algorithms. While active distribution network and demand-side integration of interest to many power utilities, they fail to be given serious consideration by power utilities as feasible alternatives in the process of system planning.

Load is traditionally forecasted at a particular bus location in medium-voltage (MV) network, and substantial literature using various techniques on load forecasting can be found in [8]. However, when the highly distributed DG or demand side integration in distribution network is taken into account in load forecasting, forecasting of the aggregate load could be very challenging. One possible solution is to isolate the effects of DG by forecasting the load of a single building, since there are considerable amount of literature on the modelling and forecasting of DG output. This motivates the author to develop an hourly electric load forecasting model for a single building.

Additionally, although many studies in literature have identified the significant potential of residential and commercial loads in DSM deployment [9], identifying the exact portion of each type of demand manageable loads in a particular location is extremely challenging, since loads are highly distributed across a large network. Therefore, the load needs to be modelled in the way that the deferrable/manageable part of the load can be accurately identified and the changes to electrical characteristics of load due to the applied DSM action can be modelled. Better understanding of the composition of various load types/devices at any time in any location is critical to develop a comprehensive methodology that can realistically assess and quantify the potential of a particular devised DSM scheme to offer system flexibility and beneficial network services, and

evaluate the corresponding effects on the network performance. It should also be noted that the implementation of DSM will give rise to the temporal variations not only in the magnitude of load demand, but also in the load composition and the corresponding electrical characteristics of loads, this will be discussed in more details in Section 5.1.

Furthermore, similar to the problem of optimal placement of DGs installation, after the deferrable/manageable portion of loads in different locations is identified, there must be an optimal location or an optimal group of locations for DSM implementation which can offer maximum benefits to the power grid, when DSM action is needed. An optimization problem can be formulated to determine such an optimal location or a group of locations with the objective of calculating the minimum amount of loads needed to be disconnected (i.e. minimizing the number of affected customers) to maintain the system within various operational constraints during system contingency or sudden shortage of variable RES.

Although the control of active power is the main focus of most DSM schemes, this inevitably changes the reactive power demand as well because it modifies the load composition, which may have significant impacts on the control strategies of voltage var optimization (VVO). Nevertheless, the majority of literature use constant power load model in the VVO analysis [10-18], which ignores the fact that load demand is predominantly voltage dependent. Recently, [19] has applied voltage dependent load models to VVO analysis, and the necessary and superiority of the more realistic voltage dependent load model has been demonstrated, but they assume the load coefficients are the same for all buses with the same type of loads and fixed throughout the day. This further motivates the author to investigate the effects of geographical and temporal variations of the coefficients in load model (due to DSM actions) on VVO dispatches.

In this thesis, demand manageable loads (DMLs) are divided into two categories, depending on their operating status during DSM implementation. One category refers to the DMLs that their operating status can only be either ON or OFF when DSM action is applied, e.g. the 'wet' load. In order words, the DSM action will only affect the corresponding power consumption simply by connecting or disconnecting these DMLs. The other category refers to the DMLs that their operating status is ON but the corresponding power consumption can be continuously varied when DSM action is applied, e.g. thermostatically controlled loads (TCLs). Instead of simply disconnecting, it is more difficult to control the power consumption of these DMLs during DSM implementation period as the physical operating principle needs to be considered to avoid violation of comfort constraints.

According to [99], the building sector is accountable for about 70% of electricity consumption in United States, and space heating, cooling and ventilation is responsible for around 50% of the energy consumed in buildings. Besides, with the initiation of ICT and AMI, the author is motivated to develop smart control methods to optimally operate the Heating, Ventilation, and Air-conditioning (HVAC) systems to reduce building electricity consumption and to enhance the role of buildings as important electricity consumers in the active distribution system operation for offering regulation services.

A physical-based thermodynamic model that is appropriate for optimal control design is required to develop an optimal controller which is able to balance energy usage of HVAC systems and comfort level. However, the shortage of such model in power engineering is the biggest obstacle to allow HVAC loads to participate in providing network services. Hence, this motivates the author to look for such model from other engineering communities such as building climate control and building construction industry.

1.3 Primary Contributions

This thesis addresses the broad area of load modelling and some of the applications in DSM within the context of the smart grid. And this research mainly focuses on various novel problem formulations related to DSM in the planning and operation of active distribution systems, rather than proposing innovative solution methodologies to solve existing problems. The primary contributions of this thesis are summarized as the following:

First of all, a novel hourly electric load forecasting model for a single building based on radial basis function neural network (RBFNN) using time, date, outdoor weather and historical load data as inputs is developed to mitigate the effects of variable and intermittent DGs on traditional load forecasting methods, especially in the high penetration level of RES situations.

Secondly, this thesis introduces an improved and comprehensive load aggregation methodology building on the work in [20-24] to develop the aggregate residential and commercial load models using the most updated load-use statistics publicly available. Compared with the majority of steady-state load models currently applied in the power system analysis in the literature, the most significant improvement is that the resulting models include short-term temporal variations in load characteristics due to the consideration of time-varying load mixes, which is particularly important for the analysis of various DSM scenarios as it enables the accurate identification of the portion of DMLs in the aggregate load at any time at various locations, as long as the information of load composition is available, which can be easily obtained from the modern smart meters. The developed load models can then be aggregated with the interconnecting medium-voltage (MV) and low-voltage (LV) networks for a wide range of applications in power system analysis. Based on the developed aggregate load models, another contribution of this research is a general methodology to model, quantify and assess the impacts of various devised DSM

schemes on the aggregate load models, power flow and network performance, which will be of interest to utility companies and policy makers. Moreover, the developed aggregate load model with time-varying model coefficients is suitable for the analysis of VVO problems in modern distribution system, particularly for the Conservation Voltage Reduction (CVR), one of the most recent advanced energy saving techniques proven by the industry to reduce power consumption and network losses, thus, a more accurate framework for CVR optimization in modern distribution system is formulated using the developed load models to investigate the effects of time-varying model coefficients of load models (due to naturally occurrence and DSM actions) on the VVO dispatches and the corresponding network performances. Furthermore, a DSM-based OPF problem is formulated to assess the ability of various type of DMLs to alleviate network contingencies (e.g. overloading, sudden shortage of RES) at different locations within a given distribution system.

Last but not least, due to the lack of accurate models describing thermal behavior of buildings in power engineering community, substantial literature in the area of building climate control and building construction has been reviewed by the author, and a mathematical R-C thermodynamic model of building based on fundamental laws of Heat Transfer and Thermodynamic that is suitable for control design with acceptable computational burden is chosen from thousands of models to serve as a bridge linking the areas of power engineering and building climate control together to provide more flexible demand and facilitate more advanced DSM programs in smart grid. Specifically, one contribution of this part is that an economic Model Predictive Control (MPC) algorithm based on the introduced thermodynamic model of buildings is proposed to effectively and optimally modulate the power consumption of commercial building HVAC system in response to varying electricity price and ambient weather to minimize the electricity costs, significantly reduce the peak demand and increase energy saving and efficiency, while respecting the comfort level. Another contribution

of this part is that an optimal building aggregator that can aggregate the HVAC loads to declare the power flexibility to the utility for providing fast and large-scale regulating power to the smart grid is developed under a novel contract framework between buildings, building aggregator and utility developed in this thesis, which can maximize and reward the flexible power reserve provided by buildings. The innovative characteristics of the proposed building aggregator lie in the ability of predicting the potential total reserve amount of HVAC loads in the target building group in a defined contract time and the ability of allocating the high frequency regulation power received from the utility to each participating building while maintaining comfort levels.

1.4 Thesis Layout

The rest of this thesis is arranged as the following:

Chapter 2 provides the literature review for all the relevant topics in this thesis. First, previous studies on DSM and various types of DSM are reviewed in details. Then a detailed literature review of load modelling, which is the most critical part of modelling DSM, is provided. In addition, the recent applications of OPF in power system, especially those related to demand side resources (e.g. DGs, energy storage systems, load control) are outlined. Furthermore, the concepts and recent applications of distribution system automation (DSA), Distribution Management System (DMS), Voltage Var optimization (VVO) and Conservation Voltage Reduction (CVR) are reviewed. Finally, this chapter concludes with an overview of the optimal control of various thermostatically controlled loads (TCLs) together with physical-based thermodynamic models in energy-efficient buildings.

Chapter 3 presents the fundamental theory of RBFNN and the detailed design of the hourly electric load forecasting model for a single building based on RBFNN, followed by a case study using the real measurement of load data from

a large high-rise commercial office building in Shenzhen China to validate the accuracy of proposed load forecasting method.

Chapter 4 outlines the aggregation methodology for developing the time-varying LV load models and representing them at the MV network, considering the temporal variations in load mixes. Both residential and commercial loads at maximum, minimum and average loading conditions are used as illustration examples.

Chapter 5 demonstrates some important applications of the aggregate load models developed in Chapter 4. Firstly, the methodology of developing the aggregate load models (both ZIP/polynomial and exponential load models) incorporating devised DSM scenarios is presented, and the corresponding impacts on the power flows and network performances are demonstrated and discussed. Next, the CVR problems using various types of load models are formulated to investigate the impacts of load model coefficients on the CVR dispatches and the corresponding resulting voltage profiles and power flows. Finally, the DSM-based OPF problem is formulated to assess the ability of various type of DMLs to alleviate network contingencies (e.g. overloading, sudden shortage of RES) at different locations within a given distribution system.

Chapter 6 starts from introducing the fundamental laws of Heat Transfer and Thermodynamics (e.g. heat conduction, convection and radiation) which dominates the temperature dynamics inside a building. Then an R-C model consisting of a series of heat transfer equations is presented to describe the temperature dynamics in a room and is extended to create a large R-C model which represents the whole building. The introduced model is then linearized and calibrated using historical data from a real existing building and the accuracy of the proposed thermodynamic model is validated by the comparison between the simulated results and the real measurements.

Based on the introduced thermodynamic model of buildings and the power consumption models of HVAC system, sophisticated control algorithms are

developed in Chapter 7 to pave the way for commercial buildings to participate in more advanced DSM schemes. Firstly, an economic model predictive controller is proposed to effectively and optimally control the HVAC system to utilize the time-varying electricity prices and the future disturbances to minimize the electricity costs, significantly reduce the peak demand and increase energy saving and efficiency, while respecting the comfort level. Furthermore, the role of energy-efficient buildings in the operation of future active distribution system is addressed in this thesis by proposing a building-aggregator-grid contract framework and formulating a robust MPC algorithm which both maximizes the profit of building aggregator and minimizes the payment of each participating building to optimally declare the power flexibility of HVAC systems to the grid as fast-response regulating power.

Chapter 8 concludes this thesis with the key contributions of this research and the discussion of the result implications. The possible directions and recommendations for future work are also discussed.

1.5 List of Publications

Journal paper published:

1. **Weijie Mai** and C. Y. Chung, "Economic MPC of Aggregating Commercial Buildings for Providing Flexible Power Reserve", *IEEE Transactions on Power Systems*, Vol. 30, No. 5, pp. 2685-2694, Sep. 2015.

Journal paper under review or preparation:

2. **Weijie Mai** and C. Y. Chung, "Model Predictive Control based Voltage Var Optimization for Active Distribution Networks with Time-varying Exponential Load Models due to Demand Side Management", in preparation for submission to *IEEE Transactions on Power Systems*.

Conference paper presented

3. **Weijie Mai** and C. Y. Chung, "Model Predictive Control based on Thermal Dynamic Building Model in the Demand-side Management", *in Proc. IEEE PES General Meeting*, Boston, MA, Jul. 2016. (**Best Paper Award**)
4. **Weijie Mai**, C. Y. Chung, Ting Wu and Huazhang Huang, "Electric Load Forecasting for Large Office Building based on Radial Basis Function Neural Network", *in Proc. IEEE PES General Meeting*, National Harbor, MD, Jul. 2014, pp. 1–5.
5. Ting Wu, **Weijie Mai**, Mingwen Qin, Chunxue Zhang and C. Y. Chung, "Optimal Operation of Combined Cooling Heat and Power Microgrid with PEVs", *in Proc. IEEE PowerTech*, Eindhoven, Jun. 2015, Page 1-6.
6. Chunxue Zhang, Bo Dai, Ting Wu, **Weijie Mai** and C. Y. Chung, "Model-based Volt-Var Optimization Using Advanced Metering Infrastructure in Distribution Networks", i*n Proc. IEEE PowerTech*, Eindhoven, Jun. 2015, Page 1-5.
7. Hei Yan Lai, **Weijie Mai** and C. Y. Chung, "Educational Simulation Platform for Micro-grid", *in Proc. 2014 IEEE PES Asia-Pacific Power and Energy Engineering Conference*, Hong Kong, Dec. 2014, pp. 1-7.

Chapter 2

Literature Review

2.1 Overview of Demand Side Management

DSM can be regarded as the measures that modulate consumers' electrical energy demand from the normal pattern and help to benefit the system in response to various supply conditions, including long-term actions intending to reduce system peak load or improve energy efficiency and short-term direct load control mechanisms under the system contingency. There are a few more terms often being used in the literature, such as demand response, demand side response, load response, load management, etc. In this work, they are all regarded as the same and the term DSM will be used throughout, unless specified.

Conventionally, the ancillary services including spinning, non-spinning reserve and other emergency reserves needed for supply-demand balancing and maintaining security margins in power supply are mostly provided by the conventional generators. With the increasing penetration of intermittent RES, the portion of traditional generators in the overall generation capacity will gradually drop, as a result of which, there is a need to exploit the flexible demand side resources to offer this system flexibility [2-3, 25].

Various DSM programs have been applied by system operators to improve supply and demand balancing by the modification of load profile for several decades. The study in [26] provides an overview of the key DSM concepts and methodologies that can enhance the performance and security of power system. Most of mature DSM programs carried out to date mainly focus on large

industrial consumers, e.g. [27-28], due to their sufficient size of load capacity to contribute to network ancillary services.

Nevertheless, with advanced development of ICT technologies, more and more DSM actions are expected to be implemented amongst residential and commercial sectors. Various approaches of aggregating and coordinating DSM measures from numerous highly distributed customers have been proposed, e.g. Virtual Power Plant or Aggregator concepts [29-30], with the intention of achieving the sufficient demand capacity to participate in Balancing Mechanism and providing beneficial ancillary services. Apart from the enabling ICT technologies, new electricity market mechanism are also required to remove the economic barriers, so as to allow DSM to be prevalent in residential and commercial load sectors [31-32].

According to the types of network services provided, the DSM schemes can be classified into several categories [26, 33-34]. It should be noted that some overlap could exist between the categories presented below, since a DSM program may have multiple objectives.

1. Load shaping

   This is the most common DSM scheme which aims at modify the shape of the system demand to obtain a flat daily load curve, generally by reducing demand at peak-load hours and shifting the reduced demand to off-peak hours, in such a way that, a greater amount of the load can be served by the more efficient base-load generation, while reducing the reliance on the costly and inefficient peaking generation. The flattening of load curves can help to reduce the generator ramping requirements and the required number of corrective actions, which in turn improves the system security and reliability [35]. The most common example of load shaping is the lower electricity tariffs offered at off-peak hours. This type of DSM will be discussed in depth in Section 7.1.

2. Maximizing asset utilization to defer investment

The cost of investment in upgrading and replacing network asset could be extremely high, and in certain scenarios, DSM can be applied to help maximize the utilization of network assets so as to defer the investment [36-37]. For instance, if a transmission line is overloaded on merely a small number of occasions throughout the year, it may be more cost-effective for the system operators to provide a DSM contract with financial incentives for the customers served by this transmission line to encourage them to reduce energy consumption when the overload is occurred, which can defer the immediate need of updating or replacing transmission line.

3. Direct load control

   Direct load control means that consumers allow their energy consumption to be directly controlled by network operator in response to supply conditions. It can offer more predictable and faster responses, compared with other DSM actions that rely on the customers' response to incentives, such as price signals. Real-time direct load control has been discussed in [38-39], which propose a similar approach to generation dispatch to dispatch the system loads, so as to mitigate the intermittent and variable renewable energy sources.

4. Providing operational reserves

   Recently, more and more studies believe that there is a great potential to provide various types of operating reserves through DSM schemes in power system. Reference [40] has summarized the advantages of providing reserve through DSM over through conventional generators, and it even claims that it is more reliable to utilize a great amount of individual DMLs than using a few large conventional generators to provide reserves, since the instantaneous response of DMLs is much faster than adjusting and re-dispatching conventional generators [41].

2.2 Overview of Load Modelling

Load modelling is to develop a mathematical or analytical expression of the variations in power flows (including both active and reactive power) to the connected load, with respect to voltage or/and frequency. There are two main types of load models, i.e. static and dynamic. Static load models are the expression of the active and reactive power demand at a specific time instant, while the active and reactive power demand in dynamic load models is expressed as a function of time using differential equations. Since this research concentrates on the steady-state analysis in power systems, only the steady-state load models will be discussed in details in this thesis. Static load models are generally classified into the following three types [42]: 1) Constant Power Load (CPL): the load draws constant active and reactive power, regardless of the magnitude of supply voltage; 2) Constant Current Load (CCL): active and reactive power is a linear function of the magnitude of supply voltage; 3) Constant Impedance Load (CIL): the power change proportionally to the square of the magnitude of supply voltage.

2.2.1 ZIP/Polynomial Load model

Generally, the loads in power system consist of different portion of CPL, CCL and CIL, depending on the exact load mix at that network location. Substantial studies have emphasized the importance of correctly modelling this load-to-voltage sensitivity in various applications of power system analysis [43-44]. The "ZIP" or polynomial model is one of the most common models in power system analysis.

The "ZIP" or polynomial load model (2.1)-(2.2) is a static load model that uses the sum of CPL, CCL and CIL to represent the demand characteristics.

$$P = P_0\left[Z_p\left(\frac{V}{V_0}\right)^2 + I_p\left(\frac{V}{V_0}\right) + P_p \right] \tag{2.1}$$

$$Q = Q_0\left[Z_q\left(\frac{V}{V_0}\right)^2 + I_q\left(\frac{V}{V_0}\right) + P_q \right] \tag{2.2}$$

where P_0 and P is the demand of nominal and actual real power of load, Q_0 and Q is the demand of nominal and actual reactive power of load, V_0 and V is the magnitude of nominal and actual supply voltage at the considered load bus, and Z_p, I_p, P_p, Z_q, I_q, P_q are the model parameters, where subscript "p" indicates active power and subscript "q" represents reactive power.

2.2.2 Exponential Load model

Another commonly used static load model is exponential load model which expresses the relationship between the demand of active and reactive power and supply voltage magnitude using two exponents, as shown in (2.3)-(2.4). It is a constant power load if $n_p = n_q = 0$, a constant current load if $n_p = n_q = 1$, a constant impedance load if $n_p = n_q = 2$. Other arbitrary values can be used for the exponents to characterize the modelled demand.

$$P = P_0\left(\frac{V}{V_0}\right)^{n_p} \tag{2.3}$$

$$Q = Q_0\left(\frac{V}{V_0}\right)^{n_q} \tag{2.4}$$

where P_0 and P is the demand of nominal and actual active power of load, Q_0 and Q is the demand of nominal and actual reactive power of load, V_0 and V is the magnitude of nominal and actual supply voltage at the considered load bus, and n_p and n_q are the model parameters for active and reactive demand, respectively.

2.2.3 Identification of Load Model Coefficients

The coefficients of load model need to be identified, once the load model form is determined. There are two widely adopted approaches to determine the

coefficient values in (2.1)-(2.4), i.e. measurement-based method and component-based method.

Measurement-based method obtains the voltage changes and the resulting variations in load characteristics to staged disturbances from the measurement and data acquisition devices at the location of interest, which are then fitted to the determined load model form [45-47]. The advantage of this approach is high accuracy since it is based on actual physical measurement data. However, this approach is inflexible because obtaining such measurement is time-consuming and costly, in addition, collecting those data for a wide range of voltage conditions and seasonal variations is usually unfeasible. The identification of load composition is also not possible, but this is an important requirement to analyze the effects of devised load changes through DSM schemes on the power system operation.

Component-based approach determines the coefficients of the desired bus load model using a “bottom-up” approach which aggregates physical and circuit based models of individual load devices. Unlike the measurement-based approach which is a “top-down” approach, no measurement from power system is needed. It is more flexible since the changes in load composition can be easily incorporated to build a new aggregate load model by simply adjusting the contribution proportion of each load type to the total demand. Although finding the accurate statistical information on the daily, weekly, and seasonal variation of load mix to implement this approach is difficult, the resulting models are particularly suitable for DSM modelling. A substantial amount of studies on developing component-based load models can be found in [20-24, 48].

The component-based approach allows the aggregate load to be decomposed, which enables the identification of the portion of load that are potentially available for DSM at any time during the day. As a result of DSM implementation, the variations in the load composition, and thus, the changes in

the electrical characteristics of loads, can be effectively and accurately modelled, which will be discussed in Chapter 5.1 of this thesis

2.3 Optimal Power Flow

Optimal power flow (OPF) has been applied to optimize a variety of power system planning and operation problems [49]. With the increasing penetration of DGs, OPF problems have been formulated to determine the maximum amount of DGs that can be integrated into the distribution network while respecting various operation constraints [50-53]. Reference [54-56] proposes to use OPF combined with linear programming techniques to improve asset utilization in distribution networks. OPF has also been utilized to minimize the load shedding required to allow the system to securely operate and avoid system collapse in system contingencies [59-64]. The control of DMLs and energy storage systems in response to real time electricity tariffs can also be optimized using OPF based approach [65-67].

2.4 Voltage Var Optimization

In the recent decades, distribution system automation (DSA) has received great attention from many power utilities worldwide with the intention of improving energy efficiency, system reliability and power quality. Similar to the role of Energy Management System tools in the transmission system operation, Distribution Management System (DMS) tools are critical components in DSA. Various appealing functionalities including VVO, fault location, service restoration and state estimation can be provided by DMS.

The VVO refers to the optimal control of capacitor banks, OLTCs and voltage regulators with the objective of minimizing the power losses, improving voltage profiles, etc. Several power utilities including American Electric Power [68], Northern State Power Company [69], B.C. Hydro [70], have deployed

many VVO applications and obtained promising results. Apart from voltage profile improvement and power loss reduction, Conservation Voltage Reduction (CVR) is another useful capability provided by VVO. The CVR aims at reducing the voltage to the minimum acceptable level with the purpose of reducing the total and peak demand, since loads are voltage-dependent and the voltage reduction results in a decrease in both active and reactive demands. Reference [71] has shown that 1% to 6% of the total demand can be reduced through proper CVR implementation.

A number of methodologies have been proposed for solving VVO problem in distribution system. For example, [72] develops a supervisory control scheme which exploits the data measured at the substation to optimally dispatch the capacitor banks and voltage regulators. Reference [73] decomposes the VVO problem into two sub-problems, at feeder levels and at substation, respectively, then solves these sub-problems by dynamic programming and a fuzzy logic control algorithm. In [74], the VVO problem is solved by a multi-objectives Genetic Algorithm combined with fuzzy logic and expert knowledge is applied to reduce the size of search space. An adaptive system is applied to solve the VVO problem in [75]. The optimal placement of capacitor for CVR problem is solved by a Genetic Algorithm in [76]. Many other work in the literature have studied the VVO problems in distribution systems [10-13], and the effects of DGs on VVO dispatches [14-18]. However, all of them use the constant-power load models in the analysis and have ignored the relationship between voltages and loads, which is inaccurate in reality.

Although a limited number of academic publications about CVR can be found in the literature, the power utilities are gradually and increasingly implementing CVR. The study in [70] has demonstrated that the demands of both active and reactive power are significantly related to the voltage magnitude. In addition, the report published by US Department of Energy [77] also acknowledges that the voltage dependence of loads has a considerable impact on

the efficiency and performance of VVO and CVR implementation. This will be discussed in details in Chapter 5.2.

2.5 Energy-Efficient Buildings

Smart energy-efficient buildings are expected to play an increasingly significant role in the emerging smart grid. It has been shown in [78] that the power flexibility provided by aggregate thermostatically controlled loads (TCLs) is similar to the characteristic of stochastic batteries, which makes them good candidates for providing fast regulating services for power system. TCLs are suitable for demand response and direct load control programs, since their thermal energy storage ability is similar to the way that chemical energy is stored in battery, which allows their power consumption to be increased and decreased.

There are various types of TCLs that have been proven to be able to provide ancillary services [79-80], such as water heaters [81], refrigerators, heat pumps [82] and Heating Ventilation Air Conditioning (HVAC) systems. Promising results have been obtained in [83-85], which use model-based control techniques to improve energy efficiency of HVAC systems. For example, an MPC framework based on a nonlinear model of cooling system is proposed in [83] to minimize the energy consumption in a large commercial building, and the authors in [85] applied sequential quadratic programming to solve a similar nonlinear problem by iteratively linearizing the constraints around the present solution, until the convergence condition is satisfied.

Reliable and accurate dynamic models are critical to model-based control techniques, and the most difficult and time-consuming task in building climate and energy control is the parameters identification in modelling process. Since an accurate thermodynamics-based building model is needed to capture temperature dynamics to ensure temperature constraints are satisfied when the control strategies are implemented, a number of thermal dynamics building models have

been proposed in the literature. The building models reported in literature can be mainly categorized into data driven models, high fidelity physical models, and simplified physical models based on R-C analogy.

Data driven models developed by fitting historical behaviors of the system cannot guarantee prediction accuracy for operating points outside the range covered by training data, and thus extensive training data with widely varying conditions is needed. TRNSYS [86], DOE-2 [87], EnergyPlus [88], etc., are typical high fidelity physical models, which emerged in 1980s and are still being used for simulation purpose currently. However, they are not suitable for online implementations because the complexity and size of models usually results in a computationally intractable optimization problem, besides, the model identification and validation process also requires excessive data collection, parameters tuning and simulation.

The issues related to data driven models and high fidelity physical models can be mitigated by using simplified physical models based on R-C analogy, which was first proposed in 1980s and showed good performance in predicting building temperature dynamics [89-91]. They represent the building mass by one or more representative lumped capacitances so that analytical solutions from the models can be easily calculated resulting in reduced computational requirements for estimating heating/cooling loads. Later, numerous studies have been concentrated mainly on: 1) what part of the building should be lumped into one capacitance [92-94]; 2) the required order of building model [95-97].

Chapter 3

Electrical Load Forecasting for Buildings Based on Radial Basis Function Neural Network

3.1 Introduction

In China, according to [98], 24.1% of total national energy use was accounted for by buildings in 1996. This increased to 27.5% in 2001 and it is predicted that buildings will account for approximately 35% of total national energy usage in 2020. Besides, 75% of total electricity consumption in United States is consumed by buildings [99]. The building sector will globally remain an important electricity end-user in the coming future due to the increasing need for better indoor environment. Therefore, building energy conservation and efficiency are of great significance both environmentally and economically.

The smart grid revolution has enabled a lot of innovative initiatives that focus on increasing building energy efficiency. For example, smart metering allows many novel services, including real time pricing, bi-directional communication and load forecasting. Specially, the prediction of future power consumption over a time-span ranging from minutes to days is essential for some smart grid applications [100], such as DSM, which is implemented by utility companies to directly control or encourage consumers to modify the amount and pattern of energy demand on the customer side, so that the available energy can be used with higher efficiency without the need of installing new generation and transmission infrastructure [101]. Therefore, building electric load forecasting is necessary because changes in load need to be known beforehand, and it is also the prerequisite for energy saving operations and optimal control of building

systems. For instance, according to [102], HVAC systems account for about 65% of the energy usage of commercial buildings and accurate load forecasting can be greatly helpful in determining the number of sets of chillers or pumps needed, the appropriate starting or ending time of pre-cooling/pre-heating and the way to adjust the running modes of the chillers [103]. Besides, the model predictive control based energy management system is increasingly becoming prevalent due to its ability of considering both the expected dynamic system behavior and the forecasts of weathers, variable RES and load demands, thus accurate load forecast of a single build is essential for the successful performance of and MPC-based energy management system.

Load is traditionally forecasted at a particular bus location in medium-voltage (MV) network, and substantial literature using various techniques on load forecasting can be found in [8]. However, when the highly distributed DG or demand side integration in distribution network is taken into account in load forecasting, forecasting of the aggregate load could be very challenging. One possible solution is to isolate the effects of DG by forecasting the load of a single building, since there are considerable amount of literature on the modelling and forecasting of DG output. This motivates the author to develop an hourly electric load forecasting model for a single commercial office building.

In major cities in China (e.g. Hong Kong, Shenzhen, Shanghai), electricity usage in large commercial buildings with full air-conditioning is 70-300 kWh/m^2, which is 10-20 times residential buildings [104-105]. Therefore, this paper focuses on electric load forecasting of commercial office buildings since they have much larger electricity consumption and thermal inertia, which can offer a greater amount of demand response, energy saving and power regulation opportunity if they operate efficiently.

Although a large amount of literature about load forecasting exists and a comprehensive review can be found in [106-109], not much has been applied to commercial office buildings for the purpose of increasing building energy

efficiency. In [110], a Gray Model was developed to estimate the cooling load which can be related to power consumption via chiller system coefficient of performance, but it involved tedious parameters identification procedure and required a lot of data that is hardly obtained. Statistical time series models are used for modelling the load according to historical load data, such as regression analysis [111-113], Kalman filtering [114] and multiplicative autoregressive models [115]. Another method is causal model which models the load as a function of exogenous variables such as weather data; examples include autoregressive integrated moving average model [116] and fuzzy autoregressive moving average model [117]. Recently researchers have focused on intelligent computational techniques for load forecasting, including support-vector machines [118-119], expert systems [120] and fuzzy logic [121-123]. In particular, [124-128] demonstrated that artificial neural network (ANN) is one of the most successful methods in forecasting area. Therefore, RBFNN is adopted in this work. Very little of extant literature on building electric load forecasting has modeled the load as a non-linear function of both historical load data and weather data based on RBFNN, as proposed in the next section.

3.2 Proposed Load Forecasting Model

3.2.1 Justification of Choosing RBFNN

The statistical time series and causal model methods mentioned above mainly work for linear prediction and they are often disadvantageous because building's loads are normally a non-linear function of exogenous factors [129]. Several computational intelligent techniques can deal with non-linearity in load prediction, but neural network is used here because it has the advantage of modeling the multivariable problem with complex non-linear relationships between variables, as these implicit relationships can be extracted via learning

with training data. Among various neural network architectures, RBF neural network is chosen for this work mainly because of its fast online learning ability, strong tolerance to noisy input data as well as good generalization and easy design implementation. The performance of RBF neural network for building load forecasting will be compared with that of traditional multi-layer perceptron (MLP) neural network in Section 3.3.

3.2.2 Theory of RBFNN

ANN has the ability of non-linear modeling and adaptation (through self-learning) to address the complex relationship between inputs and outputs by means of a highly connected array of neurons. RBF neural network is a feed-forward network characterized by the transfer function in the hidden layer which is symmetrical about the center.

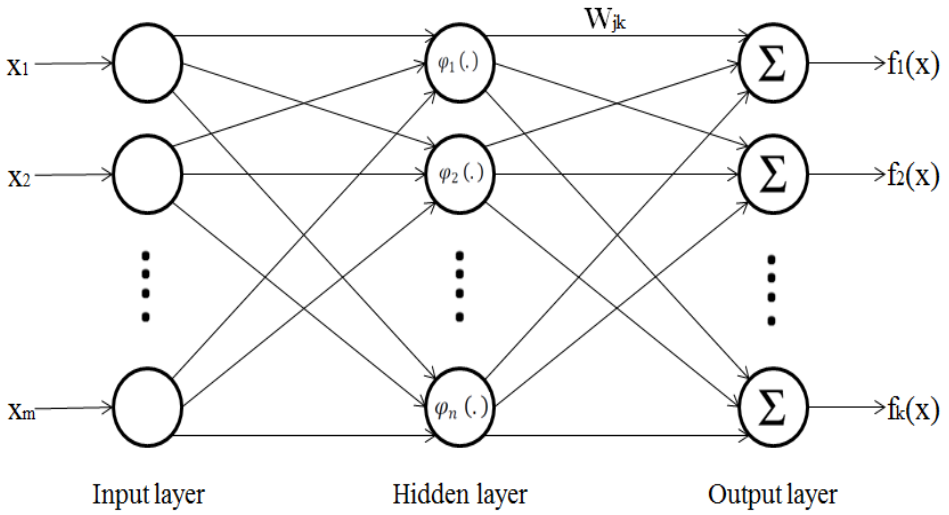

Fig. 3.1 General structure RBF neural network

RBF neural network generally consists of an input layer, a hidden layer and an output layer as shown in Fig. 3.1. Neurons of input layer function as buffers to pass each input signal x_1, x_2, …, x_m to all neurons in the hidden layer. The

neurons in the hidden layer are all connected directly to all nodes in the output layer. Gaussian exponential function is normally used as the basis function for the hidden nodes:

$$\varphi_j(\mathbf{x}) = \exp\left[-\frac{1}{2\sigma_j^2}\left(\|\mathbf{x}-\mathbf{x}_j\|^2\right)\right], \quad j=1,2,...,n \tag{3.1}$$

where $\boldsymbol{x}$ is the input vector and x_j denotes the center of the RBF unit. The output of the nodes in the hidden layer decreases when the distance between the input pattern and the center increases and, conversely, the output is greater if the input pattern is near the center. The network output is produced by a linear combination of the hidden layer outputs:

$$f_k(\mathbf{x}) = \sum_{j=1}^{n} w_{jk}\varphi_j(\mathbf{x}) \tag{3.2}$$

where $f_k(x)$ is the output of k^{th} neuron in the output layer, w_{jk} denotes the weight from j^{th} neuron in the hidden layer to the k^{th} neuron in the output layer. The associated weight of the connection between neurons acquires knowledge and distinguishes the network. Training RBF neural network is to determine the number of neurons in the hidden layer, the radius of each RBF function, the corresponding center and the optimal weights of connections between the hidden and the output layer. The details of the training algorithm can be found in [130-132]. The outputs can then be easily calculated for any input vectors after the network is well trained.

3.2.3 Hourly Electric Load Forecasting Model based on RBFNN

The hourly electric load forecasting model for commercial office buildings is depicted in Fig. 3.2. The output layer has only one neuron which yields the estimated hourly electric load. There are many factors that can affect the electric load of commercial office buildings, such as the day type, time, weather and historical load, which are used as model inputs.

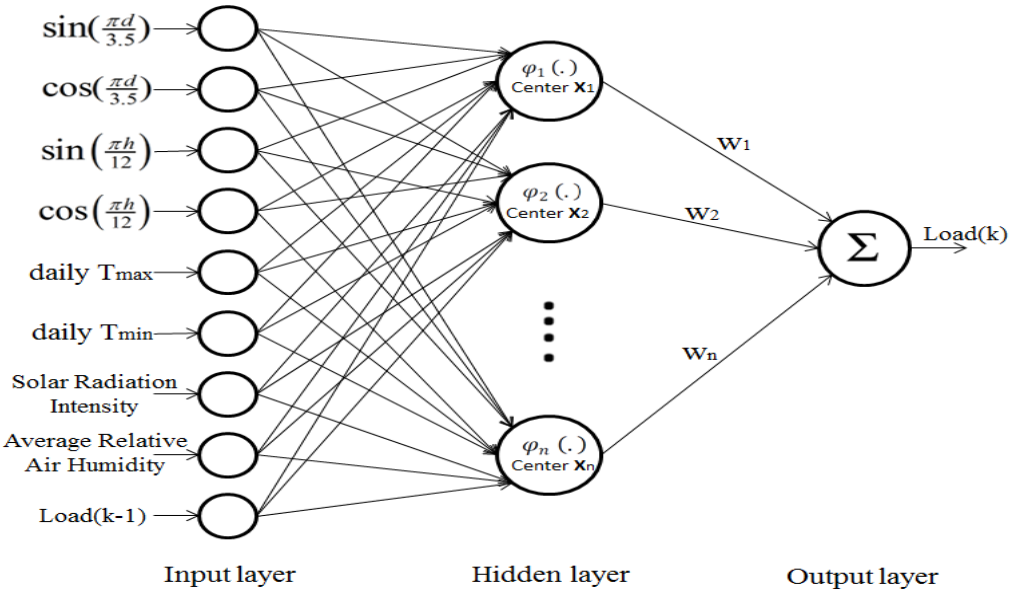

Fig. 3.2 Proposed hourly electric load forecasting model based on RBFNN

1) *Time inputs*: It is necessary to add an index in the input signals to specify the day of the week (d = 1 for Monday, d = 2 for Tuesday and d = 7 for Sunday and other holidays) and the hour of the day (h = 0, 1,…, 23), because the load pattern of commercial office buildings is greatly influenced by the schedule of work; less energy is consumed during nights, weekends and holidays. Four neurons are needed for day type and time inputs since they are to be coded as their sine and cosine values, shown as follows, before being input into the model [132-133]:

$$\sin(\frac{\pi d}{3.5}), \quad d = 1,2,...,7 \tag{3.3}$$

$$\cos(\frac{\pi d}{3.5}), \quad d = 1,2,...,7 \tag{3.4}$$

$$\sin(\frac{\pi h}{12}), \quad h = 0,1,2,...,23 \tag{3.5}$$

$$\cos(\frac{\pi h}{12}), \quad h = 0,1,2,...,23 \tag{3.6}$$

2) *Weather inputs*: The weather has a tremendous impact on power consumption of buildings on weekdays because most of the power is consumed by building HVAC system, especially for large high-rise

buildings. For example, power consumption in buildings is much higher on a hot day due to the increased energy needed for cooling. Hence, ambient temperature is a significant input for predicting electric load. However, unlike previous studies, this paper uses the daily ambient maximum (T_{max}) and daily ambient minimum (T_{min}) ambient temperatures instead of hourly ambient temperature as model inputs for two reasons, one is the accurate hourly ambient temperature data is not available in our case and the other reason is that the thermal dynamics of large commercial office buildings is very slow due to the large thermal inertia. So we believe the outdoor temperature at a given hour k does not have much influence on power consumption, i.e. it takes a few hours for the effect to be material. Apart from temperature, the daily total solar radiant intensity (MJ/m^2) and outdoor average relative air humidity are two other inputs for the model. Solar radiation greatly contributes to sensible heat load of buildings, while relative air humidity is related to latent heat load. Both sensible and latent heat load require energy for cooling to maintain the comfort level. Normalization of data before feeding the input data to the model is crucial because input variables have different magnitudes and the learning algorithm may not be able to figure out the importance of every variable without normalization. The weather data is normalized between -0.9 and 0.9, as in [125]:

$$x_n = 1.8 \times \left(\frac{x - x_{\min}}{x_{\max} - x_{\min}} \right) - 0.9 \qquad (3.7)$$

3) *Historical load input*: To predict the load at hour *k*, the most important input for the model might be the load at hour (*k*-1), which is readily available from the electric meters. A lot of factors (e.g., occupancy and building structure details, etc.) related to power consumption have not been considered; it is impossible to consider all factors. By introducing the previous load to the model, the effects brought by other unconsidered

factors until hour (k-1) are also introduced into the model and thus a higher level of acquired knowledge is obtained. Normalization of historical load data should also be carried out, using (3.7).

3.2.4 Performance Evaluation of Forecasting Model

With the objective of quantitatively examining the performance of the developed RBFNN hourly load forecasting model, statistical analysis including mean bias error (MBE), root mean square error (RMSE), mean absolute percentage error (MAPE) and coefficient of determination (R^2) needs to be conducted as follows [132-133]:

$$\mathrm{MBE} = \frac{1}{n}\sum_{i=1}^{n}(P_{p,i} - P_i) \tag{3.8}$$

$$\mathrm{RMSE} = \sqrt{\frac{1}{n}\sum_{i=1}^{n}(P_{p,i} - P_i)^2} \tag{3.9}$$

$$\mathrm{MAPE} = \frac{1}{n}\sum_{i=1}^{n}\frac{\left|P_{p,i} - P_i\right|}{P_i} \tag{3.10}$$

$$\mathrm{R}^2 = 1 - \frac{\sum_{i=1}^{n}(P_i - P_{p,i})^2}{\sum_{i=1}^{n}(P_i - \overline{P})^2} \tag{3.11}$$

where P_i is the measured load at time i, $P_{p,i}$ denotes the load predicted by the proposed model at time i, $\overline{P}$ is the mean of the measured load and n denotes the number of data points. R^2 takes values between 0 and 1, the higher the R^2, the more accurate the model. MAPE is regarded as a standard for evaluating accuracy of the load prediction model since it has been adopted repeatedly in literature, such as [132-133]. MBE is used to evaluate the model's long-term performance as it is a measure of the average error between predicted values and the measured values, while RMSE is an indication of the variation of predicted values around the measured values which can provide information on the

model's short-term performance. The forecasting model is more accurate with a lower RMSE.

3.3 Case Study and Discussion

A 39 stories real commercial office building in Shenzhen, China with floor area of about 103786 m^2 and height of 192 m was chosen for a case study for the proposed RBFNN load forecasting model. The building is used purely for office purposes and is a typical representative of the large high-rise office buildings which are very common in Hong Kong and Shenzhen. Power is mainly consumed by the air-conditioning, lighting, elevator and electronic devices. The hourly load data recorded by the electric meters from 01/08/2012 to 24/08/2013 was retrieved, provided by China Southern Power Grid for research purposes. The weather data mentioned in Figure 2 for the period from 01/08/2012 to 24/08/2013 was collected from the Meteorological Bureau of Shenzhen [134]. This data was coded and normalized as discussed in Section 3.2.3, each set with 9 input parameters and 1 output parameter, and they were divided into two groups, one for training the network and the other for validation.

In order to develop a load forecasting model with good adaptability, the training data should cover a wide range of situations, so 4776 data sets from 01/08/2012 to 15/02/2013 (24 sets each day) which include hot, cool and cold weather were used for training. The training algorithm adopted in this study is explained in [135], which finds the optimal radius and center for each neuron in the hidden layer, using an evolutionary approach. The predicted leave-one-out (LOO) error is supervised to determine the optimal number of neurons in the hidden layer; it stops increasing the number of neurons if the LOO error starts to increase because of over-fitting.

The well-trained model is validated under three different scenarios, hot, cool and cold weather. Scenario A was used to evaluate the model by 792 hourly data

sets (cold weather) from 26/02/2013 to 30/03/2013, during which the T_{min} was between 11°C and 16°C. For Scenario B there were 912 hourly data sets (cool weather), from 15/05/2013 to 21/06/2013, during which the average T_{max} and T_{min} are 28°C and 24°C, respectively. Scenario C tested the model by 912 hourly data sets (hot weather) from 22/06/2013 to 29/07/2013, during which the average T_{max} and T_{min} are 32°C and 26°C, respectively. The predicted hourly load of this large office building is derived by passing these data sets into the well-trained RBFNN load forecasting model and comparing the results with the actual hourly load to evaluate the model performance by statistical error analysis.

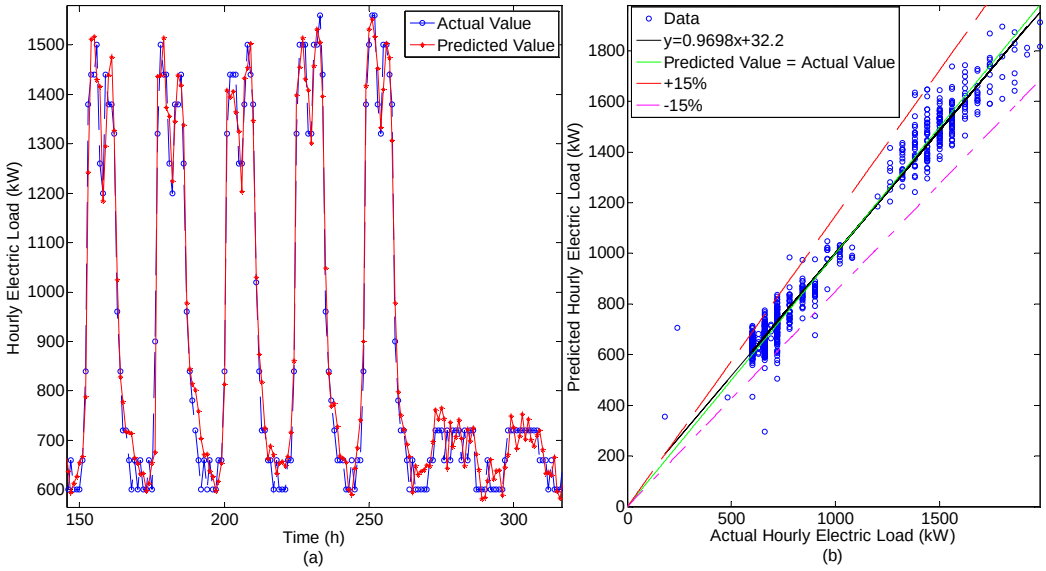

Fig. 3.3 (a) Actual hourly load vs. Predicted hourly load (by RBFNN) (Validation - Scenario A 04/03/2013 – 10/03/2013); (b) Comparison between actual and model predicted hourly load (by RBFNN) for Scenario A

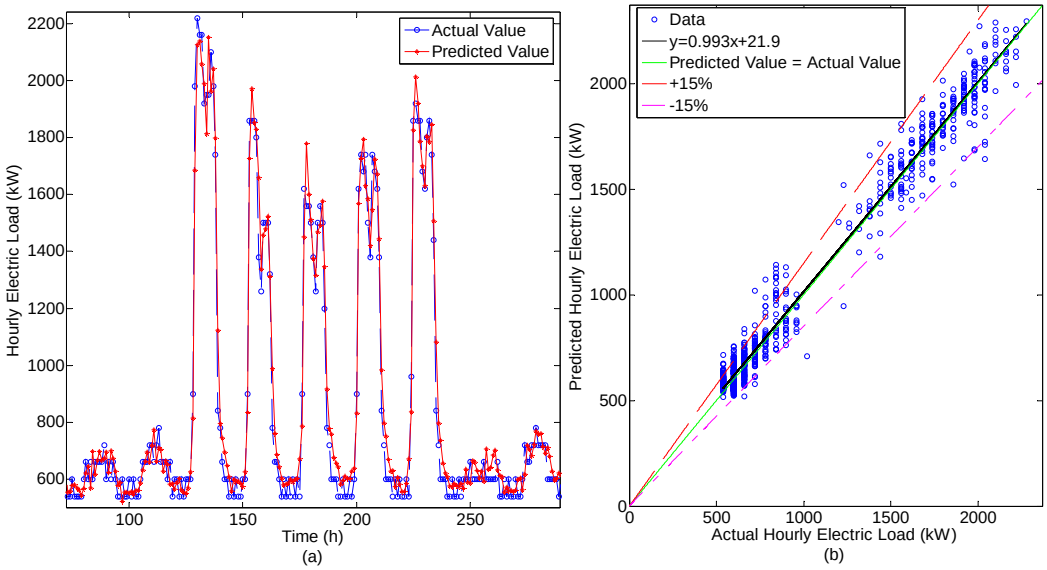

Fig. 3.4 (a) Actual hourly load vs. Predicted hourly load (by RBFNN) (Validation - Scenario B 18/05/2013 – 26/05/2013); (b) Comparison between actual and model predicted hourly load (by RBFNN) for Scenario B

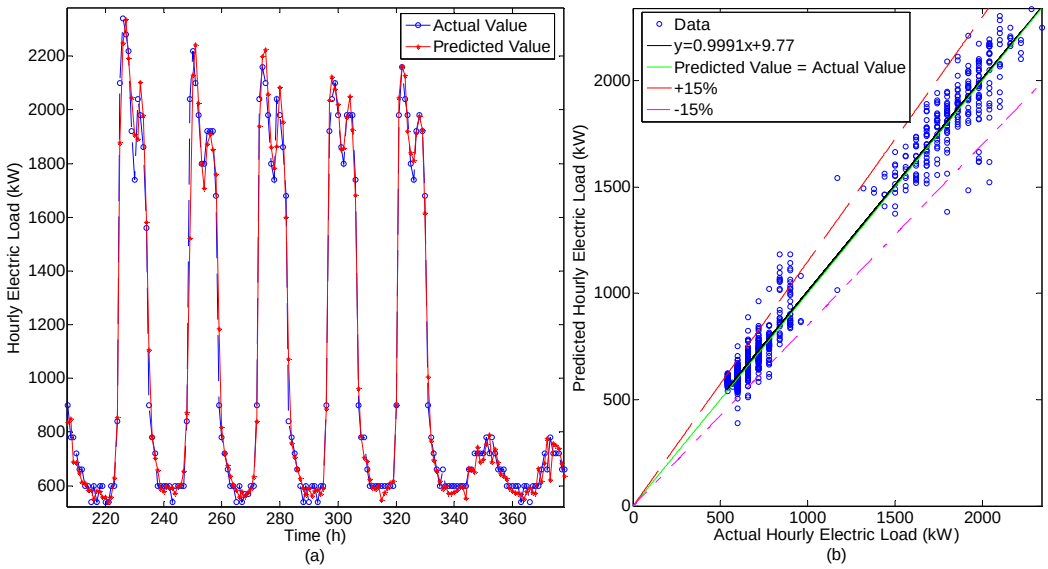

Fig. 3.5 (a) Actual hourly load vs. Predicted hourly load (by RBFNN) (Validation - Scenario C 30/06/2013 – 07/07/2013), (b) Comparison between actual and model predicted hourly load (by RBFNN) for Scenario C

For the sake of comparison, a traditional multilayer perceptron neural network (MLPNN) is implemented; it has the same input and output structure as

the proposed RFBNN with 19 neurons in the hidden layer (Rule of thumb: $2N_{input}+1$), and is trained by the same training data and tested by the data sets of Scenario A as described above. As shown in Fig. 3.6, the MLP network could not accurately predict the load and large errors are found, especially during the peak load periods on 07/03/2013 and 08/03/2013 because over-fitting occurs and the network may have tried to model random noise in the data. Optimal numbers of hidden layers and neurons in each hidden layer in MLP network must be decided to have good performance, but it involves tedious trial-and-error procedures, which is computationally expensive, thus not implemented here.

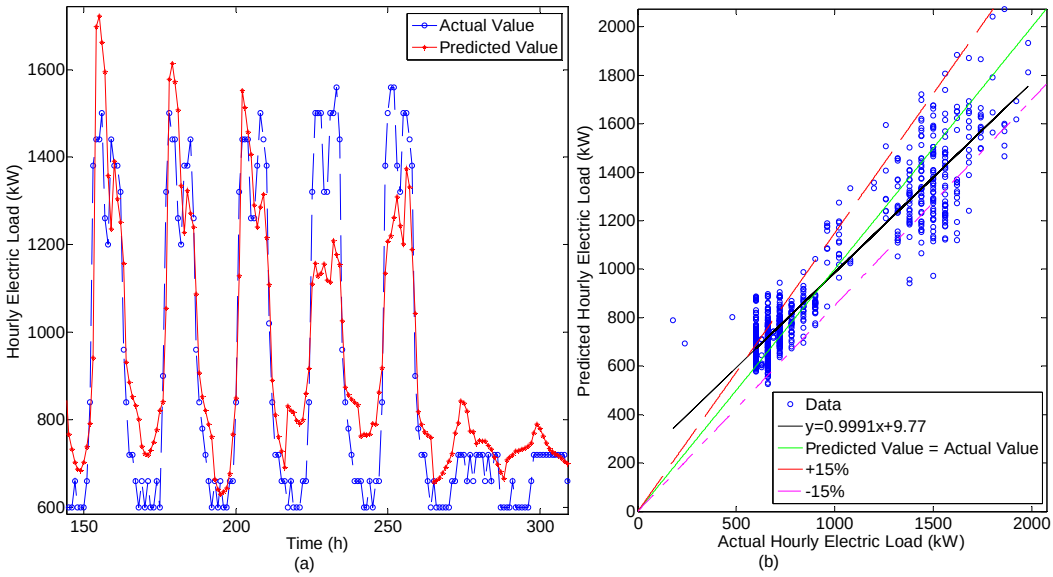

Fig. 3.6 (a) Actual hourly load vs. Predicted hourly load (by MLPNN) (Validation - Scenario A 04/03/2013 – 10/03/2013), (b) Comparison between actual and model predicted hourly load (by MLPNN) for Scenario A

Statistical analysis results presented in Table 3.1 also prove the promising performance with very low values of MAPE, RMSE and MBE, which guarantees both short-term and long-term performance. The value of R^2 is 0.97 in all the three scenarios, which means the developed model explains 97% of variability in hourly electric load of this building. As shown in Fig. 3.3(b), Fig. 3.4(b) and Fig.

3.5(b), in these three scenarios, about 95% of the hourly predicted load values have relative errors in the range of [-15%, 15%] and the linear fitting lines (color black) almost match the perfect prediction line (color green), both observations indicating good accuracy of the proposed model. It is also found that the prediction errors are slightly larger during night times and weekends when the load is smaller, but this is acceptable because non-peak period is not a big concern and the main goal is often to predict and reduce the peak load. In Fig. 3(a), Fig. 4(a) and Fig. 5(a), the model predicted load precisely follows the trend of the actual load pattern; even the small load drop at noon time on a weekday can be identified by the model, which corresponds to the lunch break when occupation level decreases. Fig. 3.4(a) shows the proposed forecasting model still does not suffer even though the load dropped quite a lot on Wednesday 22/05/2013 because of the dramatic decrease of outdoor temperature. The weekday power consumption in Scenario C (peak load about 2200 kW) is much larger than that of Scenario A (peak load about 1500 kW) as the building required more energy for cooling in Scenario C due to the hot weather. This successful prediction also proves that weather inputs play a significant role.

Table 3.1 Statistical Analysis Results of Proposed Load Forecasting Model

	MAPE	RMSE	MBE	R^2
Scenario A	0.0578	0.1643	-0.0094	0.973
Scenario B	0.0729	0.1578	-0.0192	0.975
Scenario C	0.0572	0.1511	-0.0162	0.977

3.4 Chapter Summary

In this chapter, a model for forecasting hourly electric load of commercial office buildings based on RBF neural network has been proposed and high accuracy has been demonstrated in the model validation using real building data under various weather conditions. Another benefit of the proposed method is that

it is simple to implement, without tedious trial-and-error parameterizing procedures. It only needs weather and electric power consumption data which is easy to obtain. Such prediction method could be useful in demand estimation by utilities and the intelligent optimal control of building systems for demand side management and providing ancillary service.

The future work includes testing the proposed model by using data of more real commercial office buildings in different locations to prove its adaptability and exploring the possibility of combining other computational intelligent techniques for the improvement of forecasting performance. Besides, modifications are also needed to develop a more generalized load forecasting architecture for different types of buildings. For example, hourly ambient temperature or the change of consecutive hourly ambient temperature should be used as the model inputs for load forecasting of small residential buildings because their thermal inertia are much smaller than that of large commercial buildings, thus the thermal dynamic of small residential buildings is faster. Maybe the speed and direction of wind should not be ignored in some cases as well.

Chapter 4

Aggregate Load Models with Time-varying Model Coefficients based on Component-based Load Aggregation Methodology

4.1 Introduction

The decisions for power system planning and operation highly relies on the simulation results of power flow analysis and system stability studies for various operating conditions, which requires accurate models of all network components in order to obtain accurate and useful results [43]. Several power system collapses in the history, for example, the 1987 Tokyo network collapse [136] and the 1983 Swedish black out [137], were attributed to the inaccurate load modeling. Consequently, substantial effort has been dedicated to improve the representation and models of load characteristics for diverse power system studies these years, for instance [136, 138-139], which confirms the significance of accurate load modeling. However, the electrical characteristics of loads as well as the power system operation have significantly changed since 1990s, it is necessary to improve the existing practice of load modeling and even develop models for the new emerging loads, so as to fulfill the requirements for modern power system analysis, and this is widely accepted and recognized in the research area of load modeling [140].

Traditionally, aggregate load models representing a great number of individual loads and other power system components in distribution network are used for the analysis in medium voltage networks. The behavior of aggregated load is comparatively insensitive to individual load variations at higher voltage

level network, so the impacts of individual load components is mitigated, which allows for the use of relatively simple load models in medium voltage network.

However, there are a few important reasons why a more comprehensive representation of the connected load with the supply network in distribution network is required for modern power systems. Firstly, the network performance and the aggregate load models are more sensitive to individual load variations at the distribution level due to the much smaller sized aggregates. In addition, the number of DGs in distribution network is substantially increased, for example, [141] demonstrates the influences of using different load models in distribution system analysis on the optimal placement and sizing of distribution generation units. Besides, the number of non-linear loads (e.g. inverter-interfaced DG units, consumer electronic devices etc.) is considerably increased within power system, and this will lead to various operation issues such as voltage rise, power quality (e.g. complex interactions at harmonic frequencies) and unbalance conditions. Finally, demand side management, a feasible approach to defer the investment in upgrading system infrastructure, is attracting more and more attentions, and due to the advanced development in communication technologies, distributed smaller customers, such as residential and commercial loads, which are progressively transforming into smarter electricity consumers and active participants in power system operations through DSM programs to provide network support. Therefore, there is a need of more advanced and detailed load models to help better understand the loads in low voltage network and their interactions with nearby power system components and users, which is crucial to exploit possible operational advantages in future smart grid.

This chapter introduces a component-based load aggregation methodology that combines several validated generic models of important load categories to produce the aggregate load models for residential and commercial sectors that are able to retain long-term and short-term temporal variations in load characteristics, which is particularly important to improve planning decisions and

operation strategies in the future active distribution system with a wide range of DSM programs and an growing penetration levels of time-varying, stochastic, distributed generation. This methodology is based on the method outlined in [20-24], and a considerable amount of research has been carried out by Collin [48] to update, develop and validate this component-based load model using some public load data and statistical information on load mix and load devices connected. Later, this model has been applied in [142] by Collin. However, the aggregate models developed in the above literature are out-of-date due to the increased demand and the changes of load compositions. In this chapter, this component-based load aggregation methodology is briefly reproduced, using the most updated load data and statistical information, to serve as a foundation for better understanding the following chapters which frequently utilize the produced aggregate load models for power system analysis.

4.2 Overview of Aggregate Load Modeling Approach

The advantages of the introduced load modeling approach over the traditional existing load modelling methods can be summarized as follows:

1. It can accurately represent time-varying demands using time-varying load model coefficients which vary with the change of load mix. The existing load models (e.g. [43, 143-144]) only present one set of load model coefficients for each loading condition (e.g. average, maximum and minimum loading). There are long-term (emerging or updates in load technologies), medium-term (e.g. seasonal) and short-term variations (e.g. half-hourly, hourly, daily) in the connected load. However, most of traditional existing load models do not capture the short-term variations. But the short-term variation in load composition also alters the electrical characteristics of the loads, the impacts of which really depend on the applications and the voltage levels for use in analysis. For example, using

a single lumped generic load model with fixed model coefficients and ignoring the short-term load variations is a rational approximation at medium or high voltage levels, but the aggregate load models will be more sensitive to load variation at low voltage levels, and the impacts of short-term load variations should not be ignored, especially when low voltage micro-generation that also exhibits long, medium and short-term variations is connected in the future electricity network.

2. It can be easily updated and modified to integrate and analyze expected future changes in technological modifications and load mixes. For example, the penetration of EV battery chargers and inverter-interfaced distribution generation units is expected to significantly increase.
3. Although the aggregate load model is developed from low voltage levels, it allows for aggregation to a range of voltage levels (i.e. high voltage levels in transmission network). Even though more and more engineering challenges emerge in the distribution networks, changes in load and operation in the low voltage network will still influence the transmission systems through DSM actions, DGs connection and energy storage systems etc., it allows for tracing, evaluating and quantifying these impacts.

Fig. 4.1 illustrates an overview of the component-based load aggregation methodology that applied in the following chapters. Several sets of input are needed to model the aggregate load:

1. *Load demand curves*: It can be measured or simulated, which should detail the variations in the demand of both active and reactive power over the considered period, including both short-term (e.g. hourly) and long-term (e.g. monthly) variations.
2. *Statistical information on the proportion of various load categories in each main load type and the proportion of various load types in the*

overall demand: Based on these information, the contribution of various load categories to the total demand can be obtained, thus, the load mixes is transformed into various main load categories, according to the electrical characteristics of the load devices.

3. *Generic models for main load categories*: These are combined to create the LV aggregate load model, according to the corresponding contribution to the overall active power demand of the modelled sector.
4. *Network models*: Including network configuration and component model with typical values, which will be combined with the low-voltage aggregate model to develop the medium-voltage aggregate load model.

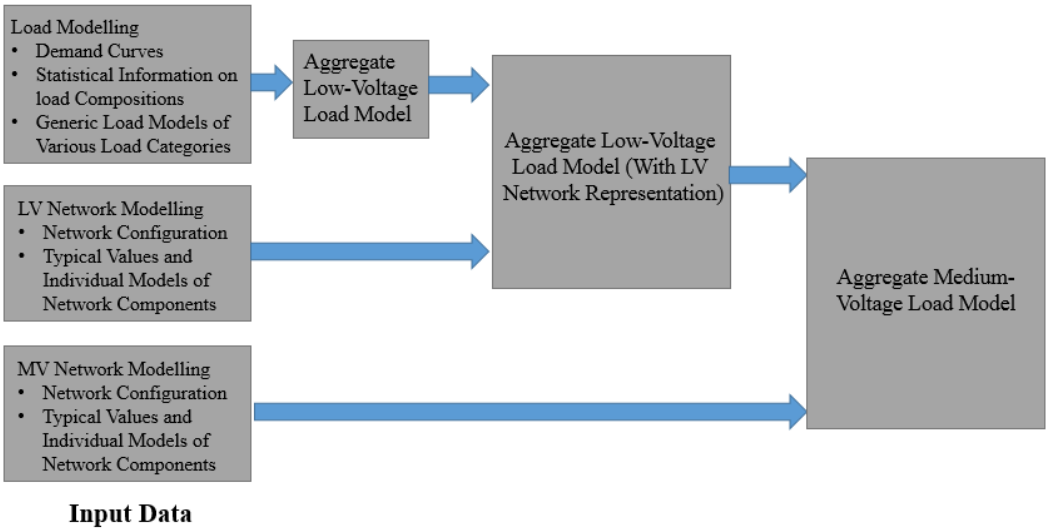

Fig. 4.1 Overview of the component-based load aggregation methodology

4.3 Example: Aggregate Residential Load Model

This section demonstrates the aggregation approach using residential load sector in UK as an illustration example, this approach can certainly be applied to other countries/areas using similar datasets as well.

4.3.1 Load Demand Curves

A considerable amount of information about load demand in residential load sector is available from existing literature [145-147] and government reports [148]. Typical residential load demand curves in UK shown in Fig. 4.2 are used to illustrate the aggregation approach, which will also be applied into various power system analysis in the following chapters. Three loading conditions which show hourly (i.e. short-term) and seasonal (i.e. long-term) load demand variations have similar profiles since the behavior of customers will not considerably change throughout the year. The seasonal variations can be attributed to the changes of load mixes that responses to the ambient conditions, for example, the demand of space heating and water heating will be different between summer and winter.

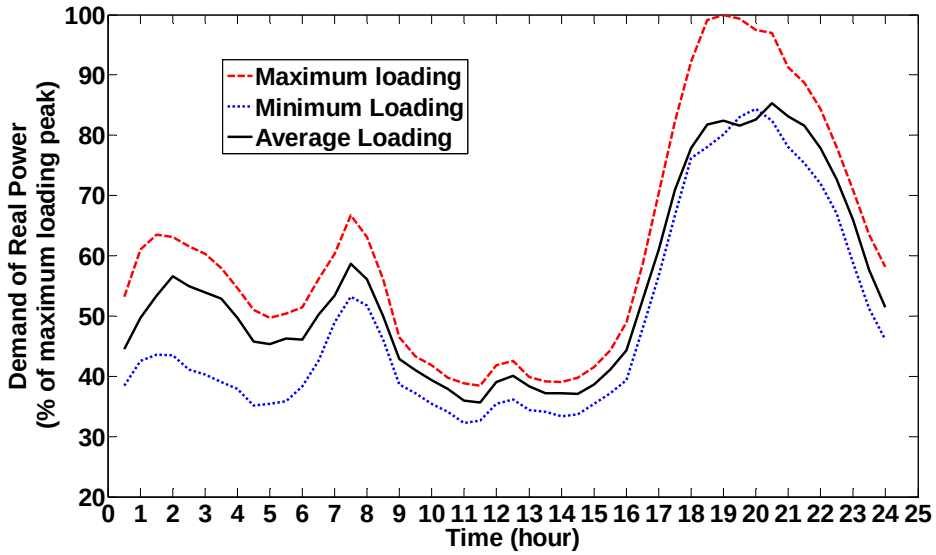

Fig. 4.2 Minimum, average and maximum loading conditions of typical aggregate daily active power demand curves for residential load.

4.3.2 Load Composition

There is substantial statistical information on load composition from various sources [145, 146-148]. Reference [144, 149-150] also attempted to decompose

the aggregate load by measuring the active and reactive power response to a staged voltage drop initiated by OLTC transformer. In this thesis, the statistical data on load composition in [148] is used to decompose the load curve into various load types, as shown in Fig. 4.3, Fig. 4.4 and Fig. 4.5. The most widely found load types in residential load include:

1. Lighting load
2. Storage, direct and top-up heating load
3. Direct domestic hot water (DHW) load and storage DHW load
4. Cold load
5. Wet load
6. Cooking load
7. Consumer electronics (CEs)
8. ICT equipment

It is obvious that most of the storage heating loads and domestic hot water loads are mainly responsible for the electricity demand at night and morning hours due to the off-peak tariffs. Cooking loads greatly increases in the early evening, while lighting, CEs and ICTs dominates in the later evening. The main difference between winter (maximum loading, Fig. 4.3) and summer (minimum loading, Fig. 4.4) is the contribution of heating load, where heating load contributes less in the summer but dominates in the winter.

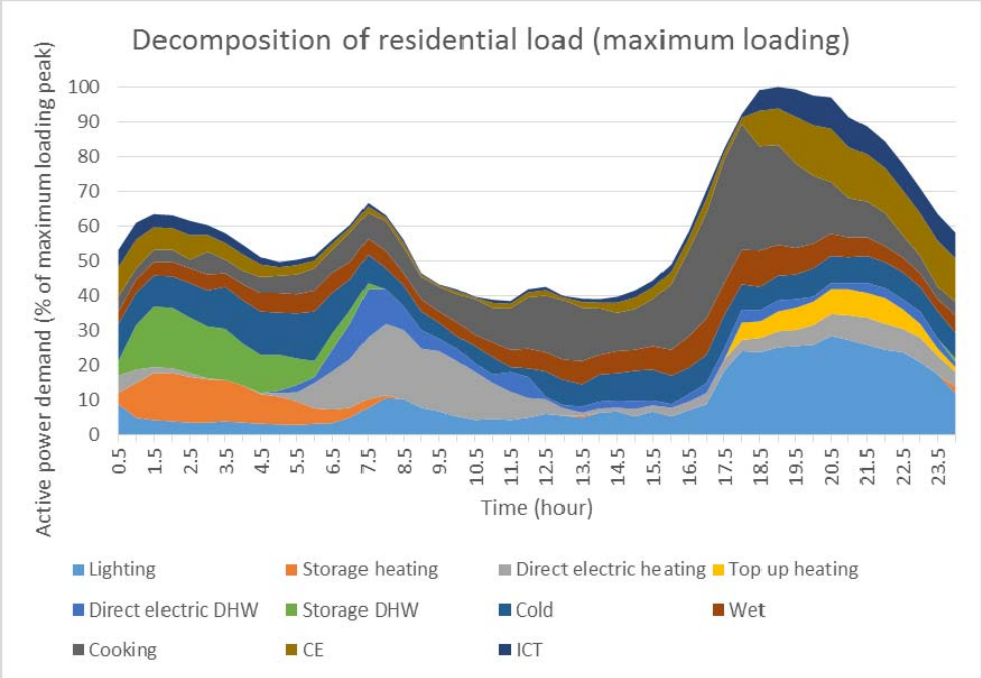

Fig. 4.3 Residential load decomposition into load types for maximum loading condition [148].

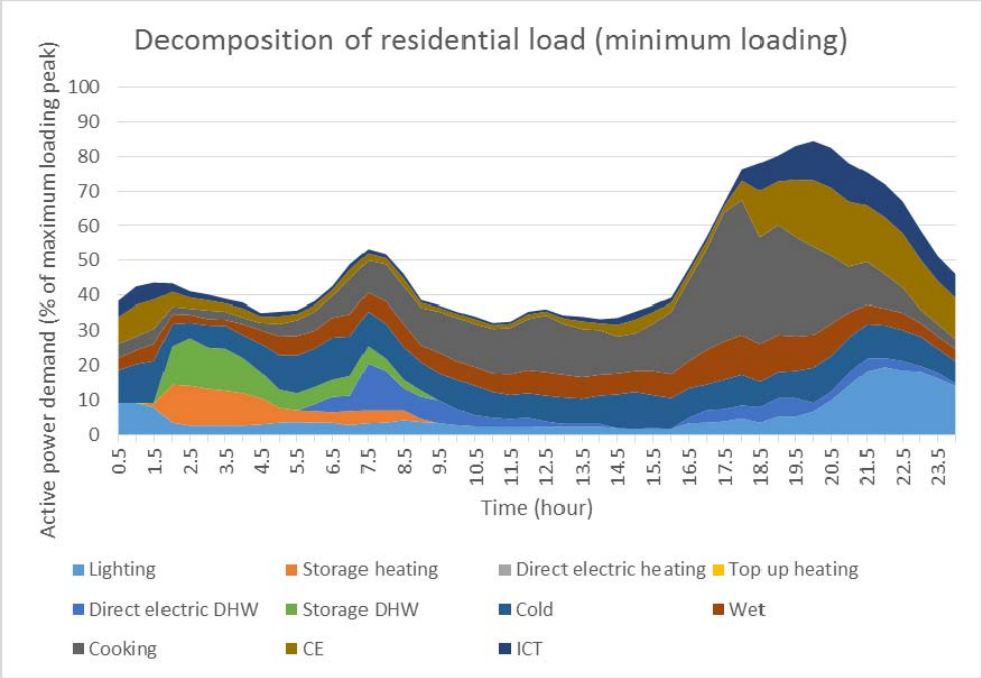

Fig. 4.4 Residential load decomposition into load types for minimum loading condition [148].

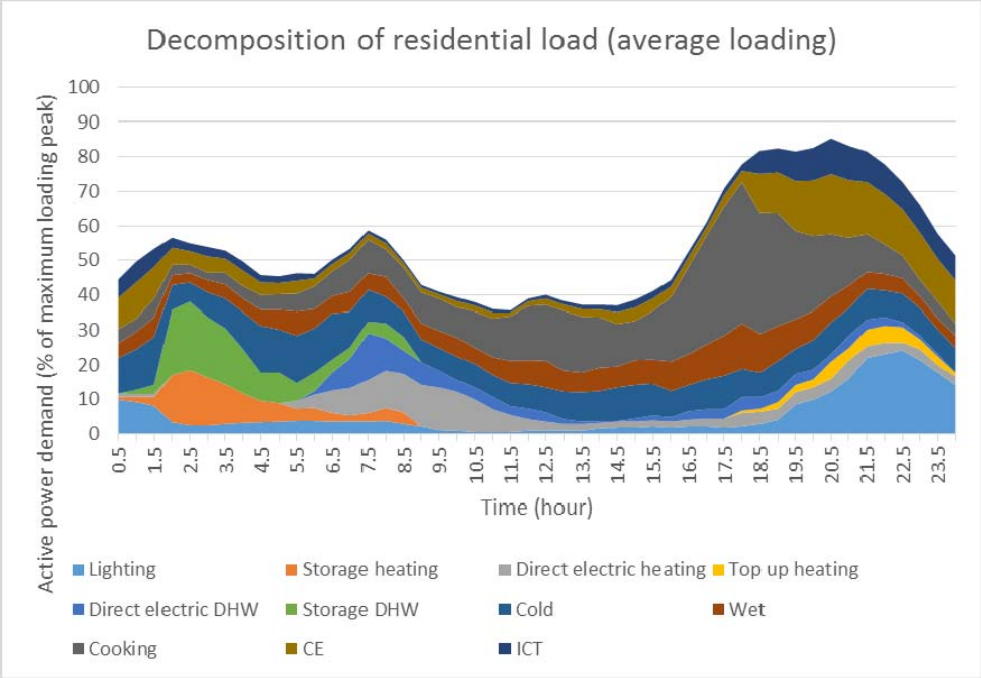

Fig. 4.5 Residential load decomposition into load types for average loading condition [148].

4.3.3 Converting Load Types into Load Categories

According to [48], an intermediate step which converts a large number of load types into a smaller number of general load categories is needed. The load types found in the residential and commercial load sectors can practically be classified into the following general load categories:

1. Power electronics load, it is also called switch-mode power supply load
2. Resistive load
3. Energy efficient lighting load
4. Directly connected motor load
5. Drive-controlled motor load

As shown in Fig. 4.6, due to technology topology variations and harmonic legislation, the above load categories can be further divided into several sub-categories with generic models that will be discussed in next section.

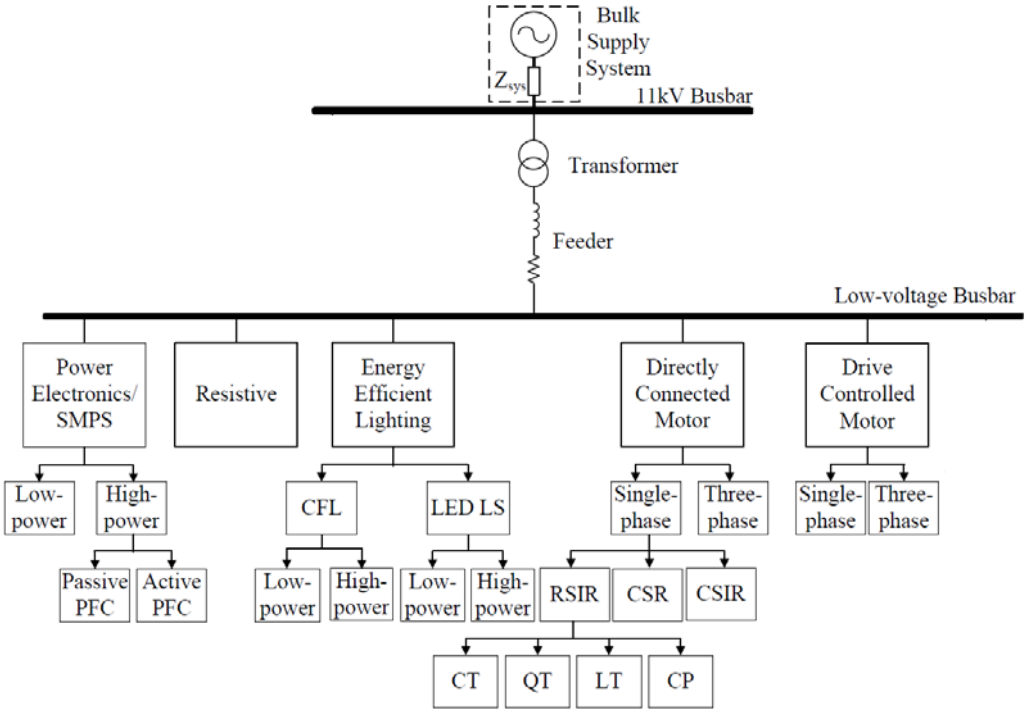

Fig. 4.6 Classification of load categories [48]

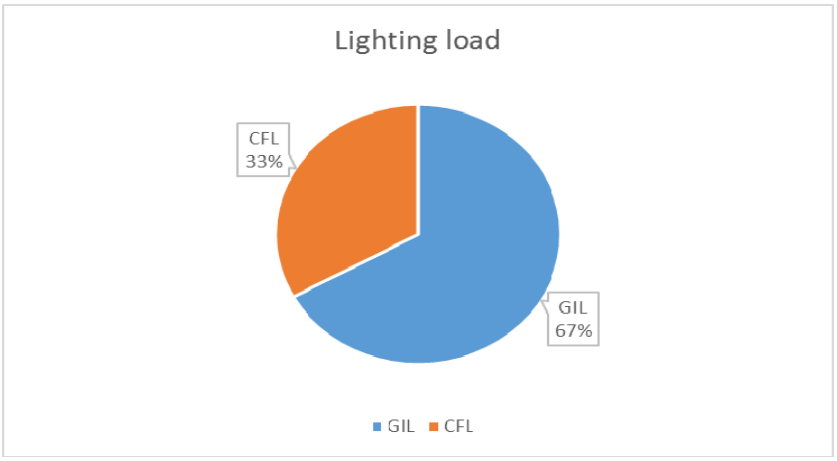

Fig. 4.7 Converting lighting load type demand into load categories with generic models

1. Lighting load

According to the statistics in [48,151-152], compact fluorescent lamps (CFL) and general incandescent lamps (GIL) are the most commonly used lighting

categories in UK domestic lighting demand, with the contribution of 67% and 33%, respectively, as shown in Fig. 4.7.

2. Storage, direct and top-up heating load

   The main operation principle of space heating load is a resistive heating element which heats the surrounding air. This entire load type demand can be represented by the resistive load category.

3. Direct domestic hot water (DHW) load and storage DHW load

   The main operation principle of water heating load is also a resistive heating element which heats the water. This entire load type demand can also be represented by the resistive load category.

4. Cold load

   Cold load refers to all types of freezers and refrigerators, they typically function by changing the state of refrigerant (i.e. between liquid and gas) via heat exchange, which is accomplished by a compressor and an expansion valve. Driving the compressor consumes electrical power, and it is reasonable to assume that the entire cold load uses single-phase induction motor (SPIM) with resistor start - inductor run (RSIR) and constant torque (CT), since the compressors used in these devices do not need high starting or running torque. A detailed review of motor load models can be found in [48].

5. Wet load

   According to the statistics in [151], wet load consists of tumble-dryers (TD) (31%), washing machines (WM) (30%), dish-washers (DW) (22%) and washer-dryers (WD) (16%). These devices consist of a resistive heating (R) element, a motor and a pump (except the tumble-dryers). Because of the need of high running torque for drum rotation, TD, WD and WM need to use SPIM with capacitor start - capacitor run (CSR), while DW utilizes SPIM with RSIR. Besides, based on the analysis of operating cycle in [48], the motor loads will operate with constant torque, while the pump will commonly present a quadratic torque (QT) load [153]. The load categories

under the wet load include resistive, SPIM RSIR QT, SPIM CSR CT and SPIM CSR QT, and the contribution of each load category to the total wet load demand is depicted in Fig. 4.8.

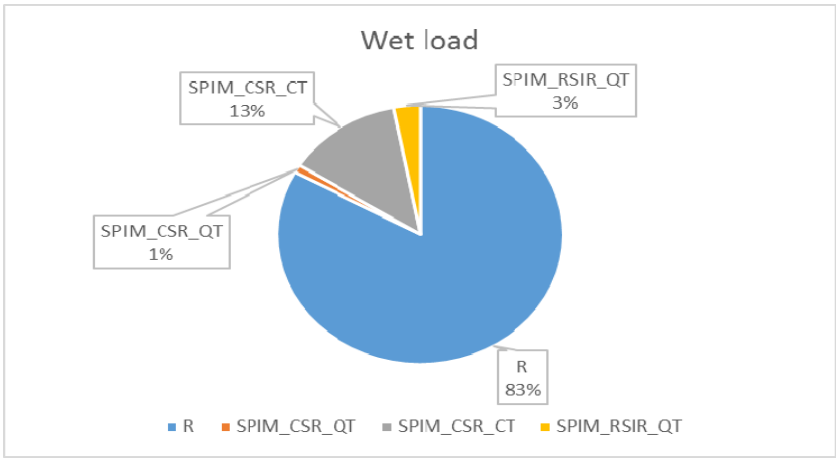

Fig. 4.8 Converting wet load type demand into load categories with generic models

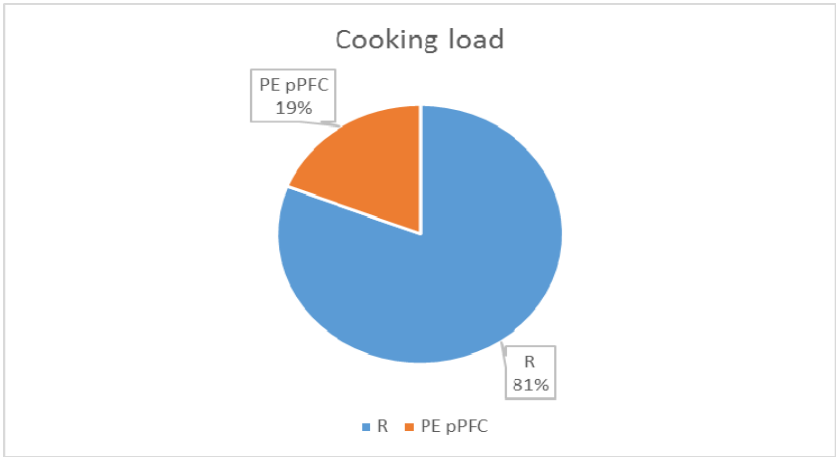

Fig. 4.9 Converting cooking load type demand into load categories with generic models

6. Cooking load

There are generally four types of cooking loads, including kettles (35%), electric oven (24%), electric hob (24%) and microwave (19%), among which,

gas accounts for 57% of cooking energy, while 43% of that is consumed by high rated power electric cooking appliances [48]. They can all be modeled as a resistive heating element, except that microwave should be modeled as power electronics loads with passive power factor correction (PE p-PFC) due to the need of rectification of the supply voltage. The contribution of each load category to the total cooking load demand is depicted in Fig. 4.9

7. Consumer electronics (CEs)

   Consumer electronics loads consist of TVs (41%), set-top boxes (19%), VCR/DVD players (9%) and other variants of power supplies (31%). According to the percentage contribution analysis in [48], and based on the harmonic legislation requirements, CEs can be divided into three sub-categories depending on the corresponding rated power, these include power electronics loads with active power factor correction (PE a-PFC), power electronics loads with no power factor correction (PE no-PFC) and power electronics loads with passive power factor correction (PE p-PFC), the percentage contribution of each category to the CEs load demand is presented in Fig. 4.10.

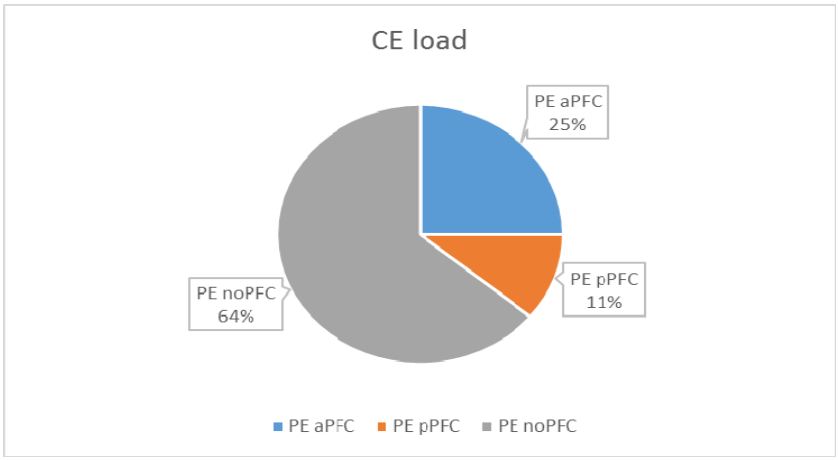

Fig. 4.10 Converting CE load type demand into load categories with generic models

8. ICT equipment

Desktops (52%), monitors (25%), laptops (18%), printers (2%) and multifunction devices (3%) are classified as ICT equipment. Depending on the level of rated power and the circuit topology used for power factor correction, the ICT equipment load types can also be decomposed into the appropriate load categories of power electronics, according to the statistical information from field measurements discussed in [48], which is shown in Fig. 4.11.

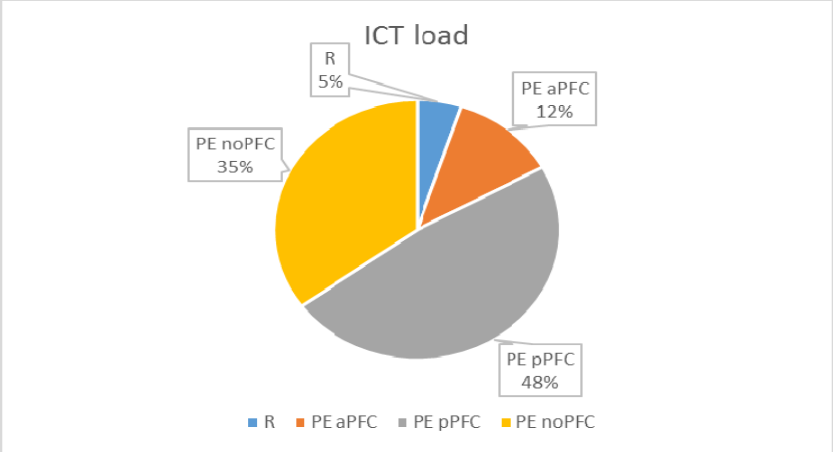

Fig. 4.11 Converting ICT load type demand into load categories with generic models

With the above analysis, the load curves for maximum, minimum and average loading conditions from Fig. 4.2 can then be further decomposed into the main load categories mentioned above, as demonstrated in Fig. 4.12, Fig. 4.13 and Fig. 4.14, respectively. It can be observed that the resistive load accounts for a large portion, as it greatly contributes to the storage space and water heaters during 0:00 – 04:00, morning cooking and electric shower during 06:00 – 09:00 and evening cooking during 16:00 – 20:00. The resistive load accounts for an even larger portion in the maximum loading in winter due to the heating need in the cold weather condition. Besides, the use of entertainment appliances significantly increase the power electronics loads in the evening.

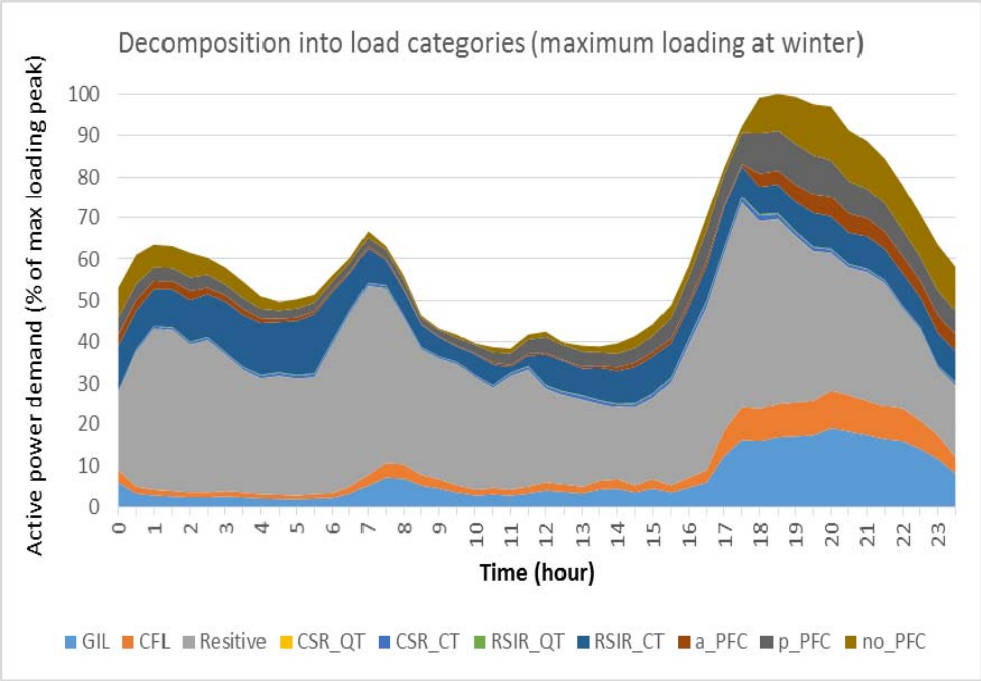

Fig. 4.12 Residential load decomposition into load categories for maximum loading condition

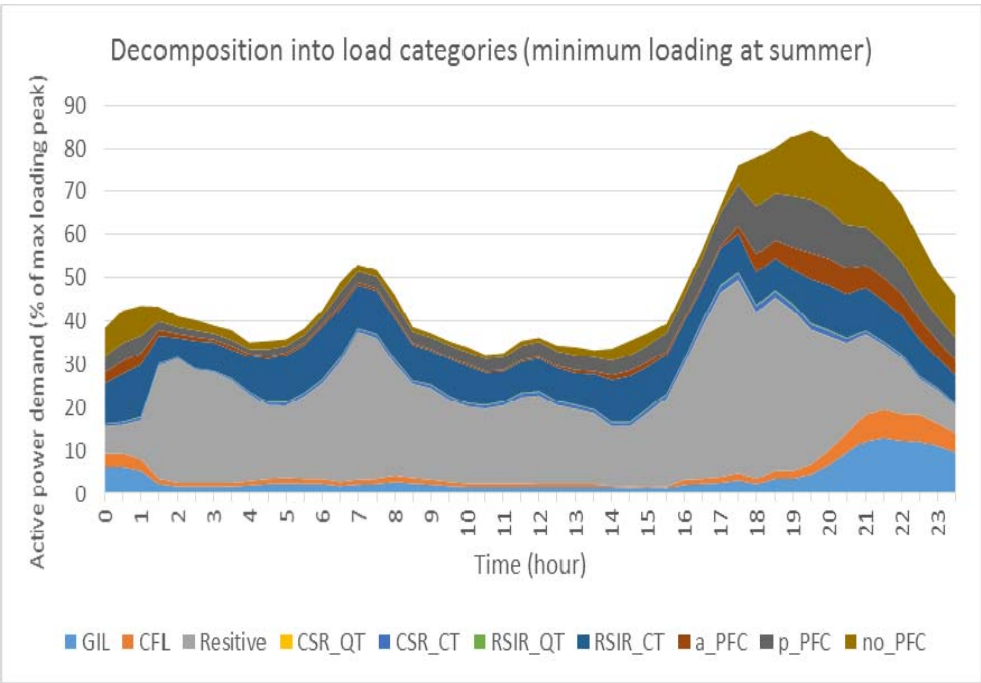

Fig. 4.13 Residential load decomposition into load categories for minimum loading condition

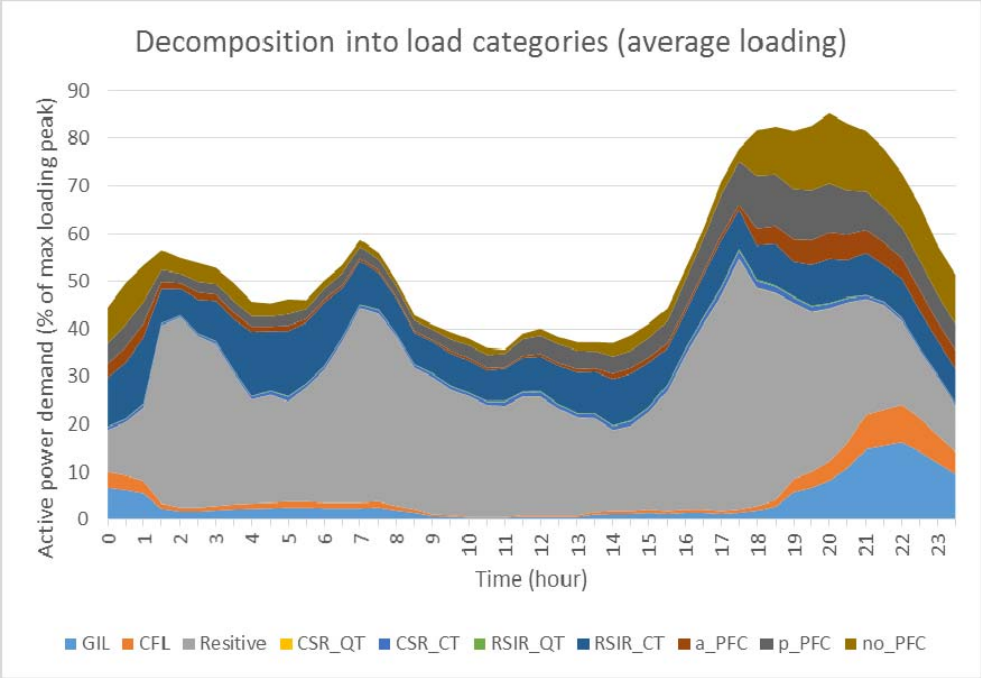

Fig. 4.14 Residential load decomposition into load categories for average loading condition

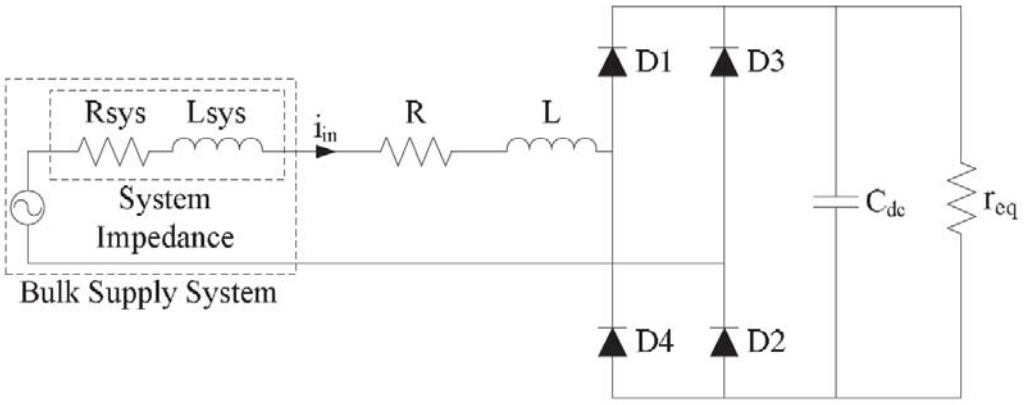

Fig. 4.15 General equivalent-circuit model of nonlinear loads

4.3.4 Generic Models

After the load profile and load types is decomposed into the corresponding main load categories discussed above, generic models of these load categories are needed to build the LV aggregate load models using component-based method. The nonlinear loads including lighting loads and power electronics loads

can be accurately represented by the circuit-based generic load models introduced in [154-155]. The rest of load categories discussed in Section 4.3.3 are connected to the power system directly, without the interface of power electronics, thus drawing continuous input current, which can be modelled using exponential or ZIP analytical models. The generic models of load categories used in this thesis will be presented below, and these are taken from previous research in load modelling [154-158].

Table 4.1. Generic values for equivalent circuit model of CFL [48]

Parameter	Generic value (pu)	Distribution	Range
X_{Cdc}	0.25	Normal	б=3.75
R	2.16e-3	Uniform	min = 1.87e-3, max = 2.38e-3
r_{eq}	$r_{dicharging} = 0.0033v_{dc} + 0.0386$ $r_{charging} = 2.96e^{-6}v_{dc}^2 + 0.0015v_{dc} + 0.183$	-	-

Table 4.2. Generic values for equivalent circuit model of PE no-PFC [48]

Parameter	Generic value (pu)	Distribution	Range
X_{Cdc}	0.036	Normal	б =0.54
X_L	6e-6	Uniform	Min = 3e-6, max = 9e-6
R	0.0017	Uniform	Min = 0.0015, max = 0.0019
r_{eq}	$r_{eq} = \frac{v_{dc}^2}{P_{rated}}$	-	-

Table 4.3. Generic values for equivalent circuit model of PE p-PFC [48]

Parameter	Generic value (pu)	Distribution	Range
X_{Cdc}	0.036	Normal	б = 0.54
X_L	0.037	Normal	б = 0.00186
R	0.0085	Uniform	Min = 0.0077, max = 0.0094
r_{eq}	$r_{eq} = \frac{v_{dc}^2}{P_{rated}}$	-	-

Nonlinear loads

The nonlinear load including CFL lighting loads and power electronics loads can be precisely represented by the general equivalent circuit model which includes an input impedance (R and L), an uncontrolled front-end diode bridge rectifier, an equivalent resistance r_{eq} and a dc link capacitor C_{dc}, as shown in Fig.

4.15. Different load categories will have different values for these components. The typical range of parameters and generic values for nonlinear loads are presented in Table 4.1- Table 4.3, and these values have been validated in field measurements in [21, 48]. Note that the values for PE no-PFC and PE p-PFC are normalized to a base power of 50W and 250W, respectively.

Linear loads

The remaining load categories identified in Section 4.3.3 draw continuous input current and can be modelled using the standard ZIP or exponential form for steady-state analysis. Their load model coefficients are summarized in Table 4.4 as follows:

Table 4.4. Load model coefficients of linear loads at residential sector [138]

Ref.	Load	PF_1	Exponential Model		Polynomial/ZIP Model					
			np	nq	Zp	Ip	Pp	Zq	Iq	Pq
[4]	GIL	1	1.55	-	0.43	0.69	-0.12	-	-	-
[18]	RSIR $SPIM_{CT}$	0.62	0.06	1.92	0.63	-1.2	1.57	1.4	-0.91	0.5
[18]	RSIR $SPIM_{QT}$	0.62	0.3	1.92	0.1	0.1	0.8	1.4	-0.91	0.5
[18]	CSR $SPIM_{CT}$	0.9	0.38	1.68	0.5	-0.62	1.11	1.54	-1.4	0.89
[18]	CSR $SPIM_{QT}$	0.9	0.53	1.68	0.22	0.08	0.69	1.54	-1.4	0.89
	Resistive	1	2	-	1	0	0	-	-	-
[48]	PE a-PFC	1	0	-	-	1	-	-	-	-

4.3.5 Aggregating Generic Models to Form LV Aggregate Load Model

The above component-based generic models can be applied directly to form the aggregate load model as they have been validated to be able to reproduce the aggregate load characteristics of the individual load categories with an acceptable accuracy in [48]. With a given system voltage, the current drawn by each load category can be obtained using the generic models, according to the proportion of each load category in the overall demand, and then the current waveforms of the individual load categories are summed to calculate the aggregate current waveform. Next, by performing a voltage sweep, the active and reactive power

demand can be calculated for each voltage step, and the exponential and ZIP/polynomial load model coefficients as well as the electrical characteristics can be extracted, thus, the voltage dependent aggregate load model can be obtained in the form of exponential and ZIP/polynomial model. The above aggregation process is described by Fig. 4.16, and the time-varying exponential load model coefficients are presented in Fig. 4.17 and Fig. 4.18. Three loading conditions generally have similar variation trends of load model coefficients. For the purpose of analysis, the day can be divided into four periods by defining 0:00-6:00 as night time, 6:00-10:00 as morning time, 10:00-16:00 as daytime and 16:00-0:00 as evening time.

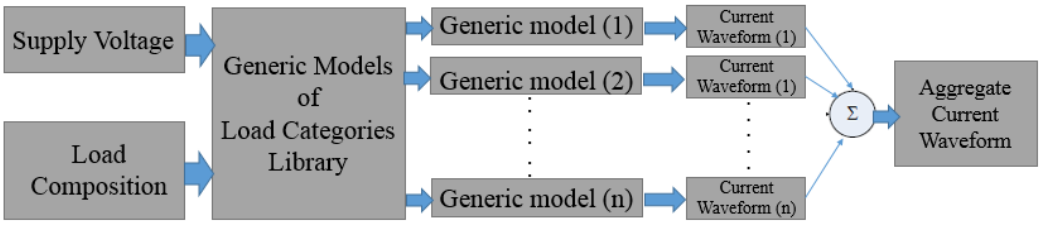

Fig. 4.16 Load Aggregation Process based on component-based method

Because of the storage space heating and water heating load during night time, i.e. off-peak electricity tariffs, the active power coefficient n_p is expected to be large due to the dominant resistive heating load. Although more heating is needed during winter months (i.e. maximum loading), the increased contribution of lighting load due to the longer dark time actually decreases the value of n_p. Another peak value of n_p can be observed, which can be attributed to the resistive cooking electric shower and cooking loads. It can also be seen that n_p is higher for maximum and average loading conditions as a result of increased resistive space heating load. Besides, n_p declines with the decrease of occupants during daytime. During evening period, n_p first rises due to the dominated resistive

cooking loads, and then reduces owing to the increase use of lighting and power electronics loads.

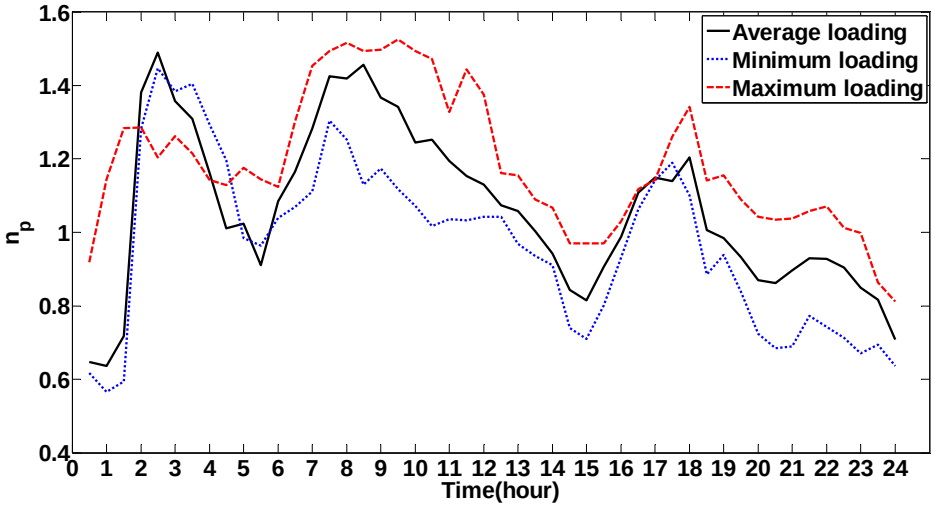

Fig. 4.17 Variation of model coefficient in aggregate exponential LV residential load model for active power

The main difference among different loading conditions is the contribution of space and water heating loads, which have negligible impacts on the reactive power characteristics of load, i.e. n_q, therefore, the variation of n_q among different loading conditions is insignificant. It can be seen that n_q gradually increase as a result of the decreasing contribution of lighting and power electronics loads during the night time. The motor load accounts for the main reactive power demand in residential load sector, which leads the maximum value of n_q for the aggregate load to lying between the reactive power characteristics of motor loads (i.e. $n_q = 1.68 \sim 1.92$). During evening, the increase of lighting and power electronic loads substantially reduces n_q, which is attributed to the fact that the reactive power characteristic of PE p-PFC and CFL is more linear than that of SPIM.

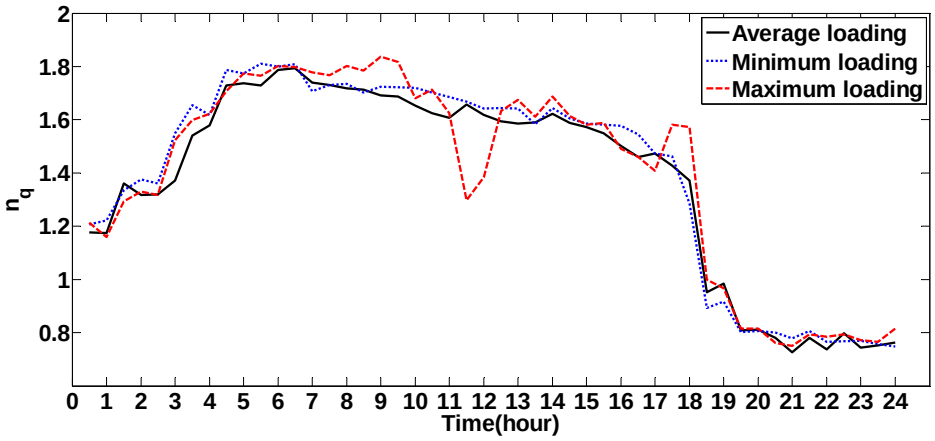

Fig. 4.18 Variation of model coefficient in aggregate exponential LV residential load model for reactive power

4.4 Network Aggregation

In order to allow for power system analysis, the low voltage aggregate load model needs to be connected to the supply network to represent the medium voltage aggregate load model, hence, the low voltage network up to and including secondary distribution transformer need to be accurately modelled and represented. Since the configuration of low voltage network is very complicated, the method proposed in [159] is used to model this as a single equivalent impedance to simplify the transformation of LV load model to the MV load model. The simplified method can be implemented in two steps: 1) Determine the equivalent impedance at each load location in the network by summing up all impedances up to the network location, and it can have multiple customers at the same bus, as shown in (4.1); 2) Calculate the overall network impedance by summing up all equivalent impedances obtained in Step 1.

$$Z_{\text{location}}(i) = \sum_{n=1}^{N} Z_{\text{customer}}(n) \tag{4.1}$$

$$Z_{\text{eq}} = \sum_{i=1}^{I} Z_{\text{location}}(i) \tag{4.2}$$

where $Z_{customer}(n)$ represents the network impedance up to customer n at location i, $Z_{location}(i)$ represents the sum of all customer impedances at location i, I indicates the number of network locations and N represents the number of customers.

The approach utilized to obtain aggregate exponential or polynomial/ZIP load model coefficients is similar to that used in [21], and the key steps can be summarized as follows:

1. Obtain the low voltage load model according to the proportion of residential and commercial load sector, the contribution of each load type and load category to the overall demand and the generic models of load categories, using the method described in Session 4.3.
2. The low voltage load model and the equivalent impedances representing the low voltage network up to and including secondary distribution transformer are connected at the secondary substations.
3. Perform a voltage sweep at the grid supply point (GSP) and calculate the active and reactive power flows at the GSP for each voltage increment.
4. Find the exponential or polynomial/ZIP coefficients using least squares estimation fitting of power flow results.

The final result is a single aggregate exponential or polynomial/ZIP representation at the GSP for each time step.

4.5 Example: Aggregate Commercial Load Model

Commercial load sector accounts for about 35% of the total electricity demand [151], and because of the substantially different load mixes and peak demand period, the characteristics of commercial load sector are considerably different compared with those of residential load sector, for example, the contribution of lighting load and three-phase motors in commercial load sector is much larger, and the majority of demand occurs within the working hours (8:00-

18:00). The same aggregation methodology which is presented in Session 4.3 will be used to develop the aggregate commercial load model, based on the analysis in [48] and the most updated statistics obtained from [151]. The developed aggregate model for commercial load sector could play an important role for power system analysis and improving system reliability performance.

The aggregation process for commercial load sector is the same as the one for residential load sector in Session 4.3, except using different demand curves and different proportions of individual load categories in the overall demand.

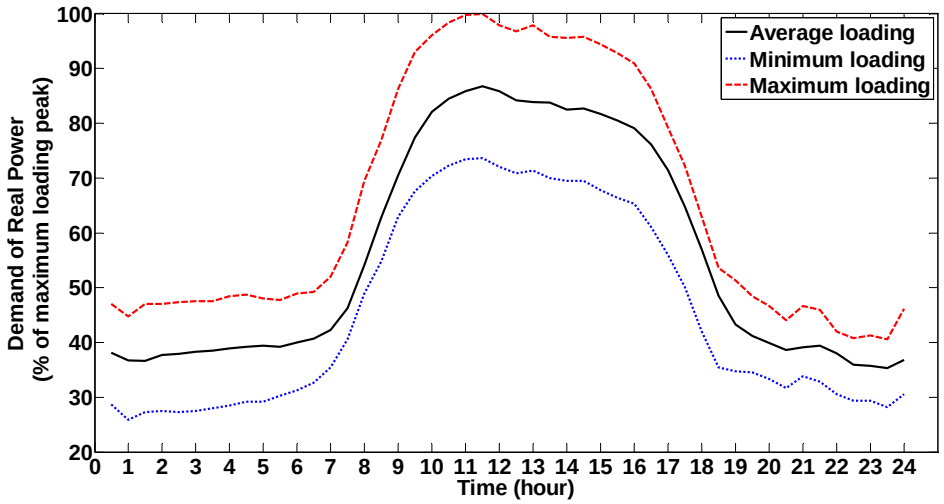

Fig. 4.19 Minimum, average and maximum loading conditions of typical aggregate daily active power demand curves for commercial load.

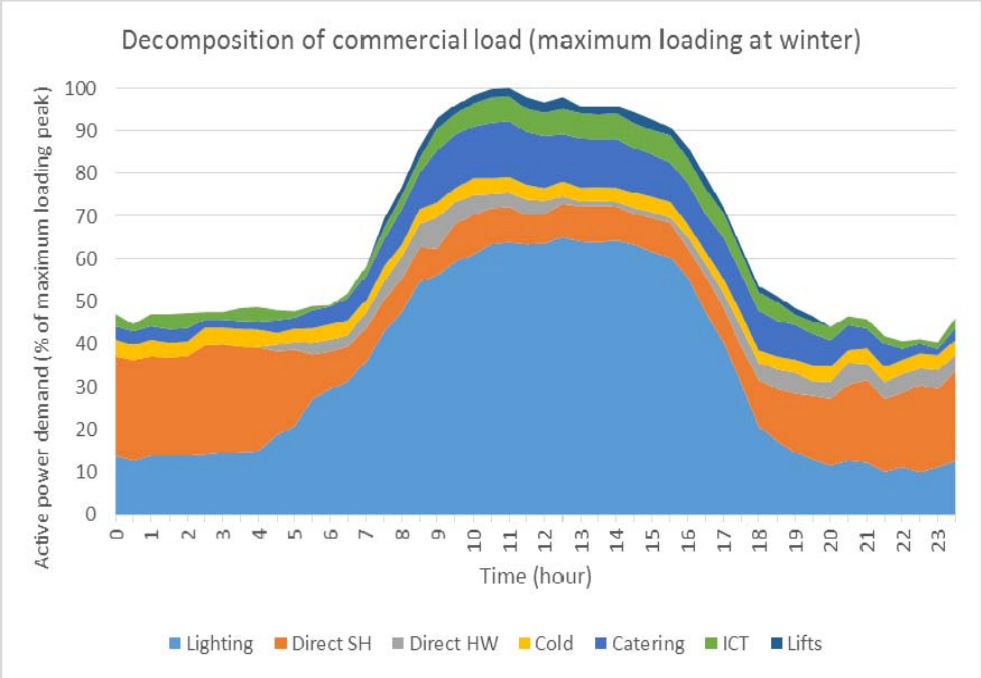

Fig. 4.20 Commercial load decomposition into load types for maximum loading condition

It starts by considering the commercial load curves for different loading conditions including maximum, year average and minimum loading conditions, which are depicted in Fig. 4.19.

Next, the daily and seasonal proportion of different load types in the overall demand for different loading conditions obtained from [148] and [151, 160-161] is shown in Fig. 4.20, Fig. 4.21 and Fig. 4.22. Clearly, the lighting load is mainly responsible for both the overall demand and the peak demand that occurs at the noon during working hours. With respect to the seasonal variations, the heating load greatly contributes to the maximum loading conditions at winter, while the cooling load forms a considerable proportion of the total demand at minimum loading conditions at summer, especially during daytime hours.

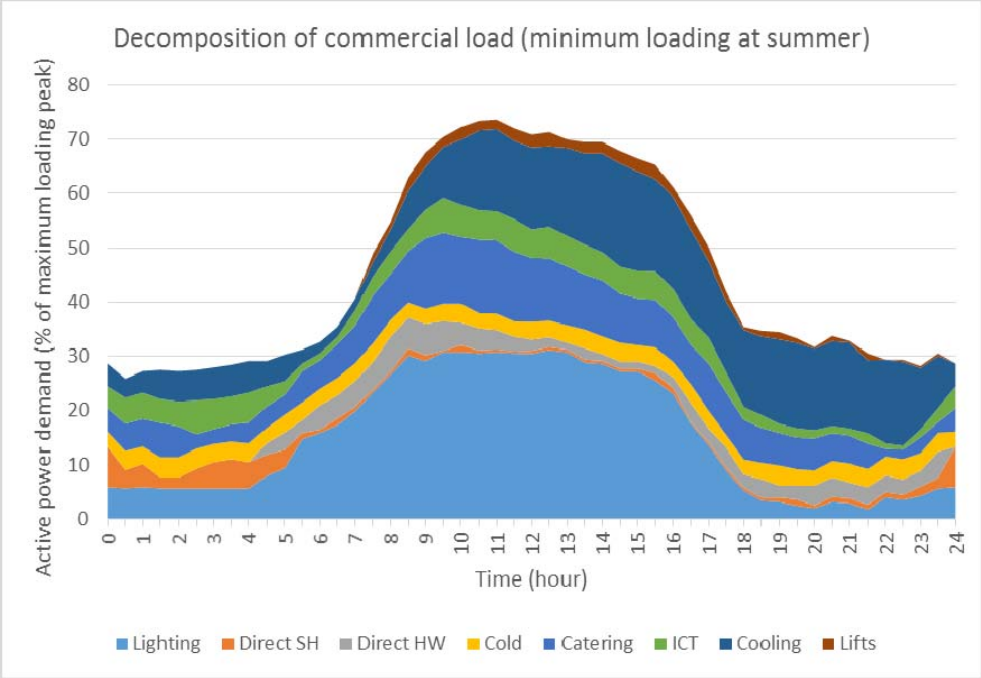

Fig. 4.21 Commercial load decomposition into load types for minimum loading condition

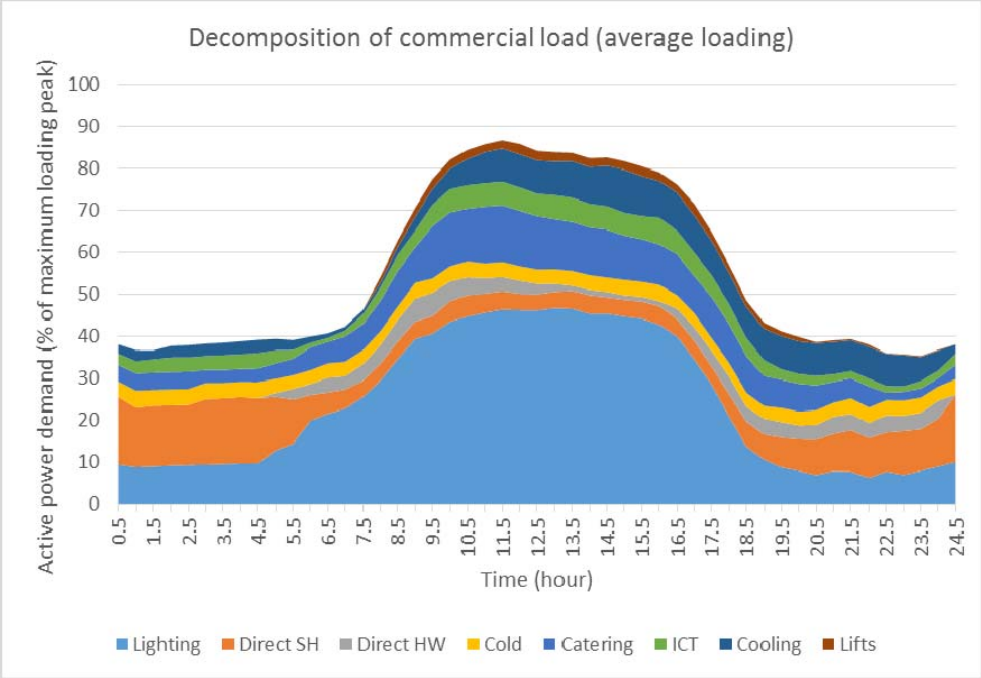

Fig. 4.22 Commercial load decomposition into load types for average loading condition

Then, based on the analysis and assumptions made in [48], this can be further transformed into the various load categories, as presented in Fig. 4.23, Fig. 4.24 and Fig. 4.25, this step will not be reproduced here, but more details can be found in [48].

Finally, the generic models of various load categories are then combined to form the LV aggregate load model for commercial sector, based on the corresponding proportions in the overall demand. The generic models that have not been previously introduced are presented in Table 4.5.

Again, using the same method outlined in Fig. 4.16, the instantaneous current waveform drawn by the LV aggregate commercial load can be obtained by summing the input current waveform of each load categories, based on their corresponding contribution to the total demand. And then, the corresponding exponential and polynomial/ZIP load model coefficients can be obtained by performing a voltage sweep of the supply voltage magnitude. The daily and seasonal variations of exponential load model coefficients are displayed in Fig. 4.26 and Fig. 4.27.

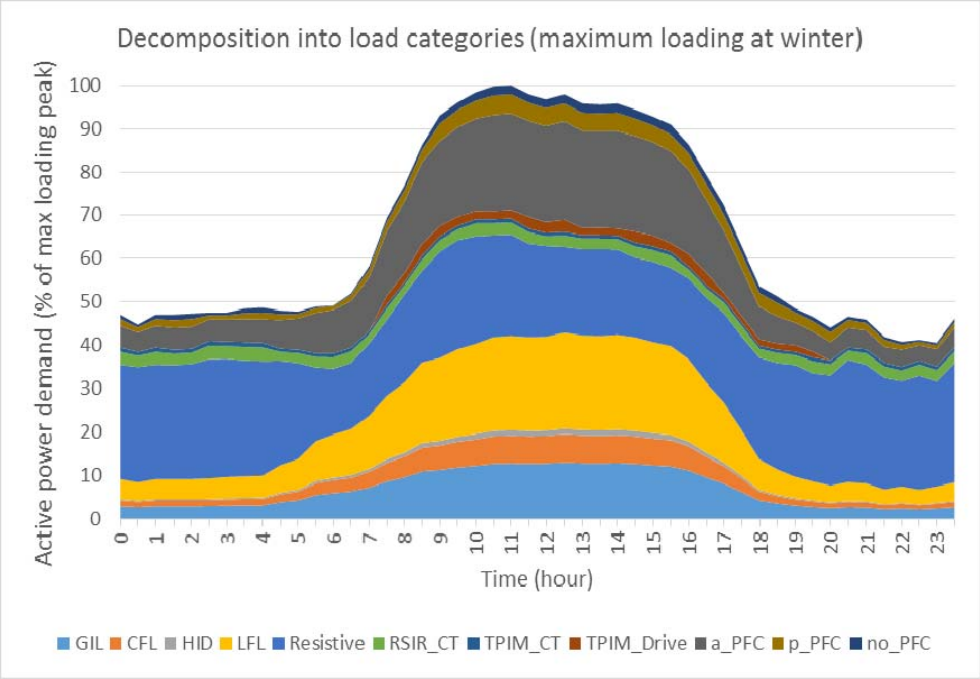

Fig. 4.23 Commercial load decomposition into load categories for maximum loading condition

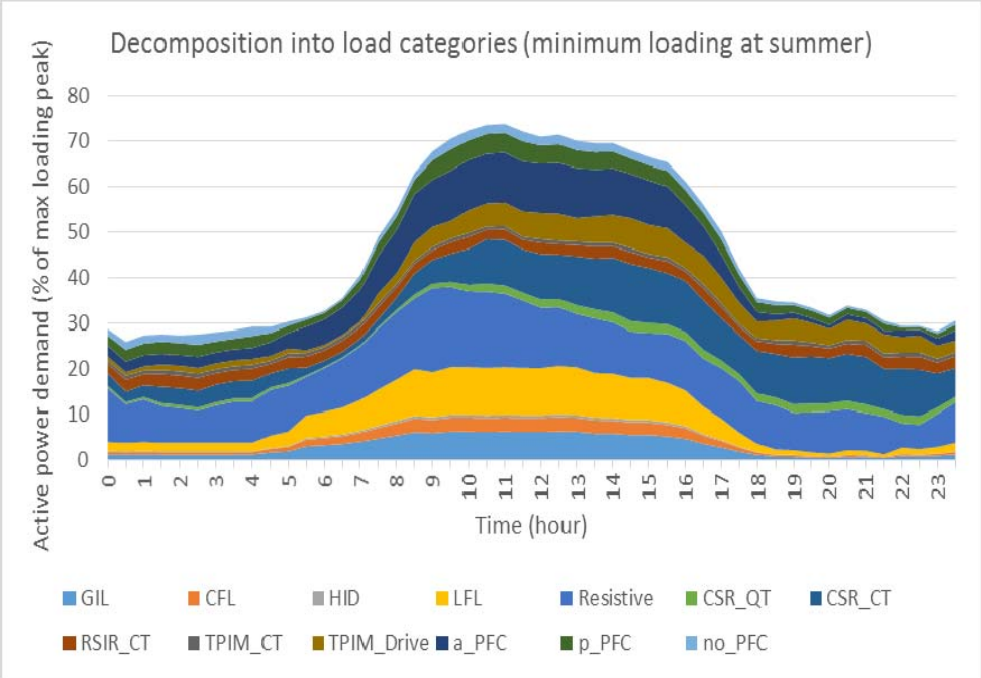

Fig. 4.24 Commercial load decomposition into load categories for minimum loading condition

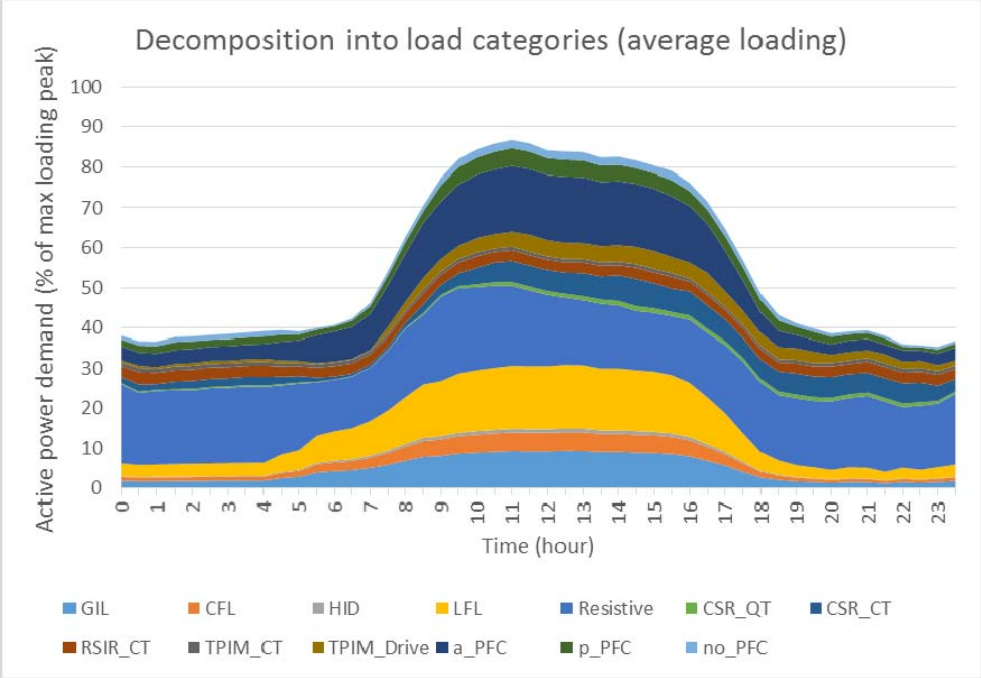

Fig. 4.25 Commercial load decomposition into load categories for average loading condition

Table 4.5 Load model coefficients of linear loads at commercial sector [48]

Ref.	Load	PF_1	Exponential Model		Polynomial/ZIP Model					
			np	nq	Zp	Ip	Pp	Zq	Iq	Pq
[39]	HID	0.96	NA	NA	0.28	0.38	0.34	2.52	-6.51	4.99
[39]	LFL	0.96	NA	NA	0.63	-1.2	1.57	8.16	-12.26	5.14
[18]	3PIM ASD	0.984	0	-0.5	0	0	1	1.22	0.45	-0.67
[18]	3PIM $RSIR_{CT}$	0.83	-0.1	1.44	0.27	-0.63	1.36	1.55	-1.7	1.15

Regarding the characteristics of active power in Fig. 4.27, the exponential coefficients of active power np for three different loading conditions are not significantly different during the working hours (8:00-18:00). The seasonal variations of np during non-working hours observed between winter (maximum loading) and summer (minimum loading) cases can be attributed to different electrical characteristics due to the changes of load mixes, i.e. heating and cooling loads. The values of np are smaller at minimum loading condition because of the larger contribution of motor loads. The increased contribution of heating load at maximum load condition only substantially increases np during non-working hours, the reason why np is not increased during working hours is that it is offset by the higher demand of Linear fluorescent lamp (LFL) lighting loads, which tend towards to constant power and constant current loads.

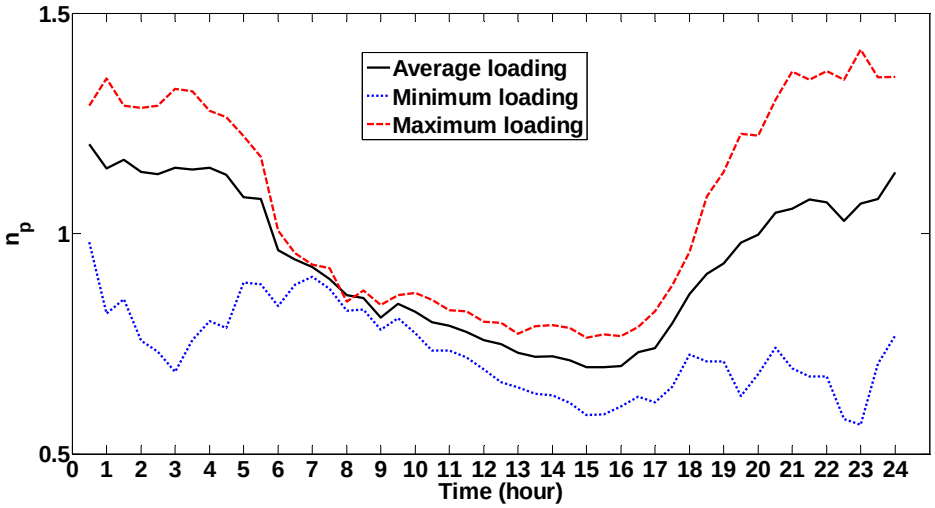

Fig. 4.26 Variation of model coefficient in aggregate exponential LV commercial load model for active power

With respect to the characteristics of reactive power in Fig. 4.28, the exponential coefficients of reactive power nq is expected to be high, due to the LFL and motor loads. It can be observed that the largest value of nq occurs at about 6a.m. for all loading conditions, because the lighting loads suddenly surge at a faster rate than the other reactive power loads around this period. Then the use of the other loads gradually reduces the variations of nq. During the evening, the lighting load becomes dominant within the load mix as the use of other loads reduces, therefore, nq gradually increase again.

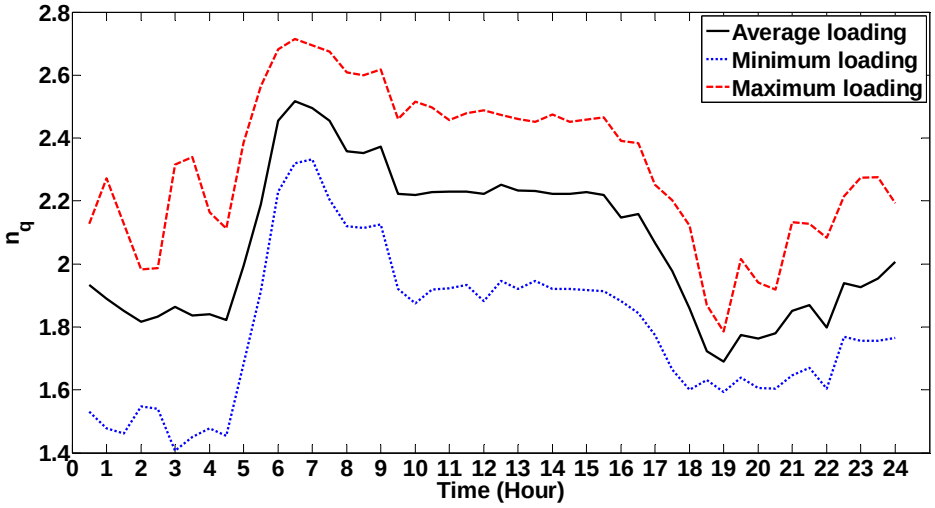

Fig. 4.27 Variation of model coefficient in aggregate exponential LV commercial load model for reactive power

4.6 Chapter Summary

This chapter outlines the aggregation methodology for developing the time-varying LV load models and representing them at the MV network, considering the temporal variations in load mixes. Both residential and commercial loads at maximum, minimum and average loading conditions are used as illustration examples. Compared with the majority of steady-state load models currently applied in the power system analysis in the literature, the most significant improvement is that the resulting models include short-term temporal variations

in load characteristics due to the consideration of time-varying load mixes, which is particularly important for the analysis of various DSM scenarios as it enables the accurate identification of the portion of DMLs in the aggregate load at any time at various locations, as long as the information of load composition is available, which can be easily obtained from the modern smart meters. The developed load models can then be aggregated with the interconnecting medium-voltage (MV) and low-voltage (LV) networks for a wide range of applications in power system analysis.

Chapter 5

Applications of Time-varying Aggregate Load Models in Active Distribution Systems

5.1 Modelling of Demand Side Management

Demand side management programs have been implemented in power system for several decades, mainly in large industrial customers. Recently, more and more electrical storage heating units used in residential customers are shifted to operate at off-peak tariffs. As the power system operates closer and closer to the operational limits, more advanced DSM is expected to be implemented to assist in improving supply-demand balancing and managing network contingencies, which is an important feature of future "smart grid".

The general term 'DSM' refers to various techniques that actively control the electricity demand via particular direct interventions or indirect incentives aiming at adjusting customers' behavior and electricity demand curves, in order to improve network performance and defer the investments in the transmission and distribution systems.

The advances in information and communication technologies could be exploited to increase the participation of residential and commercial customers in offering network support through DSM programs. Nevertheless, most of residential and commercial loads are deeply embedded and highly distributed within the LV distribution networks, large groups of customers need to be aggregated and coordinated to achieve a certain volume of demand in order to significantly contribute to network support. For this purpose, the bottom-up load modelling approach introduced in Chapter 4 can be valuable in building precise load models for various DSM programs, thus, the influences of any devised DSM

programs on system performance can be simulated for assessment before the DSM programs are implemented onto the real power systems.

5.1.1 Description of Devised DSM Scenarios

The potential and availability of loads for DSM load deferral/shifting is related to the operating characteristics of individual loads and customers' behaviors. For example, for residential loads, some are not suitable for DSM, even for a very short term, because of their function and role, such as TVs, PCs, cooking appliances, lighting, etc. The rest of loads in residential sector that are normally appropriate for load deferral/shifting include heating load (already shifted to off-peak tariffs), cold load (only short-term deferral) and wet load. As mentioned in Section 4.3.3, wet loads mainly include washing machine, tumble dryer, dishwasher and washer-dryer, and they normally complete the operating cycle within 1-3 hours, so consumers generally do not want to use them instantly or have immediate access. Besides, most of wet loads have a timer that allows the customers to choose the start or finish time of the operation. Therefore, wet load is regarded as one of the perfect candidates in residential sector to participate in DSM. By controlling wet load, this section illustrates the potential effects of DSM actions related to wet load on the load models and the power grid. The methodology used in the analysis certainly applies to other load types.

To demonstrate how the devised DSM scenarios can be accurately modelled and integrated into the aggregate load model, two DSM scenarios involving wet loads, namely DSM1 and DSM2, are considered. The impacts of DSM and the corresponding changes in the aggregate demand will also be analyzed using the following three cases:

1. The yearly average loading condition presented in Fig. 5.1 will be considered as the base case for comparison purpose, which is actually the same as the Fig. 4.5 of Section 4.3.2. The peak demand occurs at about 20:30, and the CE, ICT, cooking and lighting contribute the biggest

proportion, but these load types are not suitable for DSM because of consumer behavior.

2. DSM1: 50% of wet load is deferred from the period 17:00-21:00 (peak loading period) to the period of 21:00-1:00, the corresponding load decomposition for this scenario is shown in Fig. 5.2, and the changes of wet load labeled as 'brown' color is obvious compared with base case scenario in Fig. 5.1. Note that the DSM portion of the load is just delayed by a four-hour block.
3. DSM2: 50% of wet load is shifted from the period 17:00-21:00 (peak loading period) to late night hours (2:00-6:00), as shown in Fig. 5.3.

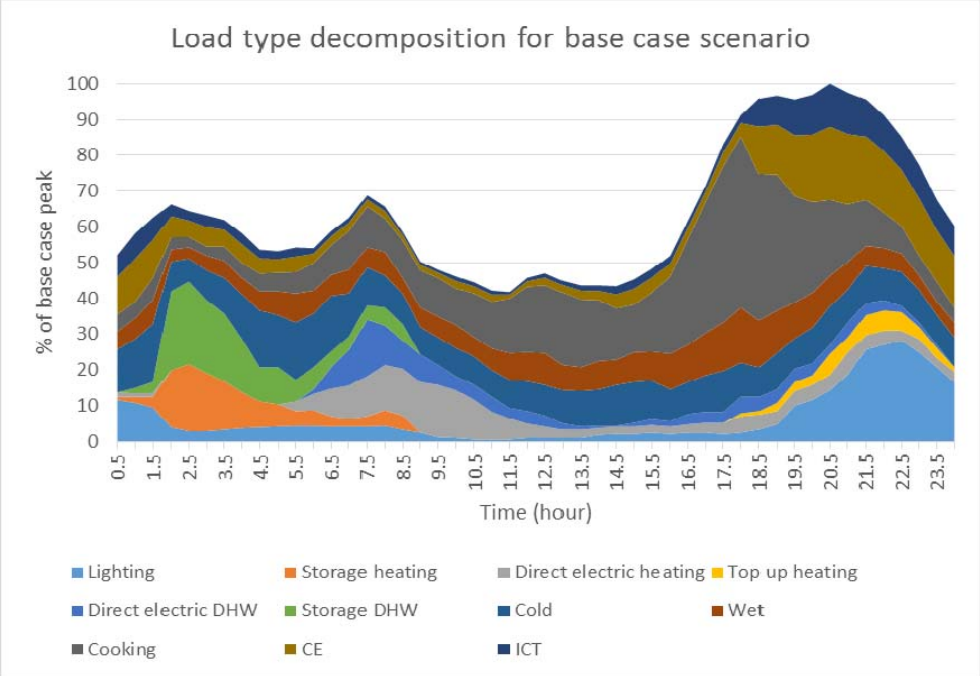

Fig. 5.1 Load type decomposition for base case scenario

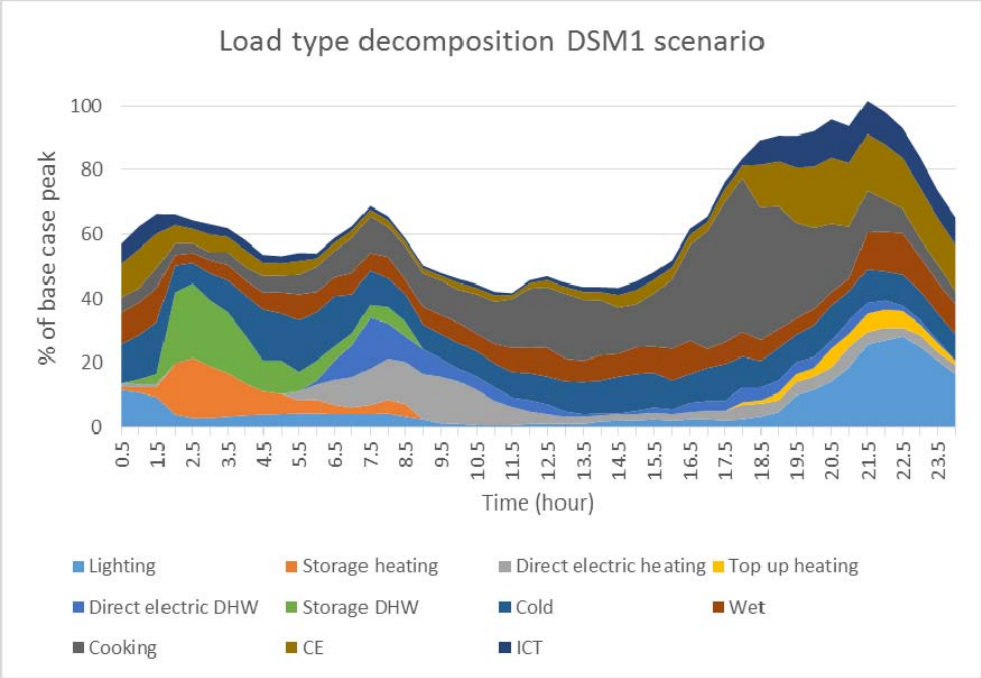

Fig. 5.2 Load type decomposition for DSM1 scenario

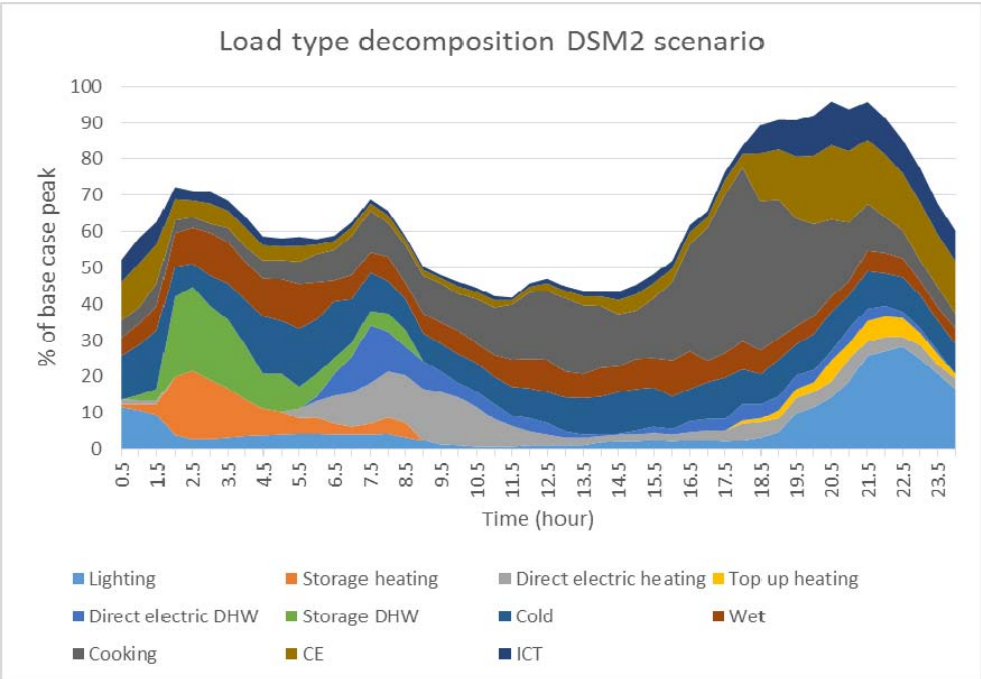

Fig. 5.3 Load type decomposition for DSM2 scenario

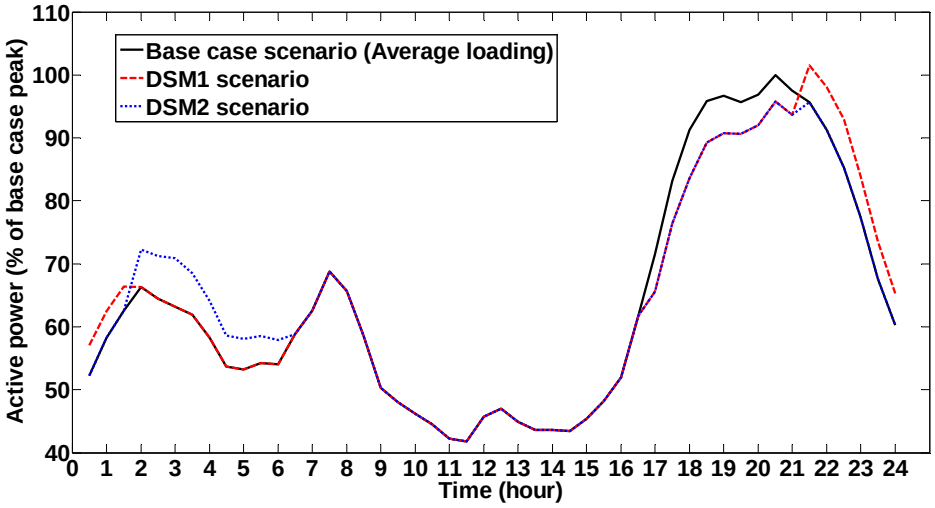

Fig. 5.4 Impacts of considered DSM schemes on active power load curves

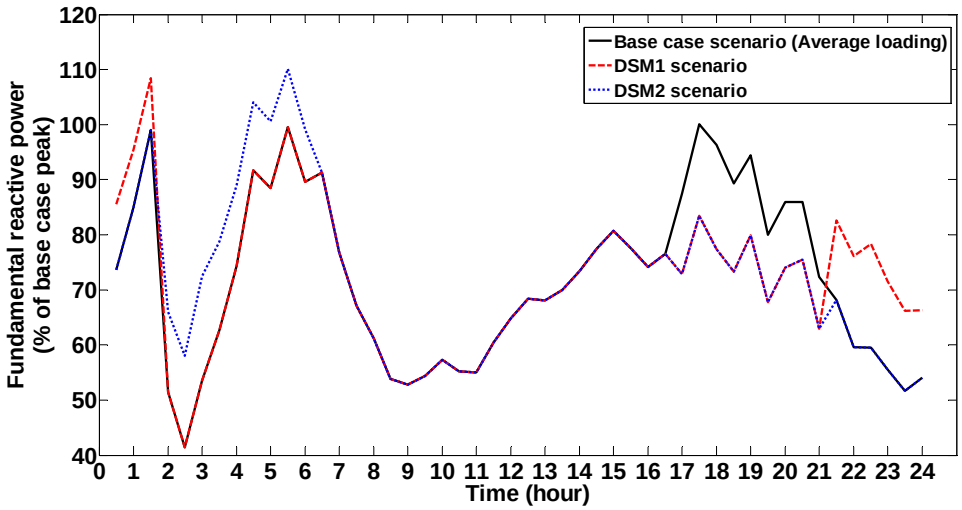

Fig. 5.5 Impacts of considered DSM schemes on reactive power load curves

5.1.2 Impacts of DSM on LV Aggregation Load Model

As depicted in Fig. 5.4, the implementation of two DSM scenarios results in a substantial reduction in active power demand during the period from 17:00 to 21:00. And a significant increase is observed when the wet loads are reconnected at 21:00 for DSM1 and 2:00 for DSM2, respectively. The peak demand, however, is not reduced by DSM1 scenario (it actually increases slightly), it is only shifted

to about 21:30 for the reason that the peak demand is spread over several hours and the demand has not significantly declined when the disconnected wet load in DSM1 is reconnected. On the contrary, DSM2 successfully cuts the peak demand by shifting a portion to late night.

Wet load contains a directly-connected single-phase induction motor for the mechanical rotation process, which consumes reactive power during operation. The displacement power factor (DPF) of wet load depends on the motor type. According to [20], about 80% of wet loads use “capacitor run” single-phase induction motor with high DPF (about 0.9). Nevertheless, the rest of 20% without run capacitors have considerably lower DPF (about 0.62), which significantly contributes to the reactive power demand of the aggregate load. It is acknowledged in the power industry that modelling the aggregate demand of reactive power is difficult, but it becomes increasingly important in the low-voltage distribution network, due to the increased number of DGs and DSM programs. As the aggregate load model introduced in Chapter 4 is able to retain all relevant electrical characteristics since the aggregate current waveform is available during the load aggregation process, the fundamental reactive power demand can be calculated for these three cases, as presented in Fig. 5.5. A substantial drop in reactive power demand can be observed when DSM is implemented with a subsequent rise in reactive power demand when the disconnected wet load is reconnected at 21:00 and 2:00, respectively.

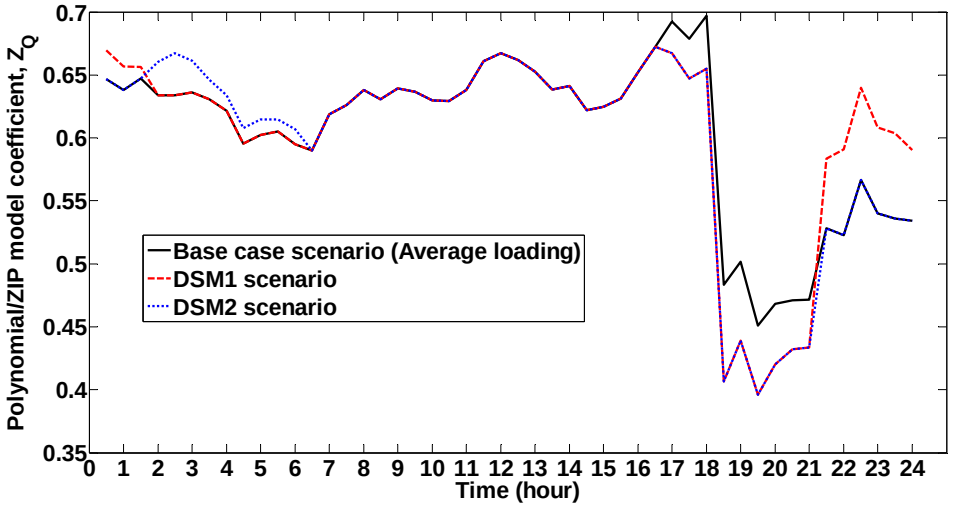

Fig. 5.6 Effects of considered DSM scenarios on Z_Q of aggregate load model

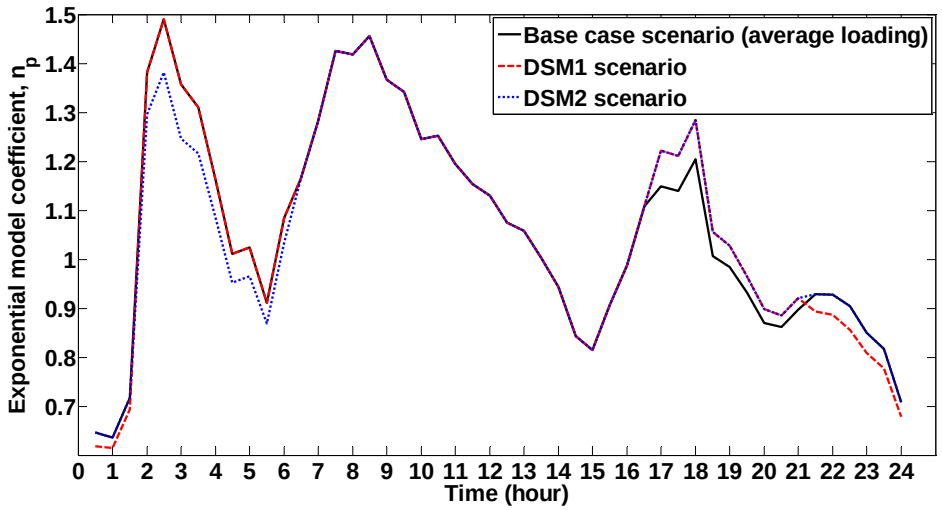

Fig. 5.7 Effects of considered DSM scenarios on n_p of aggregate load model

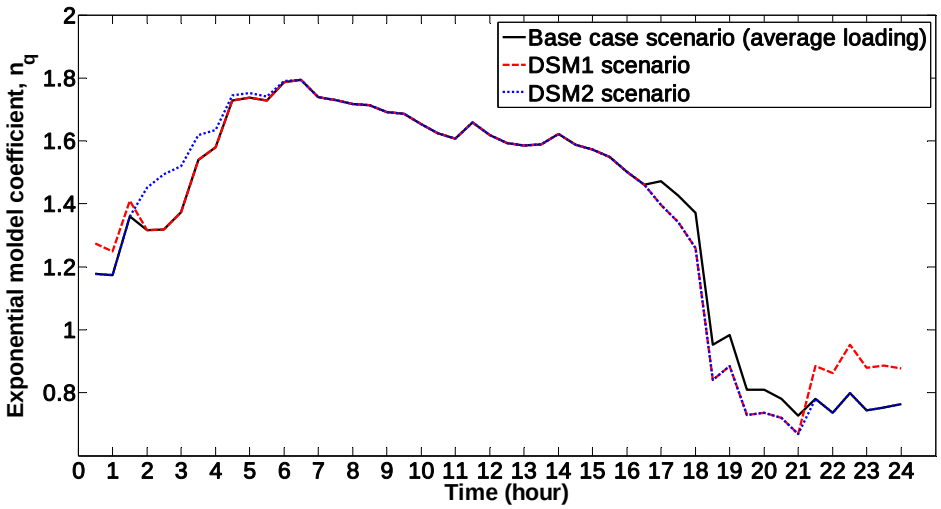

Fig. 5.8 Effects of considered DSM scenarios on n_q of aggregate load model

Fig. 5.6, Fig. 5.7 and Fig. 5.8 further shows that, the changes of load mix due to implementation of DSM scenarios will also affect the model coefficients of aggregate load model, which is often ignored for simplicity in the literature, which is, however, unacceptable for low voltage system analysis. The polynomial/ZIP model coefficients Z_Q for these three cases are depicted in Fig. 5.6. It can be observed that Z_Q decreases as soon as the DSM is initiated at 17:00, which is attributed to the fact that the percentage contribution of other load categories (with lower values of Z_Q than the motor load) increases, while Z_Q rises when the disconnected wet load is reconnected at 21:00 and 2:00, respectively. Note that the large drop of Z_Q at 18:00 is not caused by the devised DSM scenarios, but results from the increased percentage contribution from SMPS load which has a very low value of Z_Q. The above observations and justifications are further confirmed by the variations of exponential load model coefficients n_p and n_q which are presented in Fig. 5.7 and Fig. 5.8.

5.1.3 Impacts of Devised DSM Scenarios on Power Flow

In Section 5.1.2, the variations of the coefficients for polynomial and exponential load models due to DSM implementation are presented and

discussed, because polynomial and exponential load models are still the most prevalent representation in power system analysis. However, polynomial and exponential load models may offer only limited information, so it is also important to fully assess the effects of a specific DSM intervention on network performance, which will be illustrated using the modified IEEE-33 nodes network [162] in this session, and the network diagram is displayed in Fig. 5.9. Detailed data of this system can be found in [162]. There are three capacitor banks located at Bus 3, 13 and 28, as labeled in Fig. 5.9, each constantly outputting 1.0 MVar for improving the voltage profiles, especially for the end nodes in the radial system. The transformer with OLTC (ratio is between 0.9 and 1.1, step size is 0.025) is able to regulate the voltages at the secondary side and plays an important role in active voltage control, but in this study, the OLTC setting is just fixed at 1.025 to demonstrate the impacts of DSM implementation on voltage profiles, the coordinated interaction between OLTC and capacitor banks will be analyzed in Section 5.2 in details. The system is modified to include only residential and commercial load, as the focus of this thesis is on the potential for DSM in these two load sectors with the developed load models. It is much harder to develop a general model for the industrial load, since it differs significantly depending on the industry type, therefore the industrial load is ignored in this analysis.

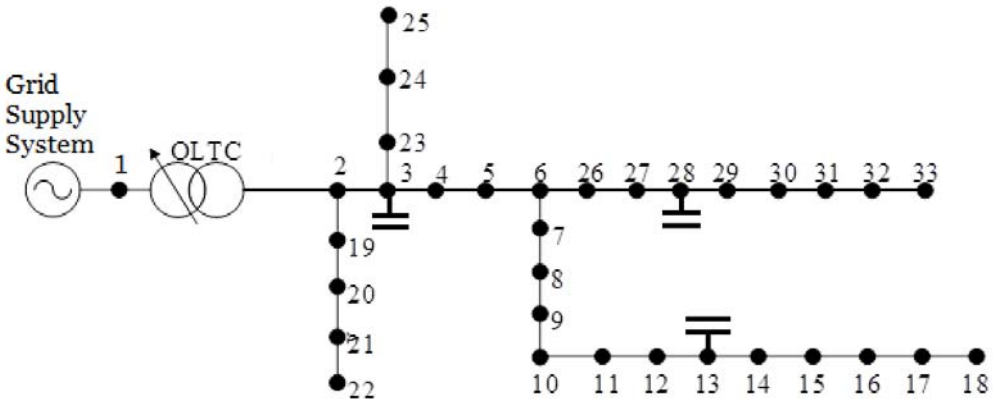

Fig. 5.9 Modified IEEE-33 nodes network

Table 5.1 Node Types for Modified IEEE-33 Nodes network

Load sector	Bus number
Residential load	2,3,4,5,6,7,8,9,12,13,14,15,23,24,25,29,30,31
Commercial load	10,11,16,17,18,19,20,21,22,26,27,28,32,33

The 24-hours injected active power from the main grid to this network, i.e. the aggregate active power demand at Bus 1, is obtained from power flow analysis and displayed in Fig. 5.10, which equals to the total load demand plus the network losses. A 4.3% decline of peak active power demand is observed when DSM1 is applied, while a 5.7% decrease of peak active power demand is recorded when DSM2 is implemented. It is also visible in both DSM scenarios that reconnecting the DSM load leads to an increase in active power demand.

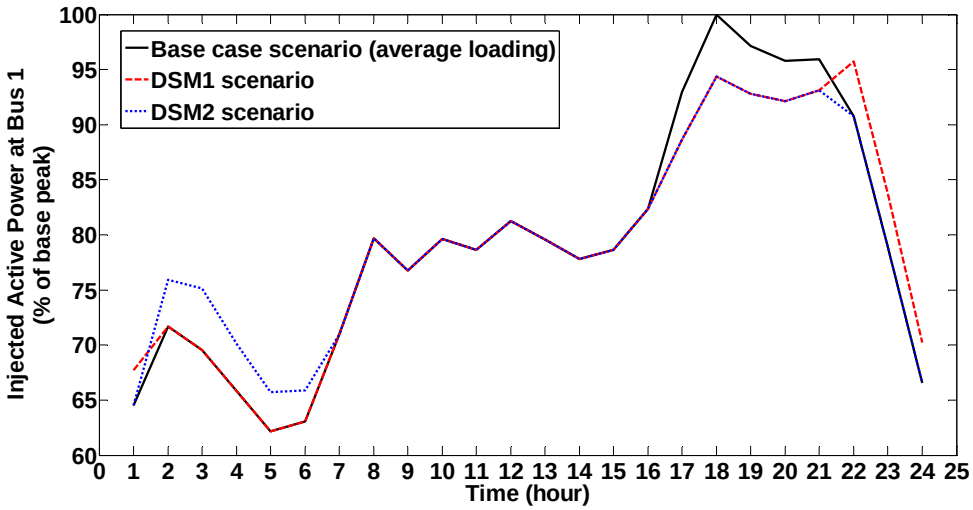

Fig. 5.10 Injected active power from the main grid

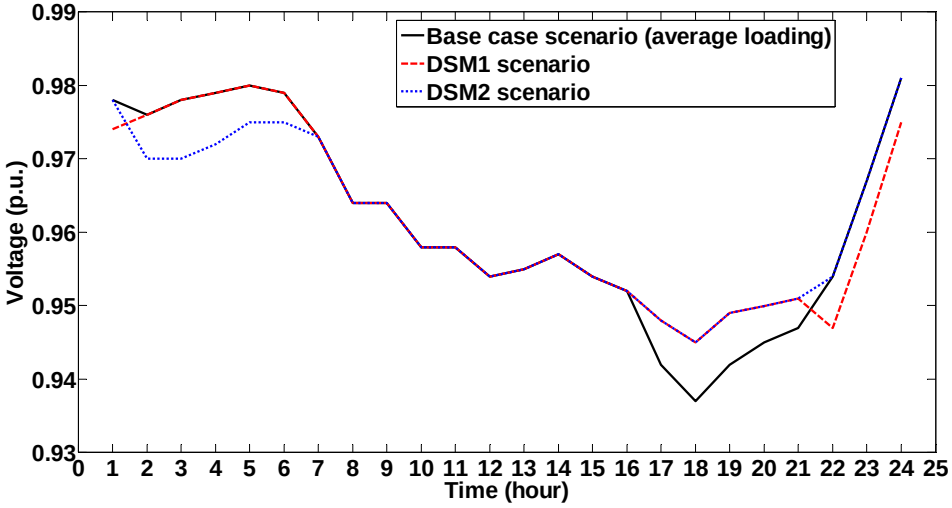

Fig. 5.11 Voltage Profile at Bus 18

The daily change of voltage profile for Bus 18 is obtained from power flow analysis and is presented in Fig. 5.11. Bus 18 is the furthest node in the network, and is expected to have the lowest voltage profile among the network. The function of voltage control in the network is basically disable since the OLTC setting and outputs of capacitor banks are constant, which is not realistic in real situation, but the purpose here is only to clearly observe the effects of implementation of DSM on the voltage profile. It can be observed that, for the base case scenario with the OLTC and capacitor bank setting defined above, the voltage profile actually violates the acceptable voltage ranges for a short time if the constraints is +/- 6%. Disconnecting half of the wet load from 17:00 to 21:00 improves the voltage profile without any violation throughout the day. Reconnecting the DSM portion of wet load at both 21:00 and 2:00 reduces the voltage levels for Bus 18, but the degree of reduction is different due to different load mixes in the aggregate load.

5.2 Conservation Voltage Reduction With Time-varying Exponential Load Models

Voltage var optimization (VVO) is regarded as a secondary control scheme to improve the power quality and voltage profiles in daily operation of distribution system, which is achieved by coordinating the schedules of the statuses/output of switched capacitors and the tap positions of on-load tap changers (OLTCs).

Due to the emergence of the smart distribution system, enhancing energy efficiency by reducing voltage on MV distribution system, which is referred as conservation voltage reduction (CVR), has gained great attention and been proved to be beneficial to the system operation. CVR is implemented to lower the customer's peak/total demand to conserve more energy by maintain the voltages at a lower level in the acceptable range, and it can be regarded as a form of demand side management that is always available. CVR can be considered as one of the VVO techniques as they utilize the same devices for volt var control, but the difference between CVR and conventional VVO is that they have different objectives. The objectives of VVO generally consist of the minimization of power loss and voltage deviation across the network, while CVR mainly aims at minimizing the energy demand.

However, as mentioned in Section 2.4, the majority of literature use constant power load model in the VVO analysis, which ignores the fact that load demand is predominantly voltage dependent. Load models play a significant role in power system operation and analysis. It is not realistic to assume the load is insensitive to voltage, and the accuracy of load model, especially the parameters of load model, have significant impacts on the VVO dispatches. In distribution systems, the load-to-voltage sensitivities, which considerably affect the effectiveness of VVO, could differ between different nodes because of the complicated load compositions. Recently, [19] has applied voltage dependent load models to VVO analysis, and the necessary and superiority of the more

realistic, accurate and voltage dependent load model has been demonstrated, but they assume the load coefficients are the same for all bus locations and fixed throughout the day. In addition, the growing penetration of DGs has enforced extra uncertainties and constraints into voltage var control, this has been addressed in the literature [14-18].

Nevertheless, to the best of my knowledge, the effects of geographical and temporal variations of the coefficients in load model and the impacts of DSM on VVO dispatches have never been discussed in the literature. The coefficients of load model are assumed to be time-invariant in [19], but in practice, they should be time-varying as the load composition is varying all the time, especially when DSM is implemented to change the load profiles in order to reduce the peak demand or relieve possible overloading of network components. Although the control of active power is the main focus of most DSM schemes, this inevitably changes the reactive power demand as well because it modifies the load composition. Therefore, the coefficients of load model change as the load compositions vary, the active/reactive demand in turn changes as the model coefficients vary, it is reasonable to predict the time-varying coefficients in load model may affect the dispatch strategies of VVO.

5.2.1 Problem Formulation for CVR

Considering the implementation of CVR in a distribution system, the objective function is to minimize the real power injected into the distribution system from the main grid, which equals to the total active power demand by all loads within the system plus the active power losses on lines and can be expresses as

$$\min_{OLTC_i,\, Q_{Ci}} P_{injected} \tag{5.1}$$

Where

$$P_{injected} = P_{demand} + P_{loss} \tag{5.2}$$

$$P_{demand} = \sum_{i \in \square B} P_{di}(V_i) \tag{5.3}$$

$$P_{loss} = \sum_{i \in \square_B} \sum_{j \in \square_B} \Delta V_{ij}^2 \frac{r_{ij}}{Z_{ij}^2} \tag{5.4}$$

Some equality and inequality constraints are required to ensure the proper operations of all components within the system. The power flow constraints can be represented by the following two equalities:

$$P_i(tap, V, \theta) + P_{gi} - P_{di} = 0 \tag{5.5}$$

$$Q_i(tap, V, \theta) + Q_{Ci} + Q_{gi} - Q_{di} = 0 \tag{5.6}$$

Most of loads in residential and commercial sectors present voltage-dependent behavior. In order to investigate the impacts of geographical and temporal variations of the load model coefficients on VVO dispatches, the exponential load model introduced in Section 2.2 is used. It should be noted that the load model coefficients are time-varying, and the active and reactive demand at each time step can be expressed as:

$$P_{di} = P_{0,i} \left(\frac{V_i}{V_0} \right)^{np,i} \tag{5.7}$$

$$Q_{di} = Q_{0,i} \left(\frac{V_i}{V_0} \right)^{nq,i} \tag{5.8}$$

The inequalities include voltage limits, thermal loading constraints of branch lines and power factor limit at the substation, as presented in (5.9), (5.10) and (5.11), respectively.

$$V_i^{\min} \le V_i \le V_i^{\max} \tag{5.9}$$

$$\left| S_b \right| \le \left| S_b^{\max} \right| \tag{5.10}$$

$$PF_{\min} \le PF_{sys} \le PF_{\max} \tag{5.11}$$

Transformers with voltage regulators and on-load tap changers are able to control the output voltage to vary in steps, depending on the tap positions.

$$OLTC_i = 1 + TP_i \cdot \Delta tap_i \tag{5.12}$$

$$TP_i \in \{TP_i^{\min}, ..., 0, ..., TP_i^{\max}\} \tag{5.13}$$

The switched capacitor banks consist of several modules, and each individual module has a capacity of ΔC_i. Depending on the adjustment position which lies

between zero and the maximum number of CB module, the reactive power injected into the distribution system is represented by

$$Q_{Ci} = NCap_i \cdot \Delta C_i \tag{5.14}$$

$$NCap_i \in \{0,1,2,...,NCap_i^{\max}\} \tag{5.15}$$

TABLE 5.2 Nomenclature for CVR problem formulation

Symbol	Definition
$P_{injected}$	total injected active power into the distribution system
P_{demand}	total active power demand by the loads
P_{loss}	total active power losses on lines
P_{di}	total active power demand at bus *i*
Q_{di}	total reactive power demand at bus *i*
V_i	voltage magnitude at bus *i*
$\square_B$	Set of buses
ΔV_{ij}	Voltage difference between bus *i* and bus *j*
r_{ij}	line resistance between bus *i* and bus *j*
Z_{ij}	line impedance between bus *i* and bus *j*
$P_i(tap,V,\theta)$	active power injected into bus *i*
$Q_i(tap,V,\theta)$	reactive power injected into bus *i*
P_{gi}	active power generation at bus *i*
Q_{gi}	reactive power generation at bus *i*
Q_{Ci}	reactive power injected by capacitors at bus *i*
$P_{0,i}$	active power demand at nominal voltage and frequency at bus *i*
$Q_{0,i}$	reactive power demand at nominal voltage and frequency at bus *i*
V_0	nominal system voltage
np,i	voltage exponents of active power demand at bus *i*
nq,i	voltage exponents of reactive power demand at bus *i*
$V_i^{\min}$	minimum acceptable voltages at each network bus *n*
$V_i^{\max}$	maximum acceptable voltages at each network bus *n*
S_b	apparent power flow through network branch *b*
$S_b^{\max}$	maximum apparent power flow through network branch *b*
$PF_{\max}$	maximum system power factor
$PF_{\min}$	minimum system power factor
PF_{sys}	system power factor
$OLTC_i$	output voltage of OLTC at bus *i*
TP_i	tap position at bus *i*
Δtap_i	voltage step controlled by OLTC at bus *i*
$TP_i^{\min}$	minimum tap position at bus *i*
$TP_i^{\max}$	maximum tap position at bus *i*
$NCap_i$	number of modules of capacitor at bus *i*
ΔC_i	step of reactive power output of capacitor at bus *i*
$NCap_i^{\max}$	maximum number of modules of capacitor at bus *i*

5.2.2 Solution Methodology

Particle swarm optimization (PSO) algorithm [163] is utilized to optimize the proposed CVR problem in this work. PSO is known to be efficient in solving complex optimization problems and has been adopted in various applications in

power system. A swarm of particles that are randomly set with initial positions within a feasible range is simulated to fly through the entire problem space to find the global optimal solution.

In this work, the position information of particles consists of the output voltage of OLTC and reactive output of capacitor banks. The fitness value can be calculated by the objective functions in (5.1). The constraints described in (5.2)-(5.15) will be handled by the penalty function in PSO algorithm. Since there are plenty of literature on PSO, the details of PSO will not be reproduced in this thesis. More details about PSO can be found in [164] and our previous work [163], which has also applied PSO in optimal energy dispatch within a micro-grid.

5.2.3 Test System Setting for Case Study

The proposed CVR that minimizes the injected active power from the grid supply system is examined on the modified IEEE 33-bus radial distribution system as shown in Fig. 5.9 with detailed data of this system in [163], which is the same as the system being used in Section 5.1.3. Switched capacitor banks are installed at Bus 3, Bus 13 and Bus 28 as labeled, each location with three modules of capacitors, each individual module with 0.5 MVar, i.e. the maximum injection of reactive power at each of these three buses is 1.5 MVar with a step size of 0.5 MVar. And it is assumed that power electronic switches are used to control the switching operations of capacitor banks, therefore, the maximum limit of the number of switching is not considered, but this constraint can be easily added in the formulated problem. The tap range and step size of transformer are: $\Delta\, tap_i = 0.025$, $TP_i \in \{-4, -3, \ldots, 0, \ldots, 3, 4\}$, i.e. the output voltage is between 0.9 and 1.1, according to (5.12). The other operational constraints include: $PF_{\max} = 0.99$ lag; $PF_{\min} = 0.96$; Vmax = 1.05 p.u.; and Vmin = 0.95 p.u.

The type of load buses is defined according to Table 5.1. The nominal active and reactive power demand, P_0 and Q_0 in (5.7) and (5.8), for residential and commercial load, are presented in Fig. 5.12 and Fig. 5.13, which is the average loading conditions shown in Chapter 4.

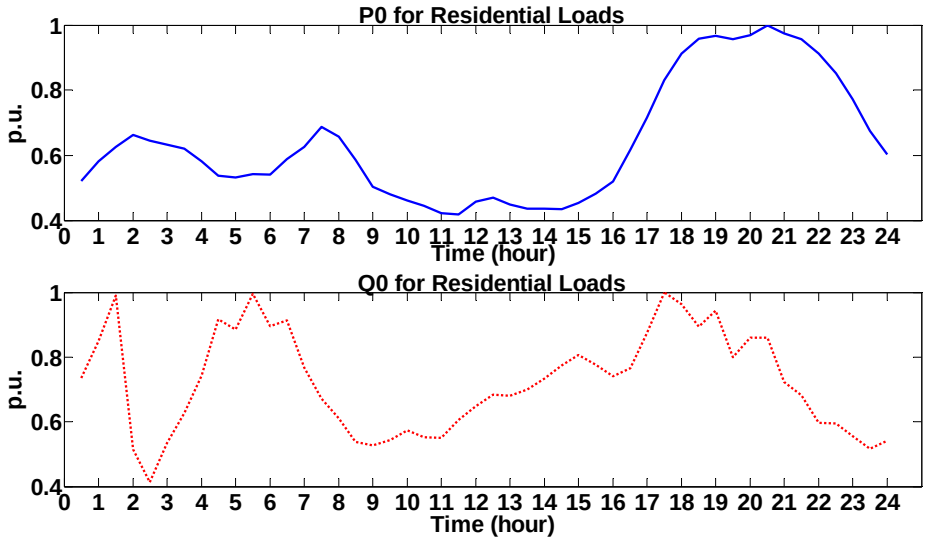

Fig. 5.12 P_0 and Q_0 for residential loads

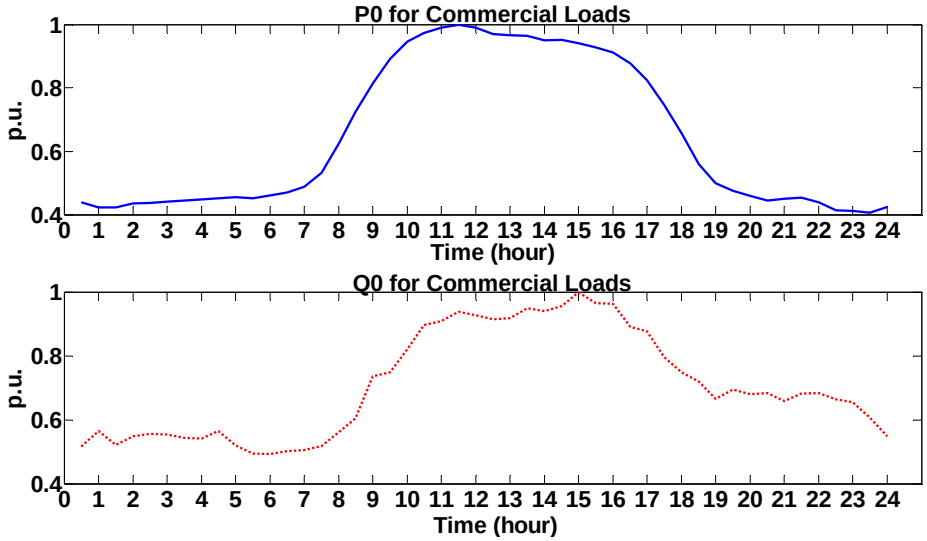

Fig. 5.13 P_0 and Q_0 for commercial loads

5.2.4 Impacts of Time-varying Coefficients on CVR Dispatch

Four types of load model are applied to the above CVR problem to investigate the effects of different load models on the dispatch strategies of CVR, including:

- Load Model 1: Constant power load model, i.e. $n_p = n_q = 0$;
- Load Model 2: Voltage dependent (VD) exponential load model, with $n_p = 1$, $n_q = 2$, time-invariant, fixed for both residential and commercial loads.
- Load Model 3: VD exponential load model introduced in Chapter 4, and the values of n_p and n_q are time-varying and vary with the load mixes, as shown in Fig. 5.14.
- Load Model 4: VD exponential load model, the values of n_p and n_q for residential and commercial loads are the corresponding 24-hours average values calculated from the Model 3 above, i.e. n_p =1.1881, n_q =1.2574 for residential load and n_p =0.9334, n_q =2.065 for commercial load. Both n_p and n_q are time-invariant.

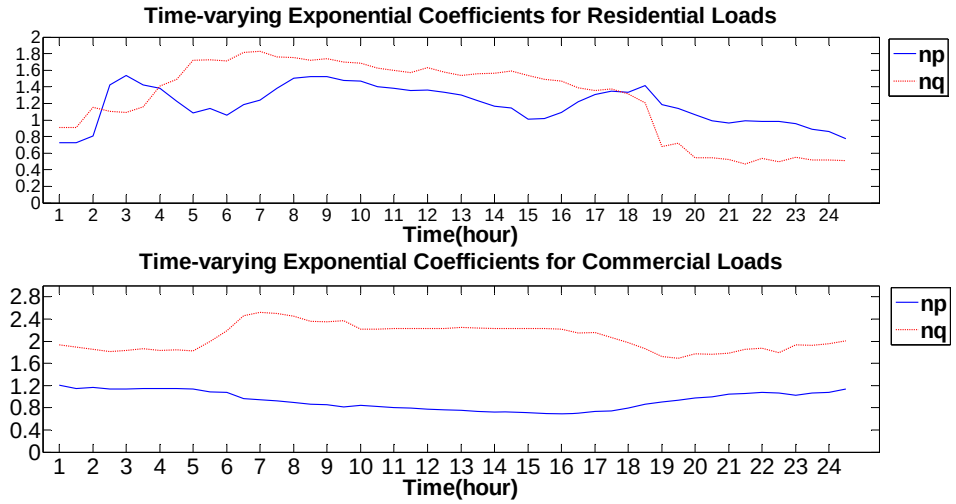

Fig. 5.14 Time-varying exponential coefficients for load models

The CVR problem defined in (5.1)-(5.15) is solved using the four load models as described above. And Fig. 5.15 – Fig. 5.18 show the daily optimal dispatch of OLTC and switch capacitors. It can be observed that the optimized values of these decision variables in CVR dispatch vary quite significantly with different adopted load models.

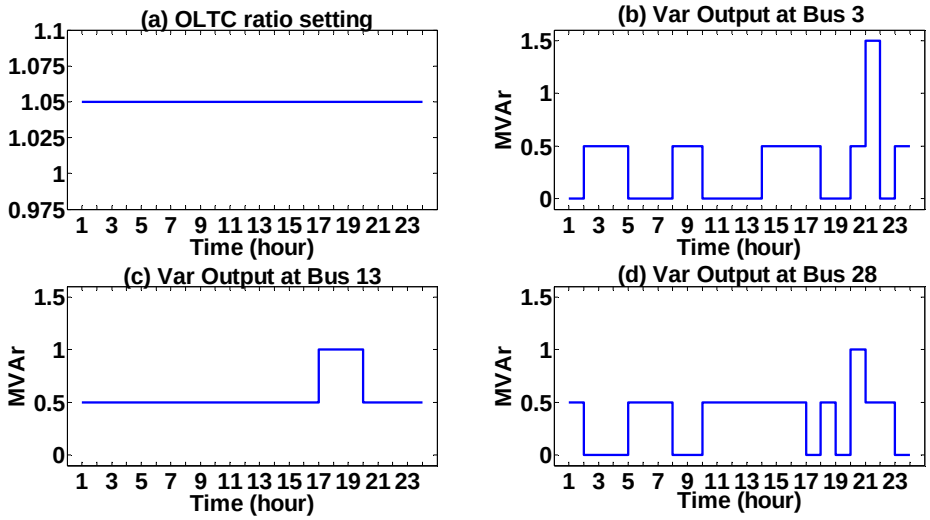

Fig. 5.15 CVR Dispatch results of using Load Model 1

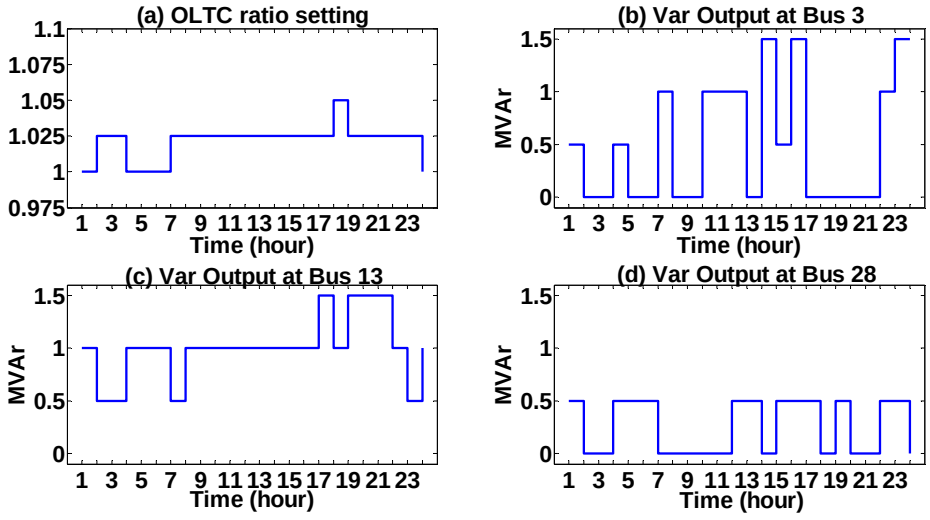

Fig. 5.16 CVR Dispatch results of using Load Model 2

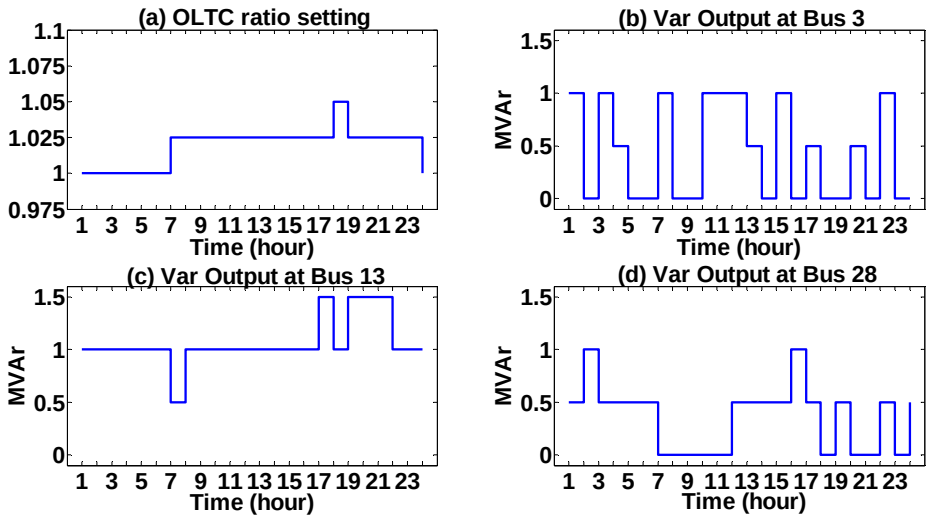

Fig. 5.17 CVR Dispatch results of using Load Model 3

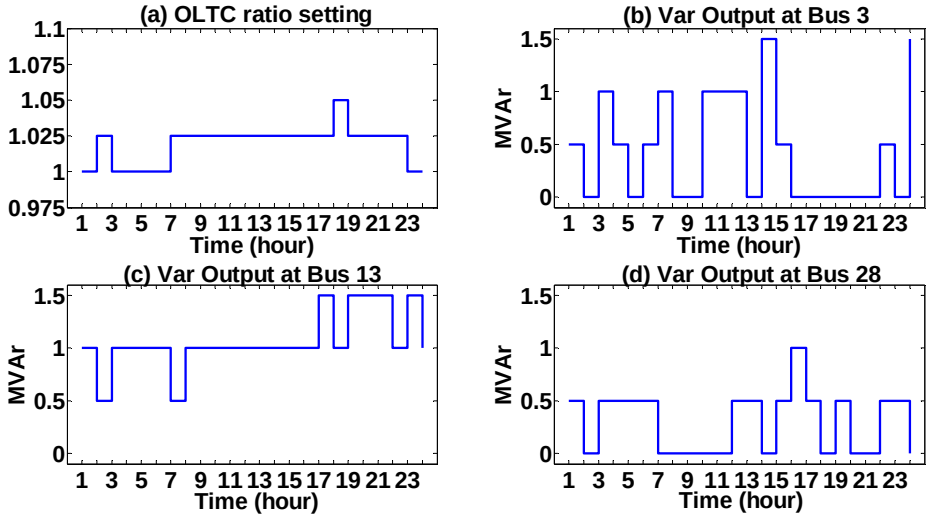

Fig. 5.18 CVR Dispatch results of using Load Model 4

Because Bus 18 and Bus 33 are located at the end of the radial feeders, their voltage profiles with different load models are shown in Fig. 5.19 and Fig. 5.20, respectively. The voltage levels with Load Model 1 (constant power load model) are obviously higher than those with VD load model, this is because power losses are linear to the square of the current, while the current flow into the constant power load is inversely proportional to the supply voltage. Therefore, when using

Load Model 1, the feeder will be operated by the OLTC in the upper bound of acceptable voltage, which is confirmed by Fig. 5.15(a). In comparison, the voltage profiles of other VD models (Load Model 2, 3, 4) are controlled to operate in the lower bound of acceptable voltage, in order to reduce the energy demand. However, although the differences among these voltage profiles exist, they are not very significant except in the period of 1:00-4:00 and 22:00-24:00.

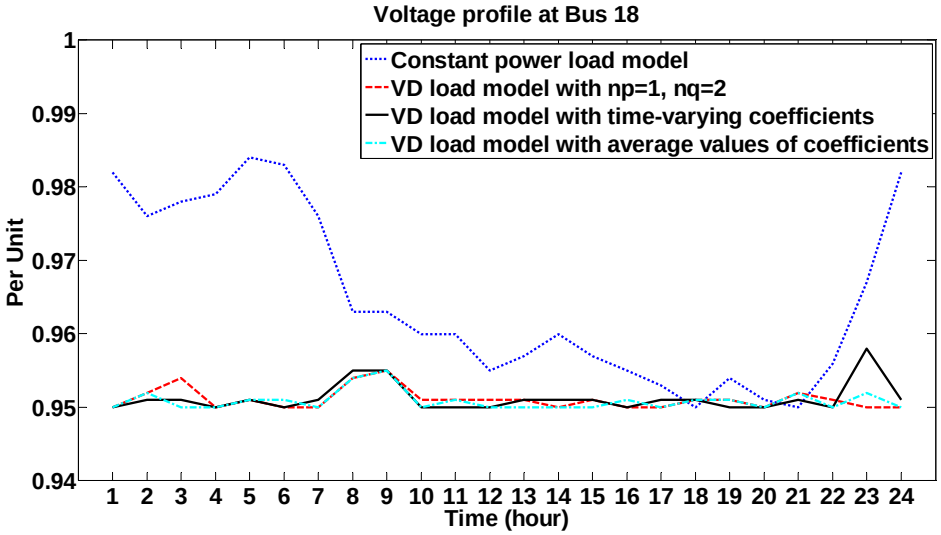

Fig. 5.19 Voltage profiles at Bus 18 when using different load models

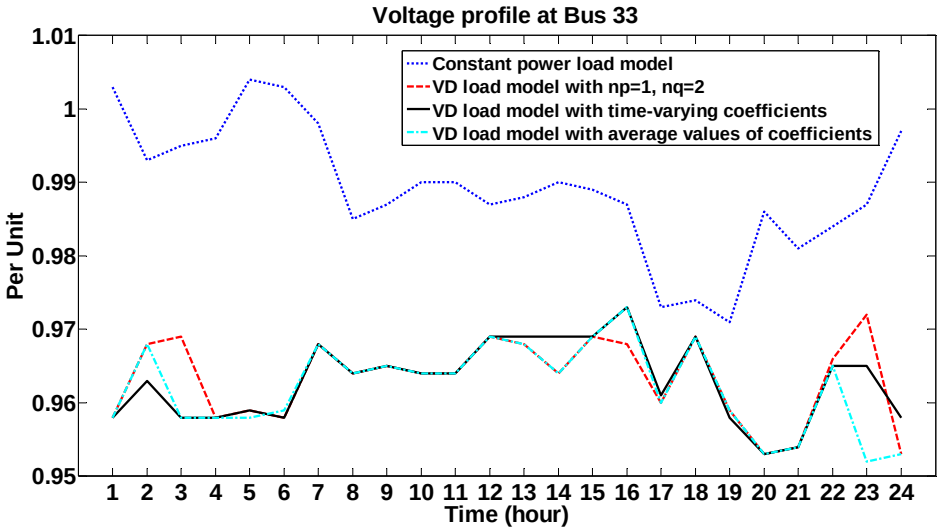

Fig. 5.20 Voltage profile at Bus 33 when using different load models

In addition, the active power demand by loads, power losses and total injected real power into the distribution system for different load models are presented in Fig. 5.21, Fig. 5.22 and Fig. 5.23, respectively, this further demonstrates the effects of different coefficients in the load models on VVO dispatches, which in turn have impacts on the energy dispatches within the system. To quantify the difference, the total injected real power for 24 hours when using Load Model 2, Load Model 3 and Load Model 4 are 112.07 MW, 109.5 MW and 111.9 MW, respectively. The percentage difference can be up to 2.3%, which is a significant number considering the only difference among various cases is the exponential coefficients in load model throughout 24 hours. Since the vast majority of loads in residential and commercial loads are sensitive to voltage in practice, and different types of loads, different load mix at different time will have various load-to-voltage sensitivities, the proposed CVR considering VD load models with time-varying coefficients are more effective and realistic.

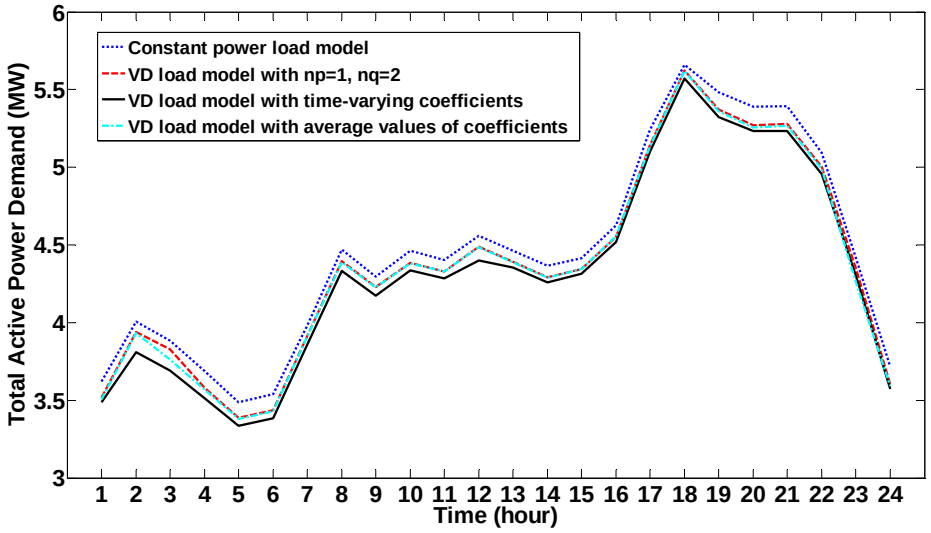

Fig. 5.21 Total active power demand when using different load models

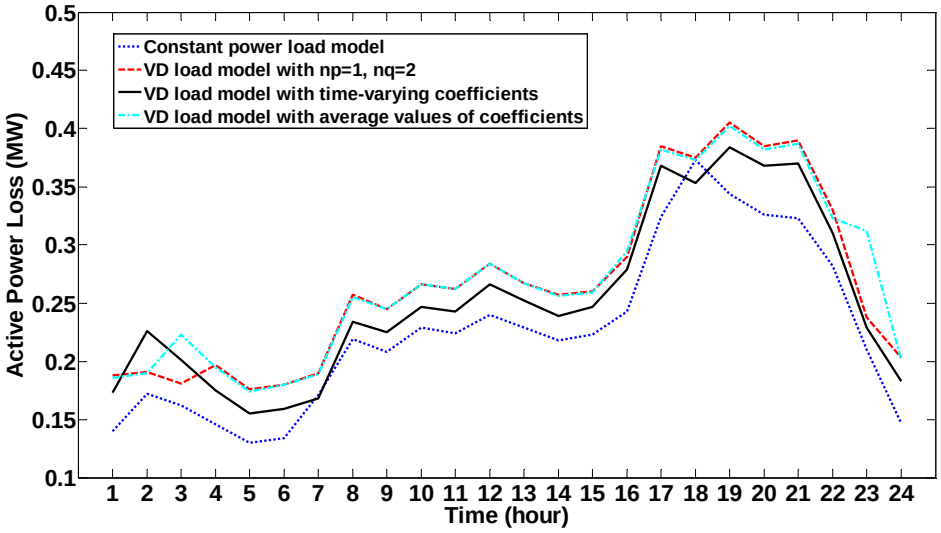

Fig. 5.22 Total active power loss when using different load models

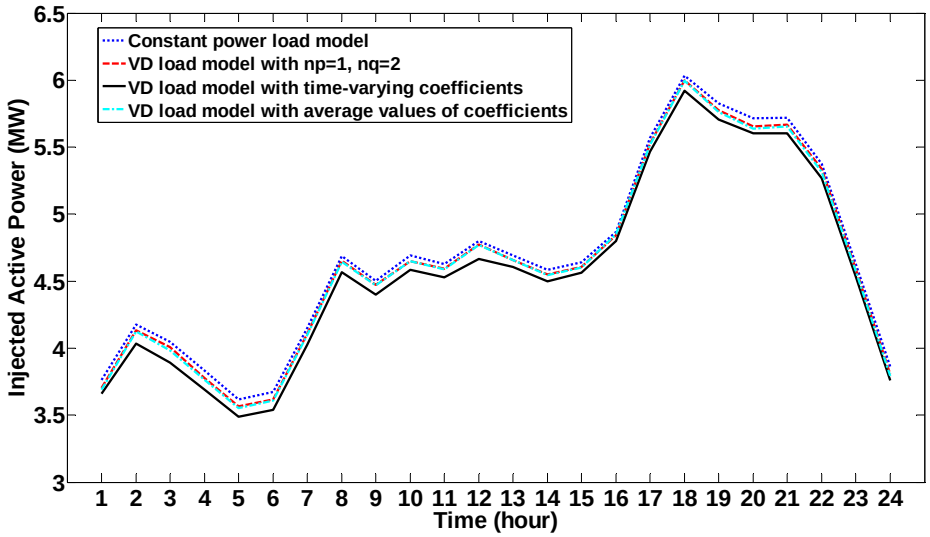

Fig. 5.23 Total active power injected from main power grid when using different load models

5.2.5 Effectiveness of Proposed CVR

In this section, in order to demonstrate the effectiveness of CVR, four scenarios with and without CVR will be simulated and compared using the same distribution system as in Section 5.2.4. The voltage dependent load model with time-varying coefficients, i.e. Load Model 3, introduced in Chapter 4 will be

used in all scenarios. The descriptions of scenarios are presented in Table 5.3 as follows.

Table 5.3 Description of four different scenarios

	OLTC	Cap 3	Cap 13	Cap 28
Scenario A	1.0	0 MVar	0 MVar	0 MVar
Scenario B	1.025	1 MVar	1 MVar	1 MVar
Scenario C	VVO with Loss Minimization (LM)			
Scenario D	CVR Optimization			

- Scenario A: No control, no reactive power support from capacitor banks;
- Scenario B: No control, but with fixed reactive power support;
- Scenario C: VVO with the objective of minimizing power losses;
- Scenario D: CVR optimization formulated in Section 5.2.1, with the objective of minimizing the sum of real power demand and power losses.

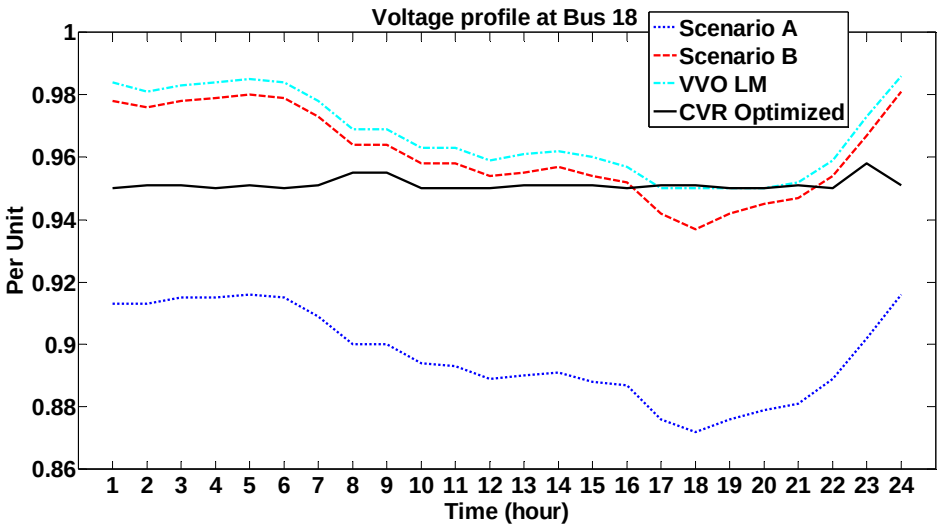

Fig. 5.24 Voltage profiles at Bus 18 for different scenarios

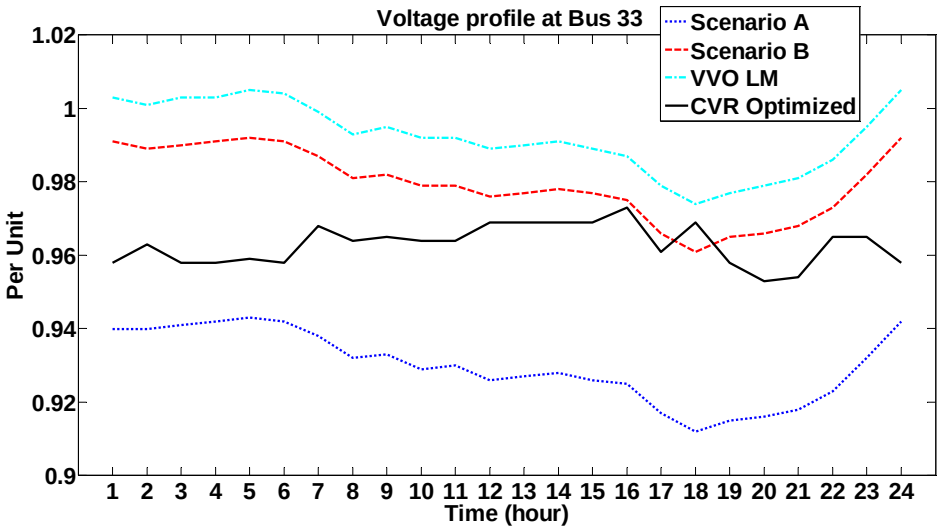

Fig. 5.25 Voltage profiles at Bus 33 for different scenarios

The voltage profiles of Bus 18 and Bus 33 are shown in Fig. 5.24 and Fig. 5.25, respectively. Due to the lack of voltage control provided by VVO, the voltage constraint is violated in Scenario A and Scenario B. It can be seen that, the voltage level of Scenario A is always less than 0.95 at Bus 18 and Bus 33, while it is violated at Bus 18 at the peak load period (17:00-21:00) in Scenario B. Since the demand is sensitive to the voltage, the proposed CVR will try to reduce the voltage level as much as possible and maintain it at the lower acceptable bound, in order to decrease the demand.

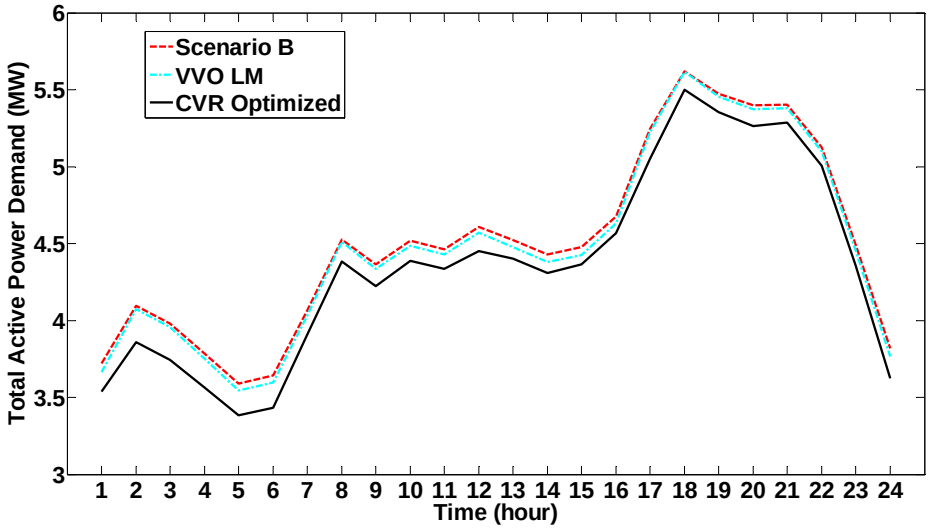

Fig. 5.26 Total active power demand for different scenarios

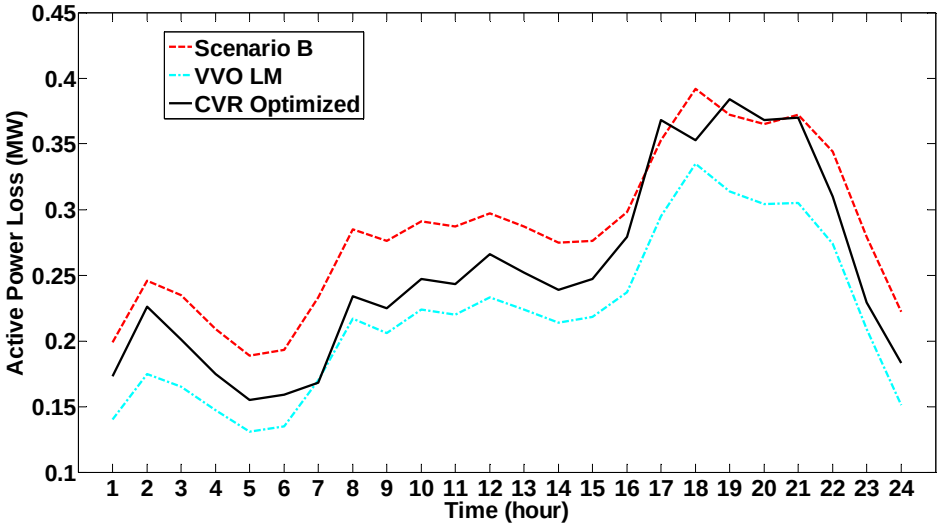

Fig. 5.27 Active power loss for different scenarios

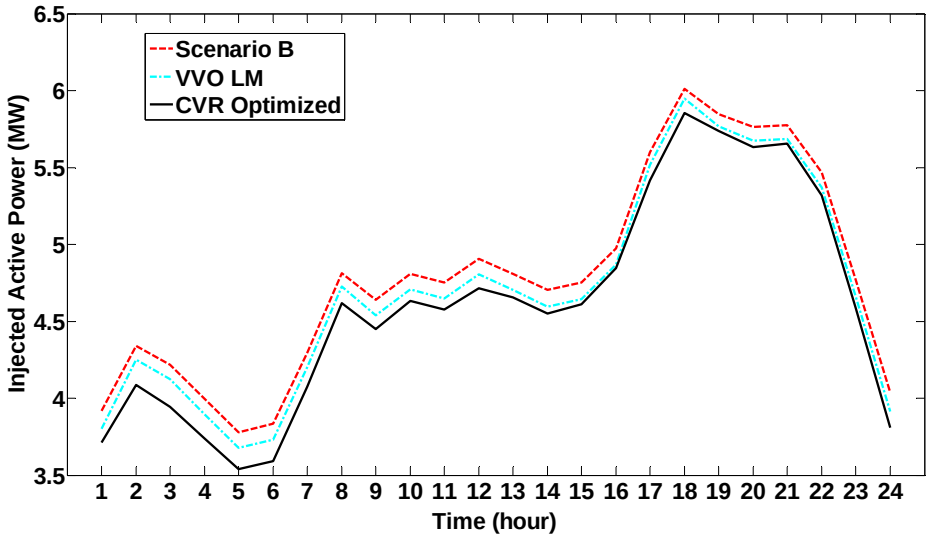

Fig. 5.28 Injected active power from main power grid for different scenarios

Since the voltage levels in Scenario A are unacceptable for most of the time, the power flow analysis for Scenario A will be ignored in the following analysis, as it is meaningless. For the purpose of comparison, the total active power demand by loads, power losses and injected active power from GSP to distribution network for Scenario B, VVO LM case, and CVR case are displayed in Fig. 5.26, Fig. 5.27 and Fig. 5.28, respectively. As shown in Fig. 5.26, the

intentional reduction in bus voltages within the acceptable range throughout the network in CVR case, achieves the minimum active power demand by loads. Although VVO LM performs the best in loss reduction compared with CVR as presented in Fig. 5.27, the demand reduction in CVR is greater than the loss reduction that can be achieved by VVO LM, therefore, the active power injection from GSP obtained from CVR is the minimum among all scenarios, as depicted in Fig. 5.28.

It is noted that the CVR is able to reduce more load demand and injected power from GSP during the light load conditions (1:00-6:00), i.e. it is more effective during these periods, which is attributed to the fact that light loading conditions result in higher voltages, which in turn leads to an unnecessary rise in load demand. The load demand can be deliberately decreased by optimal adjustment of OLTC and capacitor banks in the system. On the contrary, the voltage levels are already dropped to the lower bound at the peak load period, which limits the room for further reducing the voltage for load reduction, since the key criteria in practicing CVR is to make sure all bus voltage constraints are not violated.

5.3 Evaluation of the ability of DMLs at Various Locations to Benefit Power Network by OPF Analysis

DSM actions are generally implemented to maintain the energy balance within the power system. In the future smart grid, with the improved ICT and system infrastructures, demand manageable loads (DMLs) in some locations could be reduced to avoid the need of disconnecting an entire section of the network, in real-time response to contingencies (e.g. faults) within a power system. With the increasing penetration of distributed generation, more flexibility from DMLs is required within the distribution network. However, as discussed before, the DMLs of residential and commercial loads are deeply

embedded and highly distributed within the LV distribution networks, the implementation locations of DSM is an important issue, which has not been considered much in the literature.

Reference [165] applies reverse loadability method to determine the optimal location and capacity for DGs installation within distribution network using Optimal Power Flow (OPF), which maximizes the added capacity of DG by iteratively adding negative load at every bus, until the system constraints (e.g. voltage drops, line transfer limits) are violated. In addition, it is also proved that the adding DG at some buses provides more benefits to the network operation than the other buses.

Similarly, it is reasonable to expect there must be optimal locations for DSM implementation which can offer maximum benefits to the power grid. Therefore, this section will formulate an OPF problem to determine the optimal location and the minimum amount of DMLs required to be disconnected within the network that maintain all network constraints within the limits under a particular network contingency.

5.3.1 Problem Formulation of DSM-based OPF

When network contingencies (e.g. fault, line outage, overload, sudden shortage of RES etc.) occur, especially when the contingencies cause supply-demand imbalance and emergency generation may not be able to solve the problem, disconnecting a portion of the DMLs is an effective way to allow the power system to operate securely until the contingencies is cleared. The location and amount of DMLs that needed to be disconnected in order to keep the system within operational constraints depends on the severity and location of contingency. An OPF problem is formulated to calculate the minimum amount of disconnected DMLs that are needed to maintain secure system operation during contingency as follow:

$$\min_{\Phi_n} \sum_{n=1}^{N_{dsm}} C_n \cdot P_{0,n} \cdot \left(1 - \Phi_n\right) \tag{5.16}$$

$$P_n = \sum_{n=1}^{N} \left|V_n\right|\left|V_m\right|\left(G_{nm}\cos\theta_{nm} + B_{nm}\sin\theta_{nm}\right) \tag{5.17}$$

$$Q_n = \sum_{n=1}^{N} \left|V_n\right|\left|V_m\right|\left(G_{nm}\sin\theta_{nm} - B_{nm}\cos\theta_{nm}\right) \tag{5.18}$$

$$\left|S_b\right| \le \left|S_b^{\max}\right| \tag{5.19}$$

$$V_n^{\min} \le V_n \le V_n^{\max} \tag{5.20}$$

$$\Phi_n^{\min} \le \Phi_n \le \Phi_n^{\max} \tag{5.21}$$

TABLE 5.4 Nomenclature for DSM-based OPF

Symbol	Definition
N_{dsm}	the number of load buses with DMLs for DSM implementation
C_n	the cost of adjusting/deferring one unit of load at bus *n*
$P_{0,n}$	the original active power demand at bus *n*
Φ_n	the adjustment factor, i.e. remaining percentage of original demand after DSM
P_n	the total injected active power at bus n
Q_n	the total injected reactive power at bus n
N	the total number of buses
G_{nm}	the real parts of admittance matrix
B_{nm}	the reactive parts of admittance matrix
$V_n^{\min}$	the min. acceptable voltages at each network bus *n*
$V_n^{\max}$	the max. acceptable voltages at each network bus *n*
S_b	the apparent power in branch *b*
$S_b^{\max}$	the max. apparent power in branch *b*
$\Phi_n^{\min}$	the min. adjustment factor
$\Phi_n^{\max}$	the max. adjustment factor

5.3.2 Case Study 1

The above formulated problem is analyzed using a section of a typical distribution network in U.K., presented in Fig. 5.29, the network details can be found in [166]. The load sector mix is given in Table 5.5. This distribution system is populated with medium-voltage aggregate load models introduced in Chapter 4, using the equivalent impedance that transforms the low-voltage model to medium-voltage model. Since Chapter 4 only introduces residential and commercial load model, the light industrial load model taken from [144] is used in this analysis, and it is assumed to be constant throughout the day.

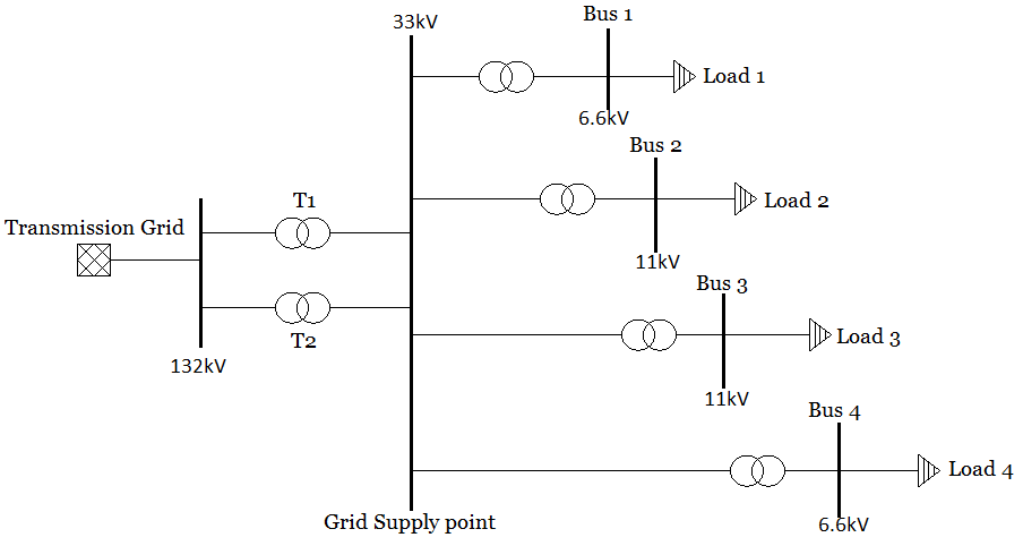

Fig. 5.29 Radial distribution network for case study

Table 5.5 Load sectors mix at each bus

	Bus 1	Bus 2	Bus 3	Bus 4
Residential	0%	75%	30%	100%
Commercial	100%	15%	35%	0%
Industrial	0%	10%	35%	0%

One of the upstream grid supply transformers (T1 in Fig. 5.29) is simulated to be faulted during the peak period at maximum loading conditions which represents the worst case fault condition, and since each transformer is rated at about 70% of peak load, another upstream transformer (T2) will be overloaded. It is assumed that there are DMLs at these four buses, the OPF formulated in (5.16)-(5.21) is applied at each locations with DMLs to calculate the minimum amount of DMLs which need to be curtailed for the purpose of relieving the transformer overloading, while keeping all system constraints (e.g. bus voltages, power flows etc.) within satisfactory limits throughout the distribution network. This static OPF is simulated in ETAP software, and the required amount of load

at each bus to be curtailed to clear the upstream contingency is determined and shown in Table 5.6.

Table 5.6 The required amount of load to be curtailed to clear the upstream contingency at each bus using different load models

Unit: MW	Bus 1	Bus 2	Bus 3	Bus 4
Constant power load model	-1.77	-1.72	-1.63	-1.37
Detailed load model introduced in Chapter 4	-1.78	-1.75	-1.68	-1.52

From the presented results, the contribution and ability of each downstream load bus with DMLs to keep the constraints under control during overload contingency can be assessed and quantified. Compared with the other buses, Bus 4 requires the least amount of DMLs (1.52 MW) to be disconnected to resolve the overload occurs at the upstream transformer, while Bus 1 needs to curtail 1.78 MW DMLs to alleviate the same contingency, which can be attributed to the higher system impedance (due to the larger physical and electrical distance) between Bus 4 and GSP. Hence, reducing the load via DSM implementation at Bus 4 results in greater decline in total power losses than implementation at the other locations, which also helps to unload the overloaded transformer. Therefore, it can be concluded that DSM implemented at Bus 4 is more beneficial to the system than at the other locations.

The differences between the obtained results using constant power load model (1.37 MW) and the detailed aggregate load model introduced in Chapter 4 (1.52 MW) is about 11%, which is quite a significant difference, because it corresponds to about 150 kW in absolute value and about 50 households assuming each with peak demand of 3 kW. This emphasizes the value of detailed load modeling with time-varying coefficients in the power system analysis under the consideration of DSM scenarios. Using constant power load models seems to tend to produce excessively optimistic results, while using the detailed time-

varying and voltage-dependent load model requires more load to be disconnected, this can be justified as follows. The power demand is constant and equals to nominal power for the voltage-independent load model, i.e. constant power load model, regardless of the supply voltage. If the load is voltage dependent, the load demand will be reduced and deviated from the nominal value due to the inherent voltage drop in the distribution network. Since the above formulated OPF problem is attempting to optimize the required amount of load that needed to be curtailed to resolve the system contingency, the load will be iteratively disconnected to re-calculate the new loading conditions. Then, as the load is disconnected, the voltage gradient across the distribution system will improve, and the demand of connected load will in turn increase. Consequently, more DMLs need to be disconnected by the network operator in the case of using voltage dependent load models.

5.3.3 Case Study 2

The DSM implementation not only changes the magnitude of load demand at the implemented location, but also alters the load composition, thus the electrical characteristics of the aggregate load. The results in Section 5.1 show that the changes of load composition due to DSM will change the model coefficients of aggregate load models, which in turn affects the bus voltages and the actual real and reactive demand drawn at the grid supply point.

In order to compare and evaluate the potential of different types of DMLs to alleviate upstream contingencies, a time sequential OPF is utilized in this section, which is a similar variation of the OPF outlined in (5.16)-(5.21). The new objective function is

$$\min_{\Phi_{l,n}} C_{l,t} \cdot P_{l,t} \cdot \left(1 - \Phi_{l,t}\right) \text{for } t = 1,...,24 \tag{5.22}$$

where the definition of variables are similar as defined in (5.16), except that subscript l indicates load type l, and subscript t represents time interval t. The

system constraints are the same as outlined in (5.17)-(5.21). The time sequential OPF means that the static OPF problem is solved at every time step.

The same distribution network is used in this case study. And a transformer (T1 in Fig. 5.29) overloading is again simulated to increase the overload level incrementally until either one of the system constraints in (5.17)-(5.21) is violated or the amount of DMLs available is exceeded. The effective reserve S_r at the grid supply point offered by a particular load type can be calculated as the MVA flow reduction across the grid supply point, i.e. initial MVA flow $S_{i,gsp}$ minus final MVA flow $S_{f,gsp}$ after time sequential OPF is carried out.

$$S_r = \left|S_{i,\,gsp}\right| - \left|S_{f\,,\,gsp}\right| \tag{5.23}$$

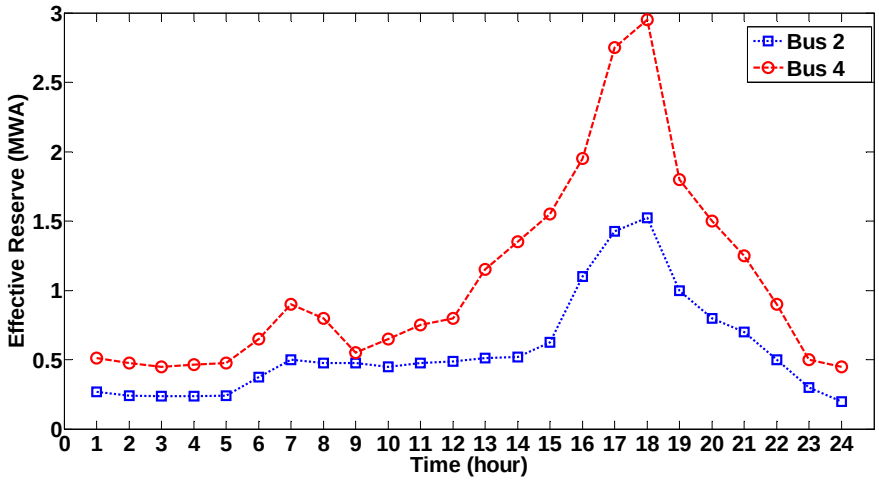

Fig. 5.30 Effective reserve offered by residential wet load at GSP

Taking into consideration the thermal and voltage constraints, the potential effective reserve provided by the wet load in residential sector at Bus 2 and Bus 4 (due to the larger portion of residential load) is calculated using the time sequential OPF, by assuming the wet load is 100% controllable (i.e. can be disconnected at any time instant), and the result is depicted in Fig. 5.30. The actual amount of deferrable wet load and the corresponding available time highly depends on the load aggregation and coordination among multiple customers in a specific DSM scheme. The reconnection of the DMLs is not considered here

because it depends on how the DMLs are controlled, for example, by a frequency control signal to the smart appliances of customers or by a price incentive signal. The focus here is to determine the amount effective reserve provided by a particular type of DMLs in the downstream at each bus at any time throughout the day that can help to resolve upstream contingency.

From the above discussion, it is illustrated that both the load composition at each bus and system location has a considerable influence on the efficiency and benefit of a devised DSM program. Precisely modelling the aggregate load will be beneficial to alleviate contingencies and maintain service to the system while minimizing the number of affected customers. As this approach can be used to assess the value, contribution and ability of each type of DMLs at any locations in the system to resolve network contingencies, it may potentially be utilized by system operators to greatly promote and improve the deployment of DSM programs at the optimal load buses throughout the network by providing customers with appropriate and attractive incentives.

5.4 Chapter Summary

Based on the aggregate time-varying load models developed in Chapter 4, a general methodology of modelling, quantifying and assessing the impacts of various devised DSM schemes on the aggregate load models, power flow and network performance is proposed, which will be of interest to utility companies and policy makers, as the impacts of any devised DSM schemes should be evaluated before actual implementation. Moreover, a more accurate framework for CVR optimization in modern distribution system is formulated using the developed load models to investigate the effects of time-varying model coefficients of load models (due to naturally occurrence and DSM actions) on the VVO dispatches and the corresponding network performances. To the best of my knowledge, the effects of geographical and temporal variations of the

coefficients in load model and the impacts of DSM on VVO dispatches have never been discussed in the literature. Simulation results demonstrate the importance of using the comprehensive time-varying load models in VVO analysis, as significant difference can be noticed under different scenarios with different load models. Finally, a DSM-based OPF problem is formulated to assess the ability of various type of DMLs to alleviate network contingencies (e.g. overloading, sudden shortage of RES) at different locations within a given distribution system, it has been shown that there is an optimal location in distribution network to deploy DSM when network contingencies occur, and the DSM-based OPF formulation can be effectively used to solve the question of "where, how much and which type of DMLs should be controlled to alleviate a network contingency".

Chapter 6

Mathematical R-C Thermodynamic Model of Smart Commercial Buildings

6.1 Introduction

Due to the relative shortage of such knowledge in power engineering, this chapter introduces the fundamental physical knowledge that from [167] for developing the thermodynamic model of buildings. The modeling techniques and methodologies that are currently and widely adopted by the researchers in the area of building climate control and building construction industry will also be discussed, as the thermodynamics in building are strongly related to the power consumption of heating ventilation air conditioning (HVAC) system in large commercial buildings, and these should be properly and accurately modelled for use in the demand side management/demand response area in smart grid.

6.2 Fundamental Principles of Thermodynamic Model for Building

Building elements include the air, walls, floors and ceilings, two fundamental thermal properties of these elements are heat transmissibility and heat storage capacity. Heat can be transferred through these elements via three different means including heat conduction, heat convection and heat radiation. Heat can also be stored in these elements and the heat storage capacity is related to the specific heat capacity and the mass of the corresponding element. Thermodynamics in building is normally modelled using a thermal network,

which is analogy to the electrical network where resistors represent heat transmission and capacitors represent heat storage. Lumped-capacitance method is used in this thesis to develop an accurate and simple thermodynamic model for large commercial building.

6.2.1 Heat Transfer

Heat conduction, convection and radiation are three main mechanisms of heat transfer.

6.2.1.1 Heat Conduction

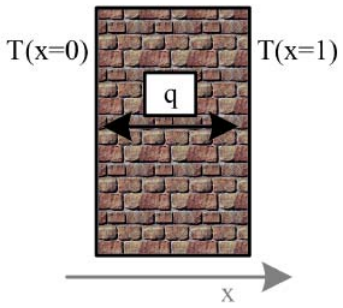

Fig. 6.1 Illustration of heat conduction [167]

Heat conduction refers to the heat transmission that takes place through the stationary medium/object/substance when a temperature gradient exists. It can be quantified using the rate equation called Fourier's Law, for example, as shown in Fig. 6.1, for the plane wall with a temperature distribution *T(x)*, the transfer rate of thermal energy $q_x(W)$ in the direction *x* is computed as

$$q_x = -kA\frac{dT}{dx} \tag{6.1}$$

Where *dT/dx* is the temperature gradient, *k* (unit: *W/m.K*) is a characteristic of the wall material called the thermal conductivity and the minus sign means that thermal energy is conducted to the direction of declining temperature. The temperature gradient can be expressed as a linear equation as in (6.2) under steady state conditions with linear temperature distribution.

$$\frac{dT}{dx} = \frac{T_{x=1} - T_{x=0}}{L} \tag{6.2}$$

Then the heat transfer can also be linearly expressed as

$$q = \frac{kA(T_{x=0} - T_{x=1})}{L} \tag{6.3}$$

6.2.1.2 Heat Convection

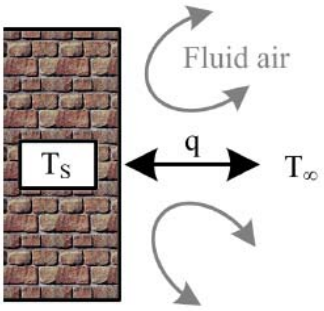

Fig. 6.2 Illustration of heat convection [167]

As shown in Fig. 6.2, the convection heat transfer can be referred as the energy transfer taking place due to bulk fluid motion and random molecular motion [167]. Using Newton's Law of cooling, the convective heat transfer q (W) can be expressed as

$$q = hA(T_s - T_\infty) \tag{6.4}$$

where T_s is the surface temperature, T_∞ is the fluid temperature, A is the area of wall, and h (unit: W/m^2.K) is called the convection heat transfer coefficient. According to the (6.4), the convection heat is transferred from the surface when q is positive ($T_s > T_\infty$), and the convection heat is transferred to the surface when q is negative ($T_s < T_\infty$).

6.2.1.3 Heat Radiation

While the heat transfer through conduction or convection needs a material medium, heat radiation does not. Heat radiation is the thermal energy radiated by

a substance with a finite temperature [167]. Fig. 6.3 illustrates the radiation transfer process.

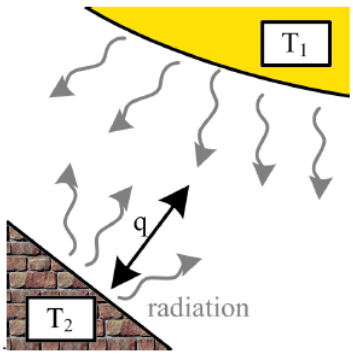

Fig. 6.3 Illustration of heat radiation [167]

Heat radiation involves some complicated physics laws and equations, more details can be found in [167]. In the context of thermodynamic analysis in building, the heat radiation through the internal walls in the building will be ignored owing to the relative small temperature range inside the building, in order to simplify the building thermal network. Two types of heat radiation will be considered in developing the differential equations representing the temperature dynamics inside the building in this thesis: 1) the irradiation from sun absorbed through the windows and the external walls into the rooms; 2) the heat emitted from the occupants and electrical devices.

6.2.2 Heat Storage

Specific heat capacity c_p is a basic property of materials, which is the quantifiable thermal energy needed to alter one unit of temperature of one unit quantity of a matter [167]. Increasing the temperature of a matter with higher c_p requires more heat, and vice versa. The capacity in storing energy (denoted by Q) of an object with specific heat capacity c_p and mass m is shown in (6.5), where $\dot{T}$ is the rate of change of temperature.

$$Q = mc_p\dot{T} \tag{6.5}$$

6.3 Configuration and Operating Principle of HVAC System

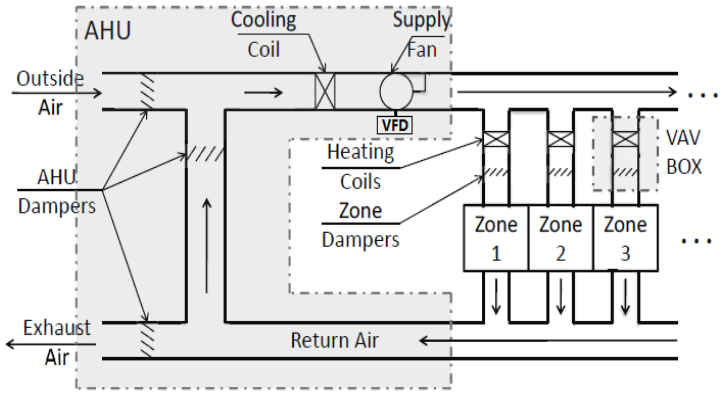

Fig. 6.4 Commercial building HVAC system schematic [168]

In a modern commercial building, the HVAC system shown in Fig. 6.4 typically consists of an air handing unit (AHU) and SF serving multiple variable air volume (VAV) boxes which together control the airflow and air temperature into a network of zones. The AHU mixes the fresh outside air with the return air, and then this mixed air is driven and distributed by the SF to the corresponding VAV box of each zone [169]. The cooling coil will cool and dehumidify the mixed air in hot and wet climates, whereas the heating coil will reheat and humidify the mixed air in cold and dry climates. The zone damper position in the VAV box determines the mass flow rate of cooled/heated air entering a zone. The differential pressure across the SF will change once the damper position is varied. To maintain the pre-specified differential pressure set-point, VFD can be commanded to change the input voltage and frequency of motor, thus SF speed can be varied to change the airflow [168]. Therefore, the combined and coordinated functions of cooling coil, heating coil and supply fan in HVAC system play a significant role in the temperature dynamics inside the buildings.

6.4 Equivalent Circuit of Thermal Network

6.4.1 Thermal Resistance and Thermal Potential

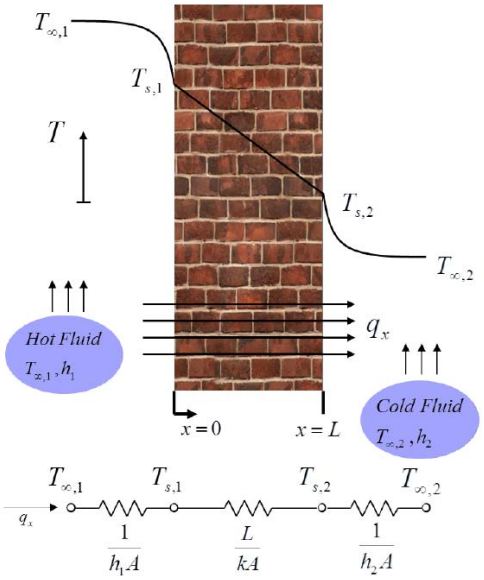

Fig. 6.5 Illustration of heat transfer though a plane wall and schematic of its corresponding equivalent thermal circuit [167]

Similar to the fact that the resistance in electrical circuit is related to the electricity conduction, the resistance in thermal network is regarded as being relevant to the heat transfer. It is acknowledged that resistance equals to the driving potential divided by the corresponding transfer rate. Similarly, the thermal resistance equals to the thermal potential divided by the heat transfer rate. Thermal potential (i.e. temperature difference) in thermal circuits is similar to the electrical potential in electric circuits. For example, Fig. 6.5 shows the temperature distribution and heat transfer (including conduction and convection) through the plane wall, as well as the corresponding equivalent thermal circuit. The equivalent thermal circuit offers an advantageous and convenient approach to conceptualize, analyze and quantify the behaviors and problems of heat transfer [167].

Following Equation (6.3), it can be derived that the heat conduction thermal resistance for $R_{t,\,conduction}$ for a wall is

$$R_{t,\,conduction} = \frac{T_{s,1} - T_{s,2}}{q_x} = \frac{L}{kA} \tag{6.6}$$

Following the Equation (6.4), it can also be derived that the thermal resistance for heat convection $R_{t,\,convection}$ at the surface of a plane wall is

$$R_{t,\,convection} = \frac{T_s - T_\infty}{q} = \frac{1}{hA} \tag{6.7}$$

Notice that q_x remains constant through the thermal network, Equation (6.8) can be easily derived from the equivalent thermal circuit.

$$q_x = \frac{T_{\infty,1} - T_{s,1}}{1/h_1 A} = \frac{T_{s,1} - T_{s,2}}{L/kA} = \frac{T_{s,2} - T_{\infty,2}}{1/h_2 A} \tag{6.8}$$

Analogy to the series connection of electrical resistance in electrical circuit, the heat transfer rate q_x can also be computed using the temperature difference between two sides of the wall and the total thermal resistance R_{total} (series connection of conduction and convection resistances) as follows.

$$q_x = \frac{T_{\infty,1} - T_{\infty,2}}{R_{total}} = \frac{T_{\infty,1} - T_{\infty,2}}{1/h_1 A + L/kA + 1/h_2 A} \tag{6.9}$$

6.4.2 Thermal Capacitance

Regarding building thermal analysis, the thermal flywheel effect refers to the thermal energy storage ability of thermal elements, to be more specific, the thermal mass provides “inertia” against temperature fluctuations. For instance, the huge building body can serve to smooth the fluctuations of indoor temperatures against the outside temperature which are always fluctuating and varying with time, because the thermal mass of building will absorb thermal energy if the ambient temperature is higher than that of the building thermal mass, and discharge thermal energy back if the ambient temperature is lower. This ability enables more advanced building climate control and has a great potential in providing more fast-responsive and flexible power reserve for smart

grid development, which is one of the motivations of this thesis mentioned in Chapter 1.

The concept of thermal capacitance is introduced into the thermodynamic building model to help analyze the transient thermal behavior inside the building. The temperature of the materials vary with time during transient heat transfer, and thermal capacitance (unit: *J/°C* or *J/K*, depending on the unit of temperature) can be regarded as the capacity of an element to store thermal energy. The thermal mass is just the specific heat capacity of the material multiplies the mass of that material. In addition, thermal capacitance $C = mc_p$ will be assigned to each node (i.e. walls and rooms of building) in thermal network to accurately capture the temperature dynamics.

6.4.3 Illustration Example

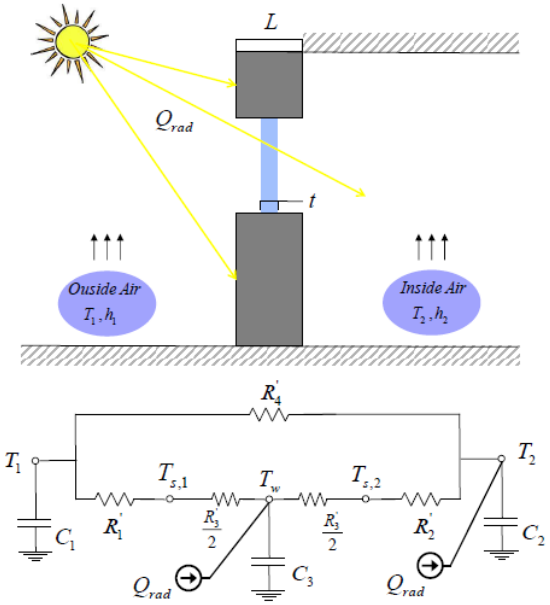

Fig. 6.6 Thermal circuit network representing a peripheral wall with a window [167]

As presented in Fig. 6.6, consider a peripheral wall with only one side exposed to the sun and the outside air as an illustration example. There are three nodes in this equivalent circuit model, namely, the outside air node with potential

T_1, the inside air node with potential T_2 and the wall node with potential T_w. And these nodes are all connected to ground via corresponding thermal capacitor to represent the thermal storage capacity.

Heat flows through both wall and window from the outside to the inside. The branch through the wall is represented by two convection thermal resistances (R_1' and R_2') and one conductive thermal resistance R_3'. The branch through the window is represented by a thermal resistance R_4'. A variable current source is used to represent the radiative heat gain from the sun.

Table 6.1 Nomenclature for illustration example

Symbol	Definition
A_{win}	Area of window
t	Thickness of window
k_w	Conductive heat transfer
A_{wall}	Area of wall, not including window
C_1	Thermal capacitance of the outside air, $C_1 = m_{a1}c_a$
C_2	Thermal capacitance of the air inside the room, $C_2 = m_{a2}c_a$
C_3	Thermal capacitance of wall, $C_3 = m_w c_w$
m_{a1}, m_{a2}, m_w	The masses of outside air, inside air and wall, respectively
c_a, c_w	Specific heat capacitance of the material of air and wall, respectively
Q_{rad}	Radiative heat gain from the sun
R_1'	Convective thermal resistance between outside air and wall, $R_1' = 1/(h_1 A_{wall})$
R_2'	Convective thermal resistance between inside air and wall, $R_2' = 1/(h_2 A_{wall})$
R_3'	Conductive thermal resistance of the wall, $R_3' = L/(kA_{wall})$
R_4'	Total thermal resistance representing the window. $R_4' = 1/(h_1 A_{win}) + t/(k_w A_{win}) + 1/(h_2 A_{win})$

6.5 Thermodynamic Model for the Whole Building

Section 6.2 review the fundamental heat transfer equations that are required for composing the plant model to represent the whole building. This section will demonstrate the process of deriving the governing hear transfer equations for temperature dynamics in all rooms and walls of the whole building and extending the single-building model to multiple-buildings model.

6.5.1 Assumptions for the Model Development

Some assumptions were made to simplify the thermal model as follows:

1) The specific heat of air c_p is constantly set to be 1.007 in this thesis. Although c_p is 1.007 when temperature is 300 K and 1.006 when temperature is 250 K, the range of temperature dynamics occurring inside a building is small enough to keep the error of this assumption within 0.1%.

2) All rooms in the building are assumed to have the same pressure as in the cooling and heating ducts of HVAC system, which means the total mass of air within the room will remain the same in the process.

3) Since lumped-capacitance method is used in this thesis, the air in a room is assumed to have only one temperature across its volume because the developed thermodynamic building model should be simple enough to facilitate the development of control methodology and reduce the computation time.

4) Since the temperature difference between inner walls of building is small, the interior radiative coupling between inner walls is ignored in this thesis as the corresponding effects on temperature dynamics should be trivial.

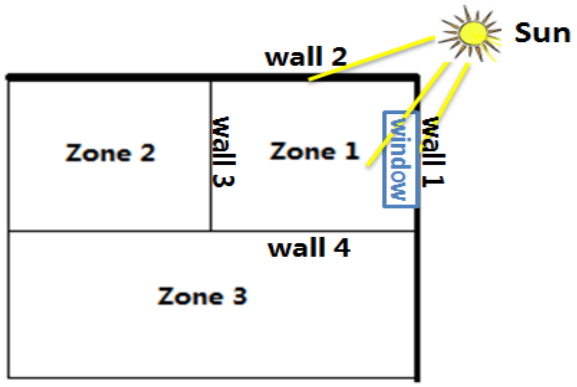

Fig. 6.7 Schematic of three-zones building [170]

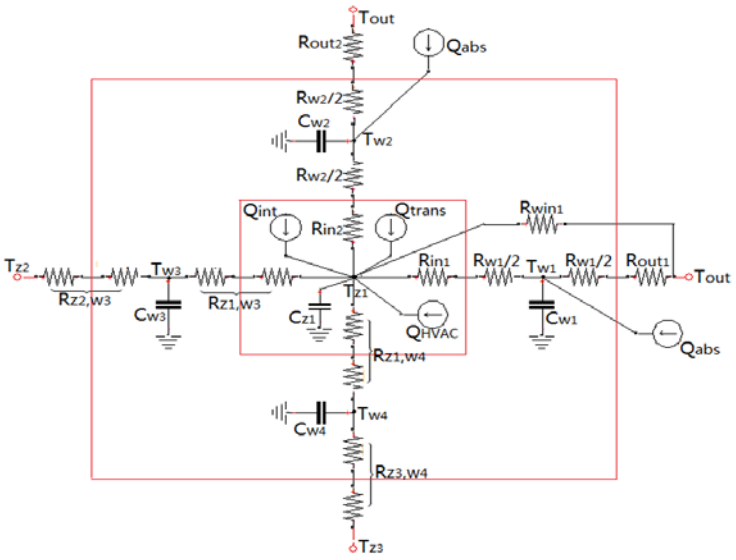

Fig. 6.8 Thermal network for Zone 1 and its surrounding walls [170].

TABLE 6.2 Nomenclature for R-C Thermodynamic Model of Building

Symbol	Definition
C_{Zi} , C_{Wi}	Thermal capacitance of zone *i* & wall *i*.
c_a, c_w	Specific heat capacity of air and wall, respectively.
m_{ai} , m_{wi}	Air mass in zone *i* and mass of wall *i*, respectively.
T_{Zi} , T_{Wi} , T_j	Temperature of zone *i*, wall *i*, node *j*, respectively.
T_{Si}	HVAC supply air temperature entering zone *I* through the ducts.
T_{out}	Outside ambient temperature.
$\dot{m}_{Zi}$	The flow rate of the mass of air entering zone *i* (airflow).
$R_{i,j}$	Total thermal resistance between node *i* and node *j*.
$\dot{Q}^i_{int}$	Internal heat gain (from electrical devices, humans, lighting etc.) in zone *i*.
Q^i_{rad}	Solar radiative heat flux density that radiates into node *i*.
A^i_{win} , A^i_W	Total window area in zone *i* and area of wall *i*, respectively.
ε^i_{win}	Glass transmissivity of window in zone *i*.
α^i_W	Solar radiation absorption coefficient of wall *i* surface.
n^i_{win}	Equals 1 if zone *i* has a window, 0 if zone *i* has no window.
ψ^i_W	Equals 1 if wall *i* is a peripheral wall, 0 if wall *i* is an internal wall.
$\mathbf{N}_{Zi}$, $\mathbf{N}_{Wi}$	The set of all neighboring nodes to zone *i* node and wall *i* node.
R^{wall}_{value} , R^{glass}_{value}	R-value of wall and glass window, respectively.
R^{in}_{value} , R^{out}_{value}	R-value of internal surface film and external surface film.
R_{Wi}	Thermal resistance of wall *i* for conduction heat transfer.
$R_{in\,i}$	Thermal resistance of wall *i* for internal convective heat transfer.
$R_{out\,i}$	Thermal resistance of wall *i* for external convective heat transfer.
$R_{win\,i}$	Thermal resistance of window *i*.

6.5.2 Model for a Single Building

Considering a three-zones building as shown in Fig. 6.7 as an example to formulate the thermodynamic model for a single building, the equivalent thermal network for zone 1 is presented in Fig. 6.8.

C_{Zi} and C_{Wi} represents the thermal mass or thermal capacity of zone i and wall i, respectively. And they are equal to the specific heat capacity multiplies the mass, i.e.

$$C_{Zi} = c_a m_{ai} = c_a \rho_a V_{Zi} \tag{6.10}$$

$$C_{Wi} = c_w m_{wi} = c_w \rho_w V_{Wi} \tag{6.11}$$

where ρ_a and ρ_w are the density of air and wall material at room temperature, respectively, V_{Zi} is the volume of air at zone i, V_{Wi} is the volume of wall i equaling to the wall thickness times the wall area.

As discussed, the thermal dynamic of the building climate is modeled as an R-C thermal network where heat transfer is represented by thermal resistance and heat storage by thermal capacitance. Every wall or zone affecting the thermal behavior inside the building is represented by a node with a thermal potential (i.e. temperature).

Note that the temperature at each node in thermal circuit is analogous to the voltage at corresponding node in electrical circuit. Similarly, heat flow in thermal circuit is analogous to the current in electrical circuit. Therefore, the changes of temperature ΔT in the zones or walls caused by the changes of heat flow ΔQ through the zones or walls with thermal capacity $C_{thermal}$ have the relationship $\Delta T = \Delta Q / C_{thermal}$, this is similar to the changes of voltage potential ΔV caused by the electrical charge Δq on the capacitors with $C_{electrical}$ capacity at that node in electrical circuit have the relationship $\Delta V = \Delta q / C_{electrical}$.

These nodes (i.e. zones or walls) are linked via thermal capacitors (C_{Zi} and C_{Wi}) to the ground and via thermal resistors to the adjacent nodes. Each internal wall node is interconnected with a zone node using two series resistors with

resistances $R_{Wi}/2$ and $R_{in\,i}$, while the peripheral wall node is interconnected with outside air node via two series resistances $R_{Wi}/2$ and $R_{out\,i}$. It means that wall i is separated into two sides, and by assuming the temperature of the centerline of the wall i is the wall temperature, the thermal resistance for conduction for these two sides is $R_{Wi}/2$, where R_{Wi} is defined in Equation (6.6). Besides, for simplicity, both sides of the internal walls and the internal sides of the peripheral walls are assumed to have the same transfer coefficient h_i of convection heat, while h_o is the transfer coefficient of convection heat for the exterior sides of the peripheral walls, therefore, following the Equation (6.7), $R_{in\,i}$ and $R_{out\,i}$, the internal and external convective thermal resistance, respectively, are defined as

$$R_{in\,i} = \frac{1}{h_i A_i} \tag{6.12}$$

$$R_{out\,i} = \frac{1}{h_o A_i} \tag{6.13}$$

In addition, the window i is just modeled as a pure resistance $R_{win\,i}$ parallel with the thermal resistance of its wall by ignoring its thermal capacitance due to its negligible mass compared to wall mass.

With the thermal capacitances and resistances defined above, the governing equation of energy balance and temperature dynamics in zones and walls of the building can be derived by performing nodal analysis. For Zone 1 in Fig. 6.7, we have:

$$\begin{aligned} C_{Z1}\frac{dT_{Z1}}{dt} = c_a \dot{m}_{Z1}(T_{S1} - T_{Z1}) + \frac{T_{W1} - T_{Z1}}{\frac{R_{W1}}{2} + R_{in1}} + \frac{T_{W2} - T_{Z1}}{\frac{R_{W2}}{2} + R_{in2}} + \frac{T_{W3} - T_{Z1}}{\frac{R_{W3}}{2} + R_{in3}} \\ + \frac{T_{W4} - T_{Z1}}{\frac{R_{W4}}{2} + R_{in4}} + \frac{T_{out} - T_{Z1}}{R_{win1}} + \varepsilon_{win}^1 A_{win}^1 Q_{rad}^1 + \dot{Q}_{int}^1 \end{aligned} \tag{6.14}$$

For Wall 1 in Fig. 6.7, we have:

$$C_{W1}\frac{dT_{W1}}{dt} = \frac{T_{Z1} - T_{W1}}{\frac{R_{W1}}{2} + R_{in1}} + \frac{T_{out} - T_{W1}}{\frac{R_{W1}}{2} + R_{out1}} + a_W^1 A_W^1 Q_{rad}^1 \tag{6.15}$$

The left hand side of Equation (6.14) and (6.15) are the heat flow into the node of Zone 1 and Wall 1, respectively. On the right hand side of Equation

(6.14), the first term denotes the heat transfer from the HVAC system to Zone 1, which is positive if $T_{s1} > T_{z1}$ for heating mode and negative if $T_{s1} < T_{z1}$ for cooling mode; the second to fifth terms account for the heat transfer from Zone 1's surrounding walls to zone 1; the sixth term represents the heat transfer from outside air into Zone 1 via window; the seventh term stands for the portion of sun radiation heat that transmitted into Zone 1 via window (i.e. Q_{trans} in Fig. 6.8). Similarly, on the right hand side of Equation (6.15), the first term accounts for the heat transfer from the air in Zone 1 to Wall 1, the second term represents the heat transfer from outside air to Wall 1 and the third term denotes the fraction of sun radiation heat that absorbed by Wall 1 (i.e. Q_{abs} in Fig. 6.8).

In fact, the above governing equation can be expressed in a general form as follows:

The energy balance equation for the Zone *I* is:

$$C_{Zi}\frac{dT_{Zi}}{dt} = c_a \dot{m}_{Zi}(T_{Si} - T_{Zi}) + \sum_{j \in \mathbf{N}_{Zi}} \frac{T_j - T_{Zi}}{R_{i,j}} + \dot{Q}^i_{int} + n^i_{win}\varepsilon^i_{win}A^i_{win}Q^i_{rad} \qquad (6.16)$$

The temperature governing equation for Wall *i* is:

$$C_{Wi}\frac{dT_{Wi}}{dt} = \sum_{j \in \mathbf{N}_{Wi}} \frac{T_j - T_{Wi}}{R_{i,j}} + \psi^i_W \alpha^i_W A^i_W Q^i_{rad} \qquad (6.17)$$

The heat flux radiated into the peripheral walls and into the rooms with windows is very difficult to accurately predict, it need to consider date, time, sky condition, the location of the considered building and orientation of the walls and windows, which requires lots of data for tedious parameter identification. Besides, internal heat generation involves the heat emitted from electrical devices and occupants with great uncertainty. For simplicity in this paper, they are approximated to be the affine function of the outsider air temperature and current CO_2 concentration in the room, respectively, as shown in Equation (6.18) and (6.19).

$$Q_{rad_i}(t) = \lambda T_{out}(t) + \gamma \qquad (6.18)$$

$$\dot{Q}_{int_i}(t) = \mu \Psi(t) + \nu \qquad (6.19)$$

where $T_{out}(t)$ is the outside air temperature, $\Psi(t)$ is the CO_2 concentration inside the modelled zone, and λ, γ, μ, ν are the parameters that need to be identified by nonlinear regression.

Now, the whole building model can be obtained by writing the heat transfer equation for every zone and wall and converting these equations into a state space form as follows.

$$\dot{x}(t) = Ax(t) + f(x(t),u(t),d(t)) \tag{6.20}$$

$$y(t) = Cx(t) \tag{6.21}$$

Where $x(t)$ is the vector of states denoting the node temperatures in thermal circuit at time t, $u(t)$ represents the vector of control inputs at time t (i.e. the flow rate of the mass of the cooled/heated air and supply temperature of the cooled/heated air entering each zone), $d(t)$ is the disturbance vector to the system at time t including the outside air temperature, sun radiation and internal heat generation, and $y(t)$ is the output vector of system including all zone temperatures at time t.

6.5.3 Linearization of Nonlinear Thermodynamic Model

It can be obviously seen from the above developed model that the dynamics of the system are nonlinear since the states $x(t)$ (i.e. T_{Zi}) are multiplied by the control input $u(t)$ (i.e. $\dot{m}_{Zi}$). There are several techniques that can be utilized to handle system nonlinearity, for example, feedback linearization, however, the high order of the model could result in substantial computational burden and messy calculations. Instead, in this thesis, the conventional Jacobian Linearization method is used to convert the nonlinear dynamics into the standard linear state space form, it linearizes the nonlinear system around a specific equilibrium point and is accurate enough for the HVAC control purposes since the temperature range inside the building is small enough. The review and detailed concept of Jacobian linearization can be found in [167].

There are infinite equilibrium operating points in this thermodynamic building model since these points can be obtained using different equilibrium inputs. Nevertheless, there is a specified equilibrium operating point where the system is working most of the time, which can be obtained by maintaining the zones' temperature identical to the user-defined set-point temperature and then solving for the inputs and the temperature of walls at the equilibrium point [170].

In order to reduce the computational effort, the nonlinear building model is linearized around an equilibrium point which is searched by a sequential quadratic programming algorithm until it locates the nearest equilibrium point to a specified operating point in which the system is working most of the time. This linearization does not introduce significant errors because of the small temperature range in building, which will be shown in next session. Then the linear building model in state space form is discretized to get the following:

$$x_{k+1} = Ax_k + Bu_k + Ed_k \tag{6.22}$$

$$y_k = Cx_k \tag{6.23}$$

where x_k is the state vector denoting the temperature of the nodes in the thermal network at time k, y_k is the output vector of system including all zone temperatures, u_k represents the vector of controllable input at time k and d_k stores the uncontrollable inputs and system disturbance at time k.

6.5.4 Parameters Identification and Model Validation

From the above developed thermodynamic model for building, it is obvious that there are a great amount of independent parameters (e.g. R_{wi}, $R_{in\,i}$, $R_{out\,i}$, etc.) need to be identified, which significantly increase the computational efforts. However, it should be noted that the thermal properties of the material of wall and window are reasonably assumed to be the same throughout the building, and the same also applies to the thickness of internal walls and peripheral walls. Therefore, the R-values of inside air film, outside air film, wall and window are assumed to remain constant across the building. Hence, the number of

independent parameters in the model can be greatly reduced. R-value being discussed in building and construction industry is the unit thermal resistance, and it is a widely adopted quantity in the area of building design. With this assumption, the parameter identification process only needs to identify the R-value of the building instead of identifying all the thermal resistances for all zones and all walls. In order to get the thermal resistance of an entire section of material for the purpose of the thermodynamic model, the R-value should be divided by the area of the material, in other words,

$$R_{W_i} = \frac{R_{value}^{wall}}{A_{W_i}} \tag{6.24}$$

$$R_{in_i} = \frac{R_{value}^{in}}{A_{W_i}} \tag{6.25}$$

$$R_{out_i} = \frac{R_{value}^{out}}{A_{W_i}} \tag{6.26}$$

$$R_{win_i} = \frac{R_{value}^{in} + R_{value}^{glass} + R_{value}^{out}}{A_{win_i}} \tag{6.27}$$

Therefore, the model parameters that need to be estimated include the thermal capacitances of zones and walls, R-value of wall, glass, insider air film and outside air film of the building.

Table 6.3 Results of parameter identification for Example Zone 1

Parameter	Value (Unit)
C_{r1}	1.673×10^3 *(kJ/K)*
C_{w1}	2.707×10^4 *(kJ/K)*
C_{w2}	2.73×10^4 *(kJ/K)*
C_{w3}	1.895×10^4 *(kJ/K)*
C_{w4}	3.898×10^4 *(kJ/K)*
R_{value}^{wall}	1.659 (m.K/W)
R_{value}^{glass}	0.124 (m.K/W)
R_{value}^{in}	0.062 (m.K/W)
R_{value}^{out}	2.149 (m.K/W)

The historical data (e.g. measured zone temperature, outside air temperature, supply air temperature, airflow etc.) collected from a real commercial building at University of California at Berkeley, was used to simulate the behavior of thermal dynamic in that building. Using the representative R-values from ASHRAE handbook [171] as initial values, the *fmincon* function in MATLAB was used to solve for the optimal parameters by an optimization problem which minimizes the difference between the simulated temperature obtained from the thermodynamic building model and the measured temperature of the zone, taking into account the constraints on the parameters. The results of parameter identification for Example Zone 1 are shown in Table 6.3. Then using the HVAC input and disturbance data from another day, the zone temperature is simulated by the building model with identified parameters and compared with the measured temperature.

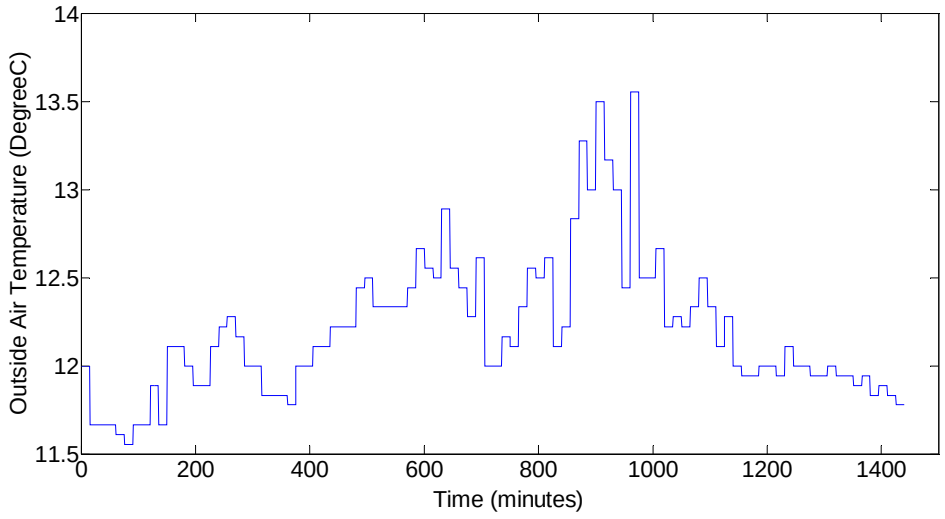

Fig. 6.9 Outside air temperature [170]

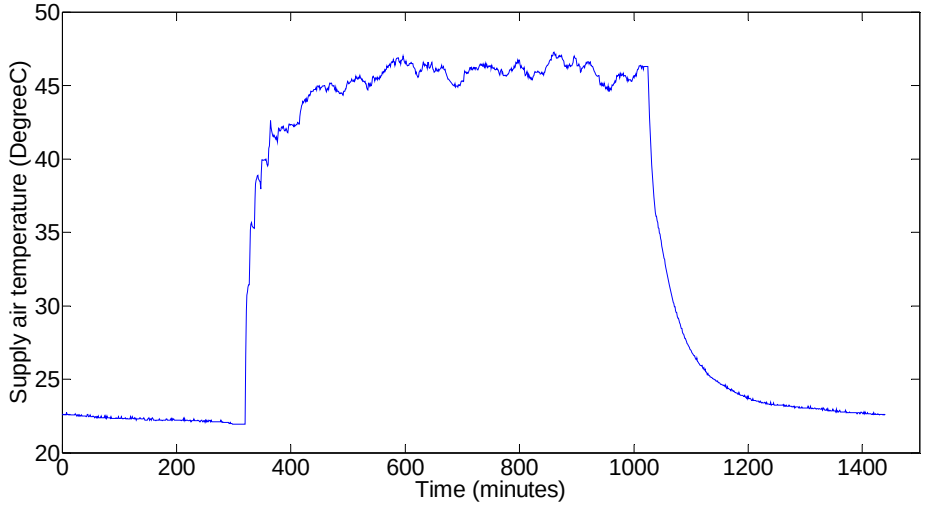

Fig. 6.10 Measured supply air temperature of HVAC system [170]

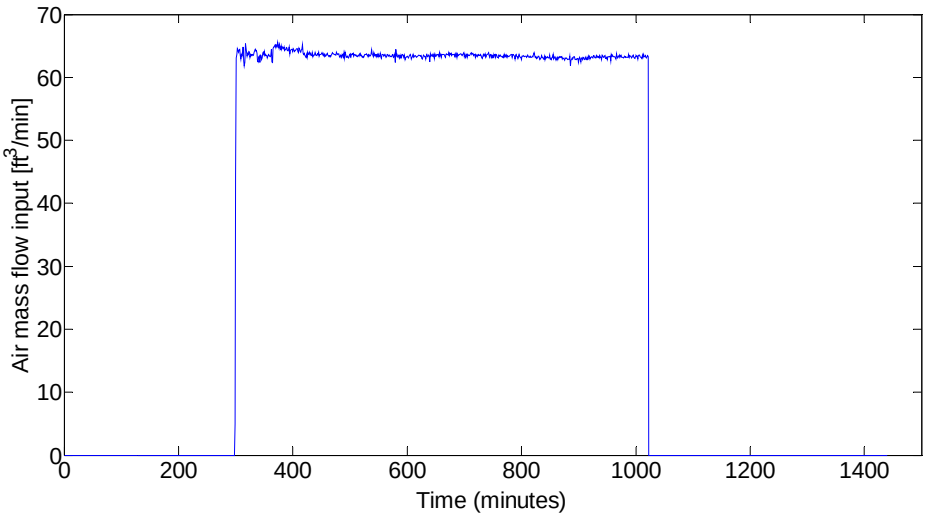

Fig. 6.11 Measured air mass flow of HVAC system [170]

The accuracy is quantified by the mean absolute percentage error (MAPE) and the mean absolute error (MAE) as follows:

$$\text{MAPE} = \frac{1}{n}\sum_{i=1}^{n}\frac{\left|T_{i,m} - T_{i,s}\right|}{T_{i,m}} \times 100\% \tag{6.28}$$

$$\text{MAE} = \frac{1}{n}\sum_{i=1}^{n}\left|T_{i,m} - T_{i,s}\right| \tag{6.29}$$

where $T_{i,m}$ and $T_{i,s}$ are the measured temperature and simulated temperature by the building model, respectively. As depicted in Fig. 6.12, in 24 hours simulation, the identified building model can accurately predict the temperature dynamics in the building with a maximum absolute error of 0.46°C which is hardly noticeable by occupants. Besides, the fact that MAPE is 0.58% and MAE is 0.12 also validates the accuracy of building model. Given the variation range of HVAC inputs as presented in Fig. 6.10 and Fig. 6.11, the range of indoor temperature of building is about 19-22 °C as depicted in Fig. 6.12, which is not very wide, thus the linearization does not cause significant errors.

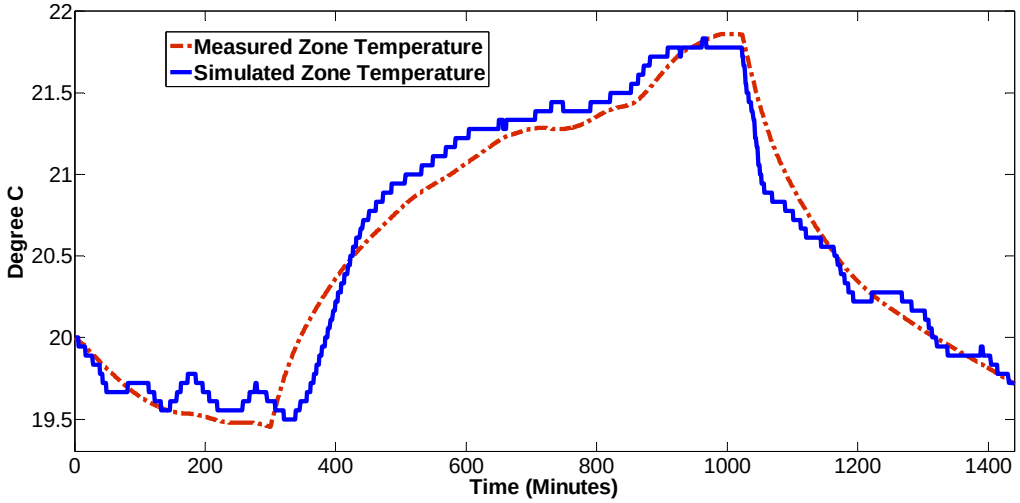

Fig. 6.12 Comparison between measured and simulated zone temperature [170]

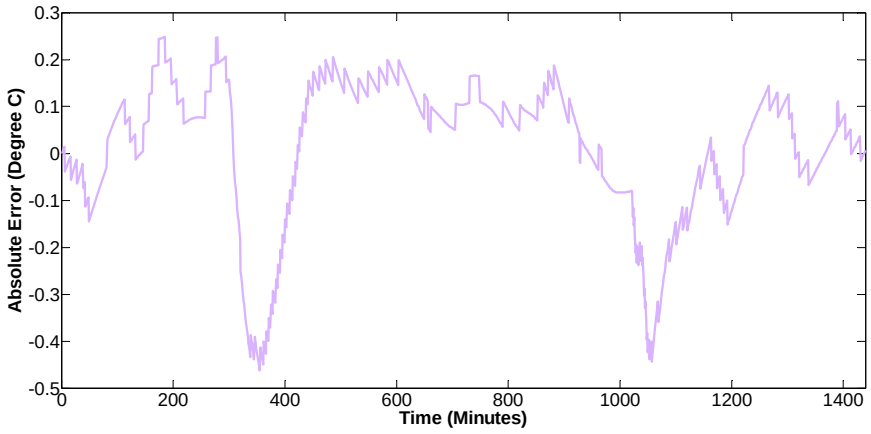

Fig. 6.13 Absolute error (simulated zone temperature minus measured zone temperature) [170]

6.5.5 Aggregation of thermodynamic building model

The model in Equation (6.22)-(6.23) can be generalized to represent a group of buildings, each with a label number *i*, in other words, the thermodynamic model for building *i* is as follows:

$$x_{k+1}^{i} = A_i x_k^i + B_i u_k^i + E_i d_k^i \tag{6.30}$$

$$y_k^i = C_i x_k^i \tag{6.31}$$

where superscript *i* refers to the label number of a building.

The above thermodynamic single building model can be aggregated by a building aggregator in order to aggregate adequate capacities to participate in the balancing market to provide ancillary service via demand response program, which will be discussed later in this thesis. The building aggregator would essentially merge the dynamic models and constraints of all concerned buildings into a large system to do the centralized optimization. The aggregated matrices are block diagonal because the dynamics of individual building are independent with each other by assuming no communication exists between buildings, the buildings are coupled through the cost function as will be discussed in Chapter 7. The aggregator building model with total number *L* buildings would be

$$x_{k+1}^{agg} = A_{agg} x_k^{agg} + B_{agg} u_k^{agg} + E_{agg} d_k^{agg} \tag{6.32}$$

$$y_k^{agg} = C_{agg} x_k^{agg} \tag{6.32}$$

Where

$$x_k^{agg} = \begin{pmatrix} x_k^1 \\ x_k^2 \\ \vdots \\ x_k^L \end{pmatrix}, y_k^{agg} = \begin{pmatrix} y_k^1 \\ y_k^2 \\ \vdots \\ y_k^L \end{pmatrix}, u_k^{agg} = \begin{pmatrix} u_k^1 \\ u_k^2 \\ \vdots \\ u_k^L \end{pmatrix}, d_k^{agg} = \begin{pmatrix} d_k^1 \\ d_k^2 \\ \vdots \\ d_k^L \end{pmatrix} \tag{6.32}$$

$$A_{agg} = \begin{bmatrix} A_1 & \cdots & \cdots & 0 \\ 0 & A_2 & \ddots & 0 \\ \vdots & \ddots & \ddots & \vdots \\ 0 & \cdots & 0 & A_L \end{bmatrix}, B_{agg} = \begin{bmatrix} B_1 & \cdots & \cdots & 0 \\ 0 & B_2 & \ddots & 0 \\ \vdots & \ddots & \ddots & \vdots \\ 0 & \cdots & 0 & B_L \end{bmatrix},$$

$$E_{agg}=\begin{bmatrix} E_1 & \cdots & \cdots & 0 \\ 0 & E_2 & \ddots & 0 \\ \vdots & \ddots & \ddots & \vdots \\ 0 & \cdots & 0 & E_L \end{bmatrix}, C_{agg}=\begin{bmatrix} C_1 & \cdots & \cdots & 0 \\ 0 & C_2 & \ddots & 0 \\ \vdots & \ddots & \ddots & \vdots \\ 0 & \cdots & 0 & C_L \end{bmatrix} \tag{6.33}$$

6.6 Chapter Summary

Due to the lack of accurate models describing thermal behavior of buildings in power engineering community, substantial literature in the area of building climate control and building construction has been reviewed, and this chapter introduces a mathematical R-C thermodynamic model of building based on fundamental laws of Heat Transfer and Thermodynamic that is suitable for control design with acceptable computational burden. This model serves as a bridge linking the areas of power engineering and building climate control together to provide more flexible demand and facilitate more advanced DSM programs in smart grid. The fundamental laws of Heat Transfer and Thermodynamics (e.g. heat conduction, convection and radiation) which dominates the temperature dynamics inside a building are first introduced. Then the R-C model consisting of a series of heat transfer equations is presented to describe the temperature dynamics in a room and is extended to create a large R-C model which represents the whole building. The introduced model is then linearized and calibrated using historical data from a real existing building and the accuracy of the proposed thermodynamic model is lastly validated by the comparison between the simulated results and the real measurements. This chapter is the foundation for Chapter 7, and the MPC controller designed in the Chapter 7 is implemented based on this thermodynamic model.

Chapter 7

Design of Model Predictive Controller Based on Thermodynamic Building Model for Demand Side Management in Smart Grid

7.1 MPC for Energy Efficiency Improvement and Peak Load Reduction

The growing penetration of intermittent renewable energy sources (e.g. solar, wind power) will increase the need for inefficient peaking generation and generator-provided ancillary services, which greatly stresses existing power grid.

Traditionally, generators are responsible for stabilizing the system frequency in the presence of power imbalances due to errors in predictions of generation or demand. However, it is a new trend in the power industry to also exploit the demand side resources, known as demand response (DR). The key idea of DR is to manage local power consumption of flexible load in response to supply conditions, e.g. high market price, peak demand or regulation signal. Intelligent and flexible demand resource with new technologies and control algorithms will allow pro-active rather than reactive participation in demand events to provide substantial demand elasticity, which will increase utilization of renewable generation sources. It can be expected that, in the future, loads will no longer dictate demand, rather become participants in eliminating supply-demand imbalances.

Buildings are responsible for more than 70% of total U.S. electricity consumption [99], and they are increasingly becoming more smart energy consumers and active participants in electric grid operations, such as pre-

cooling/discharging heuristics [172], model predictive control in day-ahead/real-time energy markets [173], non-spinning reserves [174], spinning reserves [175], frequency regulation [176-177]. In particular, commercial buildings have much larger thermal mass and heating ventilation air conditioning system (HVAC), besides, HVAC system consumes up to 50% power consumption of a commercial building to guarantee the air supply while keep the indoor temperature within comfort range [169] and the widely adopted Building Automation System enables easy local control, commercial buildings have a great potential to provide operating reserve by loosening the desired temperature range or adjusting the operating power.

Therefore, the thermodynamic building model introduced in Chapter 6 that can accurately capture indoor temperature dynamics inside the building will increase predictability and enable advanced control, thus, play a significant role in demand side management by representing the buildings in aggregate as a large dispatchable resource when the operation of HVAC system is coordinated with power grid needs.

In this chapter, an economic model predictive controller based on the presented thermodynamic building model is designed to modulate the power consumption of commercial building HVAC system in response to varying electricity price, simulation results demonstrate that peak load can be effectively and substantially curtailed and shifted to non-peak hours, besides, energy saving and energy efficiency can also be significantly improved.

7.1.1 Classical Control Methodologies for HVAC

On-off control and Proportional-Integrator-Derivative (PID) control are two classical control techniques for HVAC system, both of which have low costs and simple structure. On one hand, On-off control works only on two operating conditions, i.e. “on” or “off”, representing maximum and zero power

consumption, and this limited functionality makes on-off control method inaccurate and of low quality. On the other hand, the PID controllers have been widely adopted in many HVAC systems due to the advantages such as zero steady state offset and disturbance rejection [167], however, it is very difficult and time-consuming to tuning nested PID loops controller with multiple inputs and outputs, especially for large-scale coupled buildings [167]. In addition, these classical controllers usually set HVAC systems to work at a particular designed thermal loading [178], but the thermal loading in reality should be varying with time, occupancy levels and outside weather conditions.

7.1.2 Overview of Model Predictive Control

Model predictive control (MPC) can systematically deal with large-scale dynamically coupled systems with multiple inputs and outputs subject to the system operating constraints (e.g. state and input constraints) with performance guarantees, taking into account future predictions. The main idea of MPC is to utilize the plant model to predict the future system evolution. An open-loop optimization problem is solved at each sampling time over a finite horizon, and the optimized control signal is applied to the plant model to update the system states only during the next sampling interval. A new optimization problem based on new measurements of state and new prediction of future disturbance is solved over a shifted horizon [167].

MPC is advantageous over the conventional control techniques due to its 1) prediction capability; 2) reduced number of parameters for tuning; 3) capability of optimizing at a system level; 4) capability to maintain satisfactory performance at all operating conditions.

For control problems with multiple variables and complex constraints, MPC has successfully become the accepted standard in the process industries because of its unique ability to deal with hard constraints on states and control inputs in a

simple and effective manner. Consider the following model based optimal control problem to minimize the overall energy consumption

$$\min_{u} \sum_{k=0}^{k=N-1} E(x_{t+k|t}, u_{t+k|t}, d_{t+k|t}) \tag{7.1}$$

$$x_{t+k+1|t} = f(x_{t+k|t}, u_{t+k|t}, d_{t+k|t}), \forall k = 0,1,...,N-1 \tag{7.2}$$

$$y_{t+k|t} = g(x_{t+k|t}, u_{t+k|t}, d_{t+k|t}), \forall k = 0,1,...,N \tag{7.3}$$

$$u_{t+k|t} \in \mu, \forall k = 0,1,...,N-1 \tag{7.4}$$

$$y_{t+k|t} \in \gamma, \forall k = 0,1,...,N \tag{7.5}$$

Where *f(x,u,d)* allows to predict the future system states based on the current control inputs, states and disturbance. *E(x,u,d)* represents the relationship between the energy consumption and system states, inputs and disturbances. The variables with subscript $t+k|t$ can be read as the variable at time $t+k$ predicted at time t, x is the system states, y is the system outputs, N is the prediction horizon, u represents the control inputs of system, d stores uncontrollable inputs and system disturbances (exogenous signals).

In buildings, load shifting incorporating MPC can be used to reduce energy consumption and improve efficiency performance for HVAC system by shaping the building load profile using the inherent thermal storage of building to store thermal energy for later use.

7.1.3 HVAC Power Consumption Models

As shown in Fig. 6.4, HVAC supply fans are the main driver that distributes the conditioned air that heated or cooled by the heating coils or cooling coils to the rooms inside the building. Hence, the power consumption of HVAC system mainly consists of fan power P_t^f, heating coil power P_t^h, and cooling coil power P_t^c at time t. There are many types of model for the HVAC system in the literature of building climate control area, one of the most popular models is adopted in this thesis. According to [167], the fan power can be approximated as

a polynomial function of the total mass flow rate of supply air $\dot{m}_{f,t}$ (sum of airflow to each zone) driven by the fan to *n* number of zones.

$$P_t^f = c_1 \cdot \dot{m}_{f,t}^3 + c_2 \cdot \dot{m}_{f,t}^2 + c_3 \cdot \dot{m}_{f,t} + c_4 \tag{7.6}$$

$$\dot{m}_{f,t} = \sum_{i=1}^{n} \dot{m}_{Zi,t} \tag{7.7}$$

where c_1, c_2, c_3, c_4 are parameters that identified by fitting the recorded data (including the power consumption of supply fan and the air volume flow rate) from a real commercial building at California as validated in Fig. 7.1. The data was collected from Jan. 2013 to Aug. 2013 to identify these four parameters, which also shows that the power consumption of the supply fan with rated power 134 kW accounts for about 15% of electricity consumption in that building.

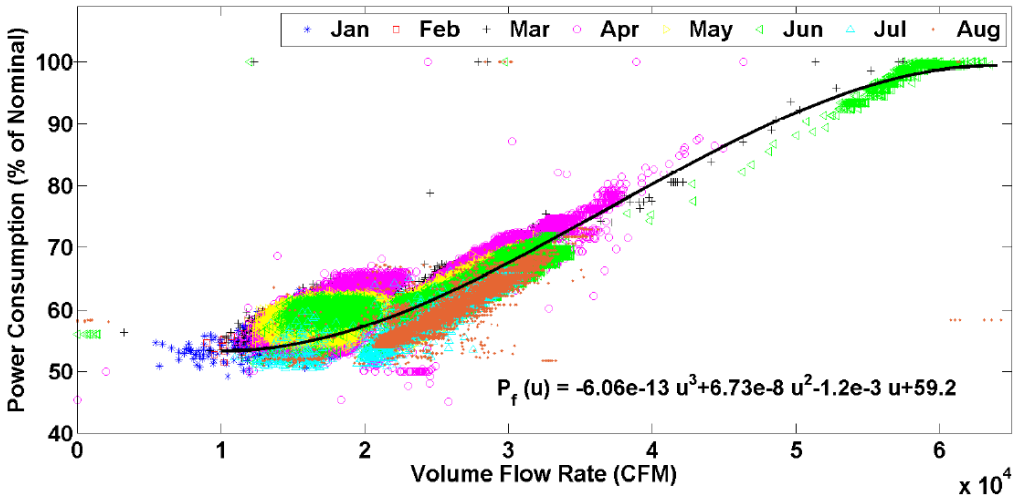

Fig. 7.1 Relationship between fan power consumption and air volume flow rate [167]

Assuming there is no air recirculation, according to [179], the heating power and cooling power at time *t* are:

$$P_t^h = \sum_{i=1}^{n} c_a \cdot \dot{m}_{Z_i,t} \cdot \left(T_{S_i,t} - T_{out,t}\right) \Big/ COP_h \tag{7.8}$$

$$P_t^c = \sum_{i=1}^{n} c_a \cdot \dot{m}_{Z_i,t} \cdot \left(T_{out,t} - T_{S_i,t}\right) \Big/ COP_c \tag{7.9}$$

where COP_h and COP_c are the coefficients of performance for the heating system and cooling system, respectively.

7.1.4 Economic MPC for Flexible HVAC Power Consumption

In the context of optimal control of buildings, MPC offers a powerful tool for model-based control of HVAC system, it has been widely adopted in the area of building climate control, but their objectives mainly aim at minimizing the HVAC power consumption, while the researchers in the area of power engineering prefer to modulating the load profiles of HVAC system in a more flexible manner, which enables the buildings to participate into the balancing market to play an important role in power system operation. In this part, we propose an economic MPC controller based on the thermodynamic building model introduced in Chapter 6 of this thesis, to utilize the time-varying electricity prices and the future disturbances to minimize the electricity costs, significantly reduce the peak demand and increase energy saving and efficiency, while respecting the comfort level.

Due to the fact that the temperature dynamics in commercial building are fairly slow, while the power consumption of HVAC system can be varied rapidly, with provided time-varying electricity prices, the building thermal capacity can be exploited to shift the power consumption to the period with low electricity prices in order to minimize the electricity cost, while maintaining the indoor temperatures within certain limits. The economic MPC has the ability to choose the optimal heating/cooling strategy in response to the time-varying energy price and the prediction of the disturbances. Consider the following optimization problem for a single building:

$$\min_{\bar{u}_t} \sum_{k=0}^{T_p-1} C_{t+k}^{hvac} \tag{7.10}$$

$$\text{s.t. } C_{t+k}^{hvac} = \beta_{t+k}^{e} P_{t+k}^{f} + \beta^{ne,\mathrm{h}} P_{t+k}^{h} + \beta^{ne,c} P_{t+k}^{c}, \quad k = 0,...,T_p - 1 \tag{7.11}$$

$$x_{t+k+1} = Ax_{t+k} + Bu_{t+k} + Ed_{t+k}, \qquad k = 0,...,T_p - 1 \tag{7.12}$$

$$y_{t+k} = Cx_{t+k}, \qquad k = 1,...,T_p \tag{7.13}$$

$$\underline{u}_{t+k} \le u_{t+k} \le \overline{u}_{t+k}, \qquad k = 0,...,T_p - 1 \tag{7.14}$$

$$\underline{T}_{t+k} \le y_{t+k} \le \overline{T}_{t+k}, \qquad k = 1,...,T_p \tag{7.15}$$

where β_t^e is the time-varying electricity prices at time t, $\beta^{ne,h}$ and $\beta^{ne,c}$ are the fixed non-electric energy price (e.g. natural gas) for heating and cooling, respectively. $\overline{T}_{t+k}$ and $\underline{T}_{t+k}$ are the upper lower limits on the temperatures in each room, respectively. $\overline{u}_{t+k}$ and $\underline{u}_{t+k}$ are the upper and lower bounds on the air mass flow rate into each zone, respectively. Minimum non-zero airflow is essential for ventilation purpose. In this study, we only investigate the potential of providing flexible electrical power consumption via the control of supply fan in HVAC system. Although we assume the heating/cooling coils are using non-electric energy, their costs still need to be considered since their power consumptions are related to the controllable airflow rate.

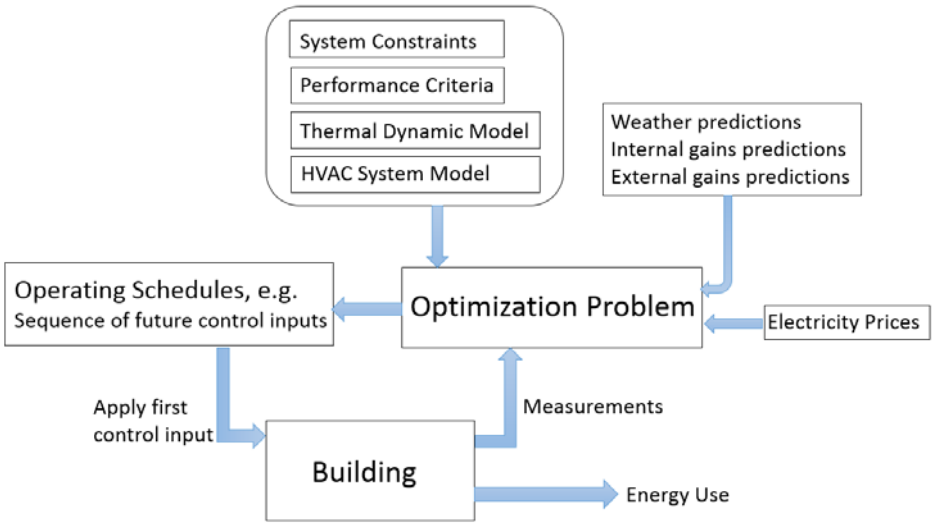

Fig. 7.2 Flowchart of proposed economic model predictive controller

As shown in Fig. 7.2, using the measurement of current states (e.g. indoor temperature, illumination) of the building as the initial states, and based on dynamic model, physical limits, design constraints and predicted disturbance, the economic MPC controller is implemented in a receding horizon manner, in

which the above optimization problem over a prediction horizon T_p (24 hours in this work) is solved at each time step to calculate the optimal input sequence $\vec{u}_t^* = [u_t^*, ..., u_{t+T_p-1}^*]$ for the entire horizon, only the first element u_t^* of the optimal input vector will be applied. At the following time step, the prediction horizon of MPC is then receded by one time step, a updated MPC problem is formulated for the next T_p time steps with new states and new prediction of disturbances, and solved for the new optimal input sequence $\vec{u}_{t+1}^* = [u_{t+1}^*, ..., u_{t+T_p}^*]$, out of which again only the first element will be applied and the horizon is receded to repeat the whole process until the interested period is covered.

7.1.5 Case Studies and Simulation Results

Due to the weather condition at the location of the considered building, only heating mode of HVAC system is needed. However, the proposed method also applies to cooling mode. Fig. 7.3 and Fig. 7.4 shows the supply air temperature of air handling unit and the outdoor air temperature over the simulation period, respectively, these are assumed to be the same for all case studies.

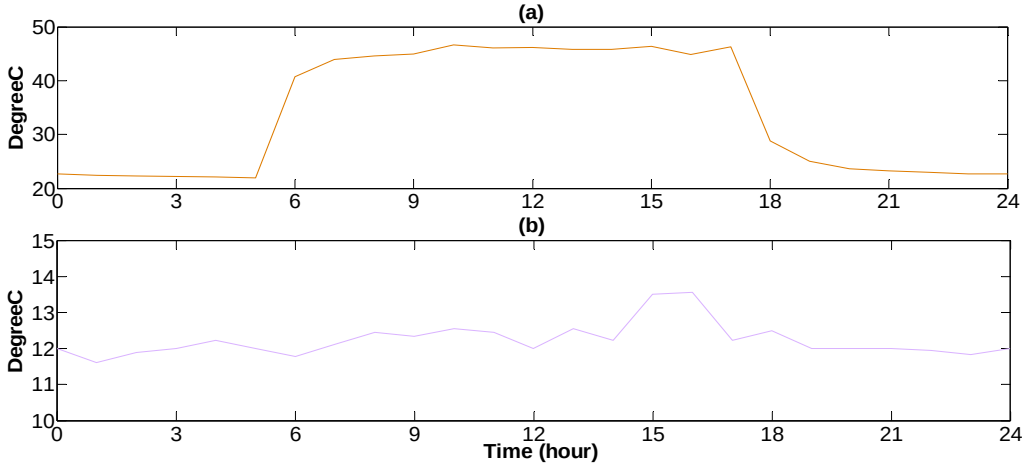

Fig. 7.3 (a) Supply air temperature of air handling unit; (b) Outdoor air temperature

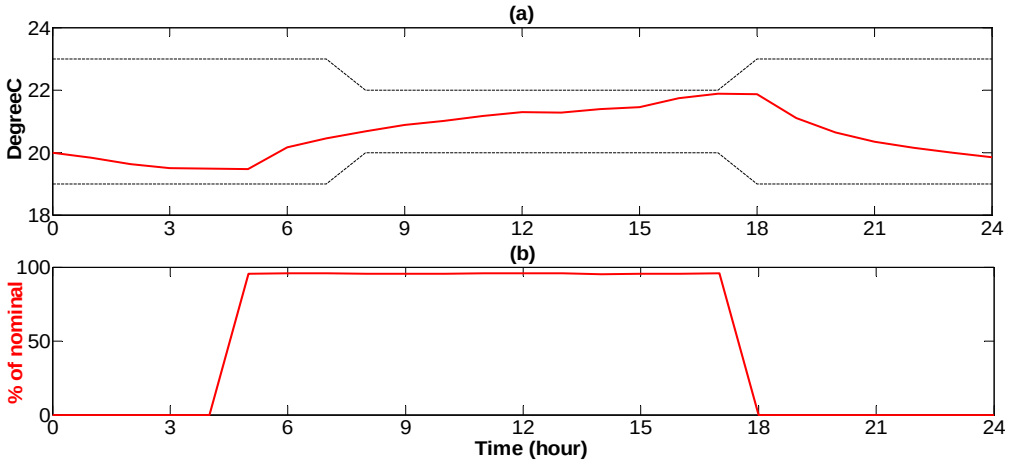

Fig. 7.4 (a) Measured indoor temperature using the original controller; (b) HVAC fan power consumption using the original controller

7.1.5.1 Original Existing Controller

The way the original controller works on the existing building is as follows: the controller releases the valves of conditioned air at 5:00 a.m. and maintains fully opened until 5:00 p.m., which unwisely lets the HVAC fan run at nearly rated power, driving the conditioned air flow to the thermal zones, and closes for the rest of the day. The discharge air temperature of HVAC system is kept constant at about 47°C during that time period as shown in Fig. 7.3(a). Fig. 7.4 (a) and (b) shows the measured indoor temperature and the HVAC fan power consumption, respectively, using the original control method. This case is regarded as the base case and will be compared with the performance of MPC controller to demonstrate the effectiveness of MPC controller.

The comfort level is defined to be between 19°C and 23°C at night and between 20°C and 22°C during working hours (8a.m. - 5p.m.). If maintaining the comfort level during working hours is enough for the HVAC system, obviously substantial energy is wasted as the temperature keeps approaching the upper bound of temperature. Due to the wide acceptable range of indoor temperature, particularly during unoccupied periods, the temperature limits can be loosened.

Consequently, model predictive controller is proposed to leverage this flexibility to reduce the peak load while achieve more savings.

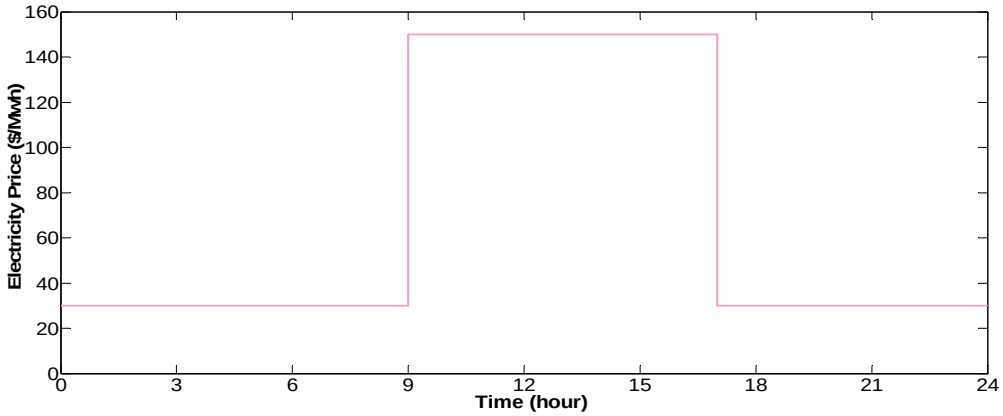

Fig. 7.5 Time-of-Use electricity price for Case 1 and Case 2

7.1.5.2 Model Predictive Controller

Economic MPC formulated in (7.10)-(7.15) is implemented on the presented building model, with a sampling time of 1 hour, a prediction horizon of 24 hours and a simulation length to 24 hours. The validated model parameters (e.g. thermal capacitances, constants in power consumption equations etc.) are taken from [84]. Yalmip toolbox is used to set up the MPC control problem in Matlab, the optimization problem in the formulated MPC problem is solved by Ipopt solver on a laptop with an Intel Core i7-4600U CPU 2.69 GHz processor and 8 GB random access memory.

For Case 1 and Case 2, the time-of-use (TOU) electricity pricing structure is set as \$150/MWh for 9a.m.-5p.m. and \$30/MWh for the rest of time, as depicted in Fig. 6. For Case 3, the day-ahead (DA) price data shown in Fig. 9 on a winter day retrieved from PJM [180] is used. In addition, we assume that we can only control the valve of air flow (i.e. control the air flow rate), and that the supply temperature of conditioned air remains unchanged as in Fig. 7.3(a).

1) *Case 1 – TOU pricing and restricted open time of air flow valve:* The valve of conditioned air flow is open from 5 a.m. to 7p.m. and closed for the rest of time.

   Compared with the results from original controller in Fig. 7.4, the peak load is substantially curtailed and shifted to the period with lower electricity price as presented in Fig. 7.6, moreover, the energy saving is huge because the proposed economic MPC strives to minimize the energy cost while respecting the comfort constraints by consuming more power to preheat the building to a higher temperature when the energy price is low (5a.m.-9a.m.), while using just enough energy to satisfy the comfort constraints when electricity price is high, so that less energy is needed during the peak load period with much higher energy price. Besides, it can be noticed that power consumption drops at 3p.m. because of the increase of the outdoor temperature and solar radiation, which helps to heat up the building. However, if multiple buildings happen to shift their partial peak load to the period between 5a.m. and 9a.m. at the same time, another undesirable peak load may be created in that period, one possible solution is to utilize the whole night time to preheat the buildings instead of using just a few hours before working hours, this leads to Case 2 as follows.

2) *Case 2 – TOU pricing and relaxed open time of air flow valve:* The valve of conditioned air flow is always open.

   Due to the relaxed open time of air flow valve, the building now can preheat or discharge thermal energy anytime during the day. Compared with Case 1, the load profile of Case 2 in Fig. 7.7 is even smoother since the peak load has been distributed to the whole night time. A coordinated optimal heating strategy among multiple buildings can be developed to avoid creating another undesirable peak load. However, it should be mentioned that, although sometimes this may increase a little overall

power consumption, it certainly helps to relief the peak load situation in power network.

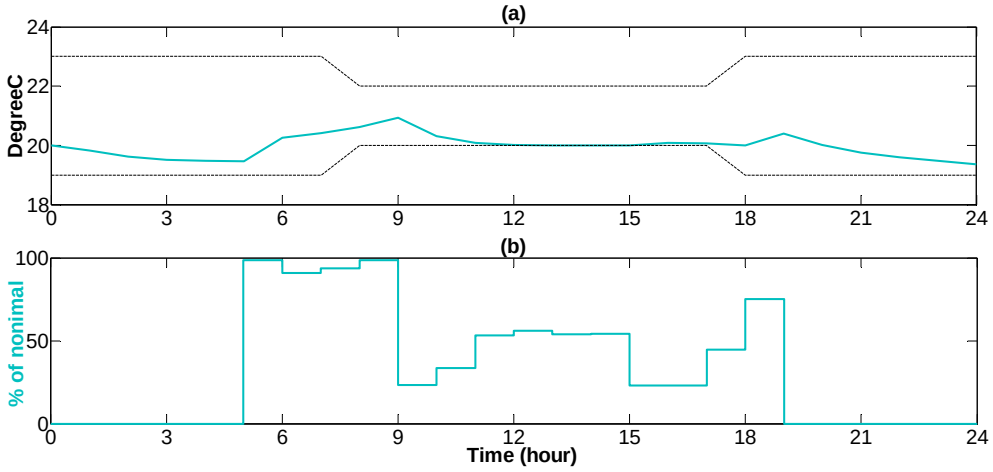

Fig. 7.6 Results of Case 1 using the proposed MPC controller: (a) Simulated indoor temperature; (b) HVAC fan power consumption

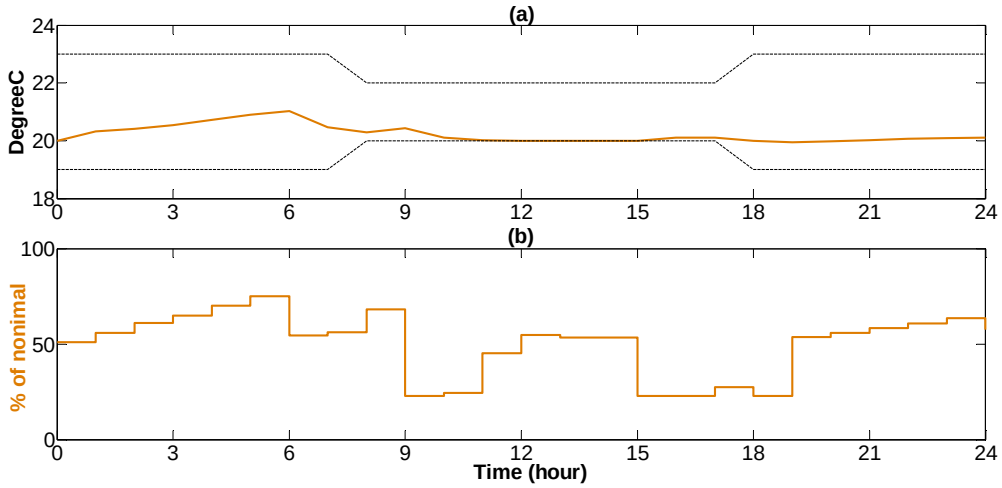

Fig. 7.7 Results of Case 2 using the proposed MPC controller: (a) Simulated indoor temperature; (b) HVAC fan power consumption

3) *Case 3 - DA pricing and relaxed open time of air flow valve:* DA pricing and relaxed open time of air flow valve: The valve of conditioned air flow is always open.

What we observe and discuss in Case 1 and Case 2 also applies to Case 3, as presented in Fig. 7.9, even though the real day-ahead price data is applied. For example, the period 7a.m.-9a.m. is the preheat period in both Case 1 and Case 2, however, because of the much high electricity price during this period in Case 3, the controller decides to preheat the building from 3a.m. to 6a.m., so that less energy is needed during the period with high electricity price.

Compared with the original control, about 50% of cost saving has been observed in the MPC simulation. From the results demonstrated in Fig. 7.6, Fig. 7.7 and Fig. 7.9, it can be concluded that the proposed economic MPC controller can effectively and optimally control the HVAC system to utilize the time-varying electricity prices and the future disturbances to minimize the electricity costs and significantly reduce the peak demand.

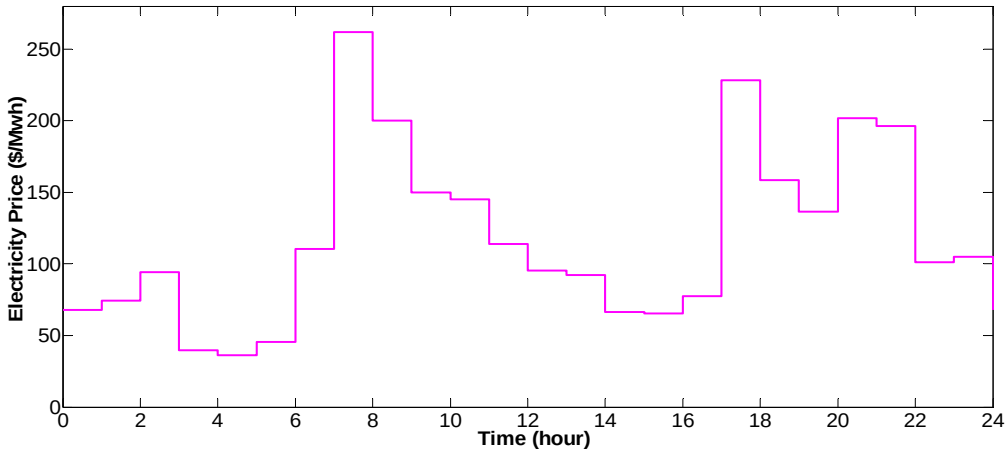

Fig. 7.8 Day-ahead electricity price for Case 3

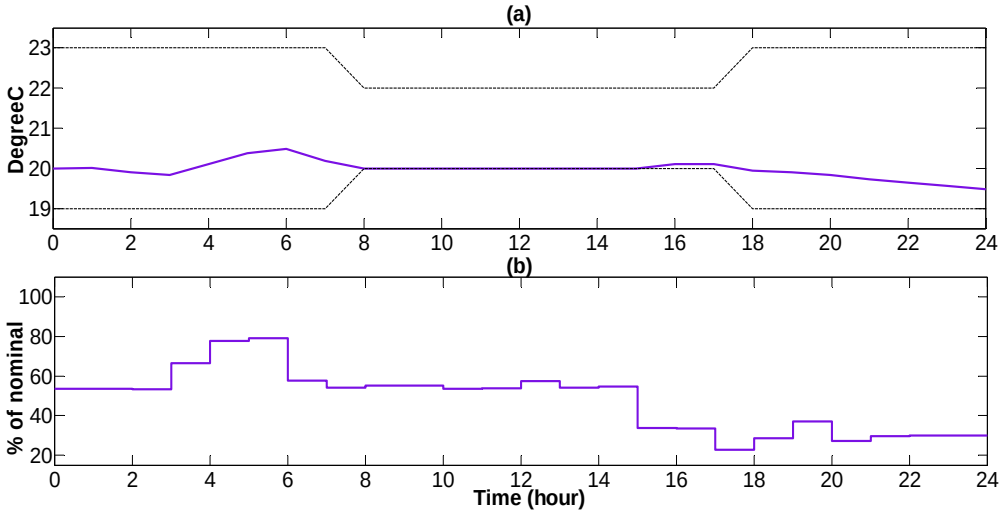

Fig. 7.9 Results of Case 3 using the proposed MPC controller: (a) Simulated indoor temperature; (b) HVAC fan power consumption

7.2 MPC of Aggregating Commercial Buildings for Providing Flexible Power Reserve

Smart grid will be subject to greater volatility and uncertainty due to the increasing reliance on the intermittent renewable energy sources (RES) [181-182]. An identified critical operational issue of significantly increasing the penetration level of RES is that both the capacity and ramp-rate of the regulation reserve are required to increase substantially for the continuous balance of supply and demand. However, in order to operate efficiently and reduce the wear and tear costs, the conventional regulating generators are limited by ramp-rate constraints, and they often fail to accurately track the area control error signal. Hence, a new trend is to exploit the flexible demand side resources that could provide more regulation reserve and the desired fast-response ancillary services (AS), known as demand response (DR).

The idea of DR is that end-use customers can actively participate in changing their electric use from the normal pattern and help to stabilize the system in response to supply conditions. Plug-in electric vehicle (EV) has been regarded as

a flexible energy option for AS provision [183-185], besides, buildings are also natural candidates because they account for 74% of total U.S. electricity consumption in 2013, 38% for residential buildings (RB) and 36% for commercial buildings (CB) [99]. Smart CBs should play a more important role in power system operation because, firstly, thanks to the much larger thermal mass and heating ventilation air conditioning system (HVAC) in a CB, it could offer a greater amount of DR than a RB could. Secondly, Building Energy Management System (BEMS) has been widely adopted in CBs, which enables direct communication with the building aggregator or the grid operator. AS provided by CBs can thus be obtained at low costs, without additional infrastructures such as smart meters. Lastly, variable frequency drives (VFD) are installed in most CBs to operate the HVAC supply fan (SF). Fan speed can be changed by BEMS continuously and frequently (in order of seconds), thus modulate fan power to track regulation signal [167, 169]. Reference [169] estimates that about 70% of the currently needed total regulation capacity in U.S. are potentially available from HVAC fan equipped with VFD in all CBs.

Existing literature on DR is mostly related to demand control in low frequency (i.e. peak load shaving/shifting). For example, a dynamic DR controller was proposed in [186] to reduce peak load of RBs by controlling HVAC set-points; the effectiveness of model predictive control (MPC) in reducing the energy costs for CBs is validated in [187-189], the peak load is effectively shifted away by precooling with time-of-use pricing; an electricity market with different DR penetration level from various CBs was simulated using agent-based modeling and simulation techniques in [190], showing that price-responsive demand has noticeable impacts on the electricity market. However, in order to provide AS to the grid, demand control in higher frequency (seconds to minutes) is needed. Aggregating thermostatically controlled loads in RBs for providing frequency regulation and load balancing services has attracted a lot of attention [81-82, 191-193], including the water heaters [81], heat pumps

[82], and small HVAC units [17]. Nonetheless, the literature on controlling CBs to provide AS is inadequate, to the best of our knowledge, [169] and [194] are two representative examples. A feasibility study of providing frequency regulation and non-spinning reserves by controlling dimmable lighting system in CBs is conducted in [194], and [169] showed the fan power of central HVAC in CBs can be manipulated up and down extremely fast to track the regulation signal without noticeable impacts on the indoor environment. However, the regulation signal is passively tracked by the controller designed in [169], which implies the provided flexibility may not be maximized and the building operator may be unwilling to participate without any incentives in real situation.

Reference [167] proposed a MPC control algorithm for a single commercial building to declare the power flexibility to the utility for direct load control in high frequency, nevertheless, the data transmission burden could be overwhelmed for the utility to aggregate the flexible power on large-scale since the power capacity of a single building is rather small. A feasible solution for this is to use distributed building aggregators to aggregate the flexible power of different groups of buildings in different areas, so that the utility only needs to communicate with the building aggregators. Therefore, in order to encourage more CBs to participate in AS market, we propose a contract framework between CBs, building aggregator and utility that can maximize and reward the flexible power reserve provided by CBs; we also design an optimal building aggregator that can aggregate the HVAC loads in CBs to declare the power flexibility to the utility for providing fast and large-scale regulating power to the smart grid. These are the main contributions of this work. In addition, the innovative characteristics of the proposed building aggregator lie in, 1) the ability of predicting the potential total reserve amount of HVAC loads in the target building group in a defined contract time; 2) the ability of allocating the high frequency regulation power received from the utility to each participating building while maintaining comfort levels. As compared to [167], we not only

investigate the feasibility of providing flexible power reserve by multiple commercial buildings instead of a single building, but also validate our proposed approach by incorporating real day-ahead price data and different temperature bounds for different buildings.

By storing excess renewable energy as thermal energy in the envelope of buildings, the flexible central HVAC loads in CBs can be utilized to absorb the variability associated with RES and increase the penetration level of RES. But an accurate thermodynamic building model is needed to capture temperature dynamics to ensure temperature constraints are satisfied. Therefore, another contribution of this work is that we review the building modeling techniques comprehensively and present a well-suited building model in details for providing flexible and fast-response power reserve.

7.2.1 Feasibility

As discussed before, the power consumption of HVAC system mainly consists of three components, including heating system, cooling system and supply fan. In Section 7.1, we have proposed a MPC controller to determine the optimal heating/cooling strategy to minimize the energy payment of the building without violating temperature constraints, where these three components are coordinated as a whole in order to reduce the peak demand and increase energy saving and efficiency. It demonstrates that smart buildings can become critical components in smart grid and play an important role in power system operation by some appropriate demand response programs, especially in eliminating the imbalance between supply and demand. However, this response is still not fast enough. In this chapter, we aim at investigating the much faster flexibility in power consumption HVAC systems, in particular, the power consumption of supply fan. We only investigate the potential of providing flexible and fast-response electrical power consumption via the control of supply fan of HVAC

systems, which accounts for approximately 15% of the total electric consumption in a large commercial building.

To the best of our knowledge, the feasibility of providing flexible and fast-response (in order of minutes or seconds) power reserve by the supply fan in HVAC system has only been studied in [167] and [169], which both showed that the fan power can be manipulated up and down extremely fast to track the regulation signal without noticeable impacts on the indoor temperature.

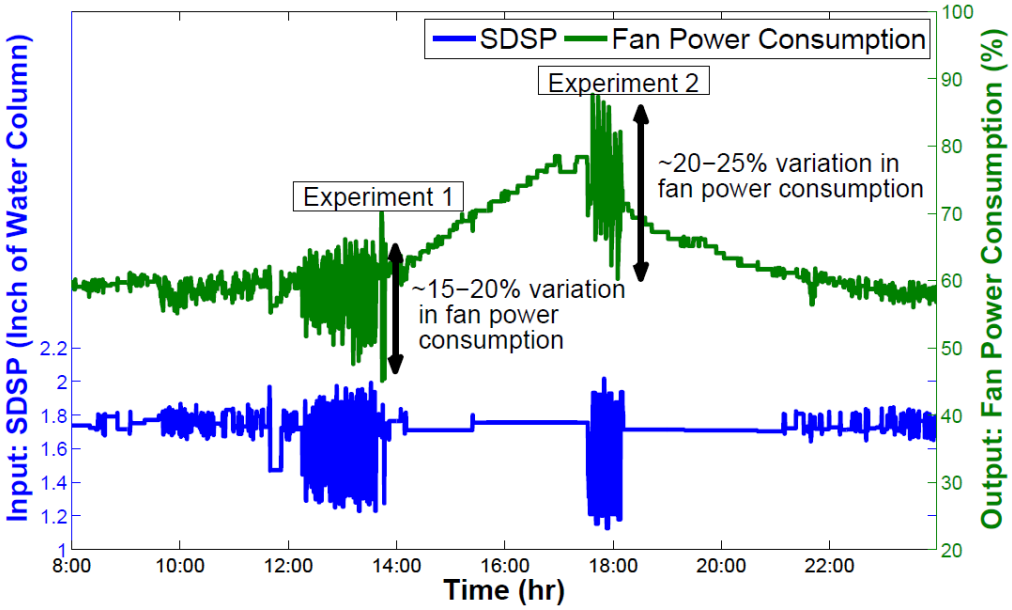

Fig. 7.10 Manipulation of the power consumption of supply fan [167]

In [167], an about 14000 square-foot commercial building installed with Siemens Building Management System named Apogee was used to conduct this feasibility experiment, this building has two sets of 9 supply fans with a total capacity of 134 kW. The Supply Duct Static Pressure (SDSP) set-point is used to keep the pressure inside the ducts of HVAC system (Fig. 6.4) around the pre-defined set-point and can be controlled by the Building Management System. The speed of supply fan can be varied via the control of the SDSP set-point. The speed of two sets of fans will increase to raise the pressure to the set-point if the

pressure drops below the set-point, and vice versa. Two experiments were conducted on 17 May, 2013, and the SDSP set-point was manipulated frequently and quickly within 1.2 and 1.9 inch Water Column during these two experiments, which should normally be maintained at 1.75 inch Water Column. Experiment 1 was conducted to randomly vary the SDSP set-point every minute at the period of about 12:00pm-14:00pm, while experiment 2 was conducted in the same procedure but every three minutes at the period of about 5:30pm-6:15pm. As depicted in Fig. 7.10, the power consumption of supply fan can be controlled by the SDSP set-point to change up to 25% around the nominal power within several seconds. Besides, Fig. 7.11 shows the indoor temperature of fifteen rooms randomly chosen was maintained with the user-defined comfort levels to demonstrate these experiments had no noticeable and sensible impacts on the indoor temperature inside the building. Hence, it is indeed feasible to use the existing BEMS software to control the power consumption of supply fan to track the high-frequency power regulation signals from utility.

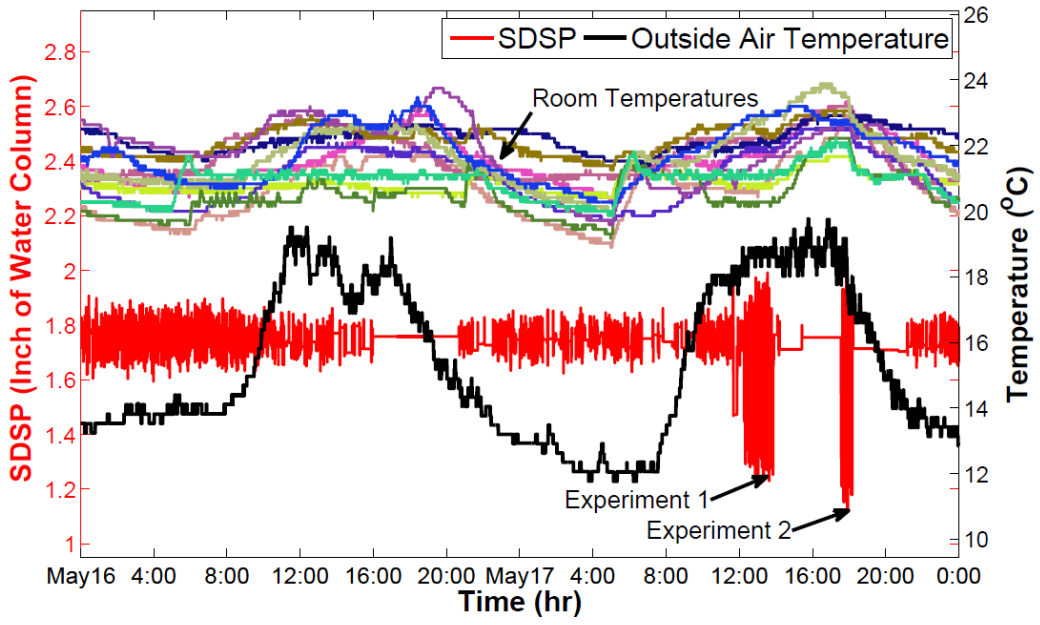

Fig. 7.11 Temperatures of 15 randomly selected rooms in the experiments [167]

Table 7.1 Nomenclature for BAG contractual framework

Symbol	Definition
β_t^e , β_t^{up} , β_t^{down}	Time-varying electricity price, upward flexibility reward rate, downward flexibility reward rate, respectively.
T_p	Prediction horizon.
T_c	Contract length.
$\vec{u}^*$, $\vec{u}^{lb}$, $\vec{u}^{ub}$	Baseline, low bound, and upper bound of input vector sequence of aggregated building model, respectively.
$P_t^{*f,i}$, $\underline{P}_t^{f,i}$, $\overline{P}_t^{f,i}$	Baseline, low bound, upper bound of HVAC fan power consumption for building *i* at time *t*, respectively.
$P_t^{*f,\mathrm{ag}}$, $\underline{P}_t^{f,\mathrm{ag}}$, $\overline{P}_t^{f,\mathrm{ag}}$	Baseline, low bound, upper bound of aggregated HVAC fan power consumption at time *t*, respectively.
$P_t^{f,\mathrm{up}}$, $P_t^{f,down}$	Total upward and downward flexibility of aggregated HVAC fan power at time *t*, respectively.
$\alpha_t^{i,\mathrm{up}}$, $\alpha_t^{i,down}$	Proportion of total upward and downward flexibility provided by building *i* at time *t*, respectively.
P_t^{reg}	Power regulation signal sent by utility at time *t*.
$P_t^{i,reg}$	Power allocated to building *i* according to the regulation signal received at time *t*.
φ_t^{down} , φ_t^{up}	Downward and upward flexibility of airflow at time *t*, respectively, i.e. $\vec{u}^{lb}=\vec{u}^*+\vec{\varphi}^{down}$, $\vec{u}^{ub}=\vec{u}^*+\vec{\varphi}^{up}$
$C_t^{hvac,ag}$	Total cost charged by utility for the baseline HVAC power consumption of the building group at time *t*.
$P_t^{*h,i}$, $P_t^{*c,i}$	Baseline heating power, and cooling power of HVAC system in building *i* at time t, respectively.
R_t^{ag}	Total reward to the buildings for flexible power at time *t*.
$\beta^{ne,\mathrm{h}}$, $\beta^{ne,\mathrm{c}}$	Fixed non-electric energy price (e.g. natural gas) for heating and cooling, respectively.
$\underline{T}_t$, $\overline{T}_t$	Lower and upper limits on building temperature at time *t*, respectively.
$\underline{u}_t$, $\overline{u}_t$	Lower and upper limits on the airflow into each zone at time *t*, respectively.

7.2.2 Building-Aggregator-Grid (BAG) Contract Framework

A certain amount of reserve from a CB can be provided as the AS via DR by increasing or decreasing HVAC fan power in response to the regulation signal from utility, without violating the specified comfort range [167, 169]. A single building cannot place bids on the balancing market due to the inadequate capacities, but an aggregation of CBs can be a viable solution.

According to a similar concept about EV aggregator proposed in [185], a building aggregator will strive to maximize its profit, which is a fixed percentage of the reward offered by utility for providing the power capacity for regulation. The regulation service is rewarded based on the available power capacity rather

than the actual dispatched energy because the regulation signal dispatched by grid operator fluctuating above and below zero generally averages out to approximately be zero over time. As the power capacity of aggregator is actually the sum of that of each building, consequently, the profits of the aggregator could be maximized by performing an optimal control such that each building offers as much power flexibility as possible whenever the regulation reward is high. Since the payment of each building is the cost for purchasing electricity minus the reward from the utility for providing flexibility, optimal HVAC control to minimize the payment of each building logically results in the maximum aggregator profits.

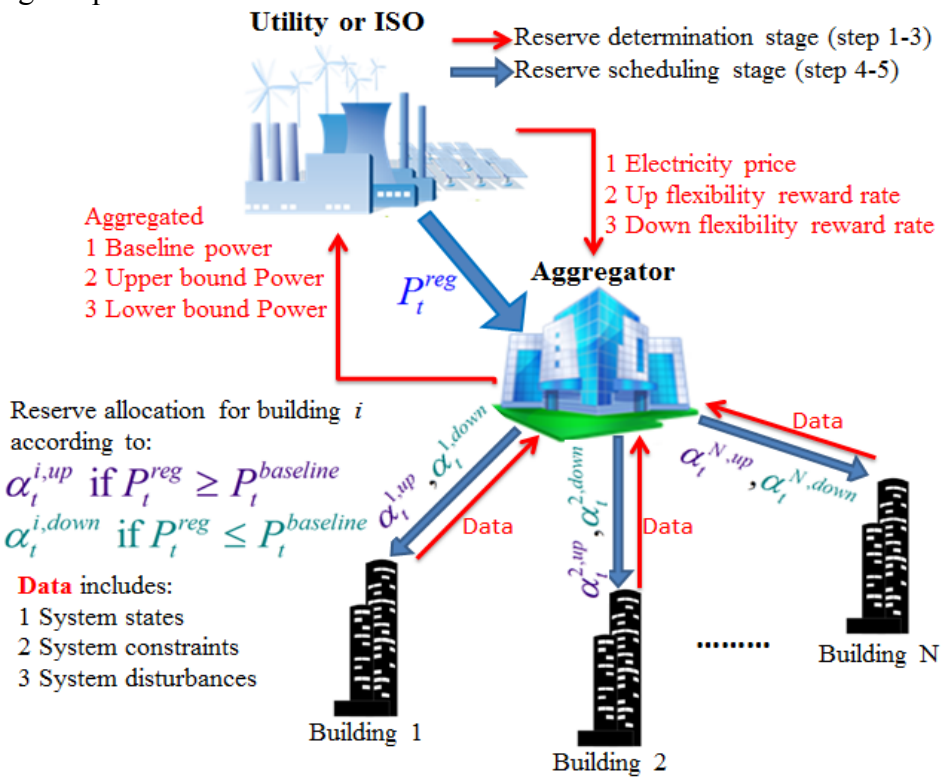

Fig. 7.12 The proposed architecture for BAG contractual framework schematic

By extending the work in [167, 169], we focus on two key functions that should be fulfilled by the building aggregator. Firstly, in the reserve determination stage, the aggregator needs to seek reward rate offers from utility, and then predicts the potential total reserve amount of the target building group

with the given incentives, along with the proportion that each building can provide. Secondly, in real-time reserve scheduling stage, the aggregator receives the high frequency regulation signal from utility and allocates the target amount to each building based on the proportion determined in previous stage.

Suppose the models of *N* number of buildings are aggregated into a system in the form of (6.30)-(6.31), the BAG contract is implemented by the following steps as shown in Fig. 7.12:

1) The utility or independent system operator (ISO) declares the time-varying electricity price β_t^e, upward flexibility reward rate β_t^{up}, and downward flexibility reward rate β_t^{down} for the next T_p time steps to the building aggregator, or they can be the aggregator bidding prices. Each involved building should also inform the aggregator of their corresponding measured or predicted disturbances (e.g. outside weather conditions and internal heat gains), state constraints (e.g. desired temperature ranges), and input constraints for the next T_p time steps, as well as the current states of building groups (i.e. zone temperatures).
2) By solving optimization problem (7.22)-(7.31), which will be discussed in Section 7.2.3, for the next time T_p steps, the building aggregator computes the *baseline* $\vec{u}^* = [u_0^*, ..., u_{T_p-1}^*]$, *lower bound* $\vec{u}^{lb} = [u_0^{lb}, ..., u_{T_p-1}^{lb}]$, and the *upper bound* $\vec{u}^{ub} = [u_0^{ub}, ..., u_{T_p-1}^{ub}]$ of input vector sequence of the aggregated building model, such that for any airflow profiles $\vec{u}_t = [u_0, ..., u_{T_p-1}]$, for all $t \in \{0,1,...,T_p-1\}$, $u_t^{lb} \le u_t \le u_t^{ub}$ is feasible, meaning no constraints are violated. Then the corresponding *baseline* $P_t^{*f,i}$, *lower bound* $\underline{P}_t^{f,i}$, and *upper bound* $\overline{P}_t^{f,i}$ of HVAC fan power consumption for building *i* at time *t* can be obtained using Equation (7.6). Therefore, at time *t*, the **total** *baseline* $P_t^{*f,\mathrm{ag}}$, *lower bound* $\underline{P}_t^{f,\mathrm{ag}}$, and *upper bound* $\overline{P}_t^{f,\mathrm{ag}}$ of aggregated HVAC fan power consumption is just the sum of $P_t^{*f,i}$, $\underline{P}_t^{f,i}$, $\overline{P}_t^{f,i}$, respectively, for $i \in \{1,...,N\}$. At time *t*, the **total** upward flexibility (UF) $P_t^{f,\mathrm{up}}$ and

total downward flexibility (DF) $P_t^{f,down}$ that the aggregator can provide are

$$P_t^{f,\mathrm{up}} = \overline{P}_t^{f,ag} - P_t^{*f,ag} \tag{7.16}$$

$$P_t^{f,down} = P_t^{*f,ag} - \underline{P}_t^{f,ag} \tag{7.17}$$

And the proportion of UF and DF provided by building *i* is

$$\alpha_t^{i,\mathrm{up}} = (\overline{P}_t^{f,i} - P_t^{*f,i}) / P_t^{f,\mathrm{up}} \tag{7.18}$$

$$\alpha_t^{i,down} = (P_t^{*f,i} - \underline{P}_t^{f,i}) / P_t^{f,\mathrm{down}} \tag{7.19}$$

3) The building aggregator and the utility agree upon a contract length T_c, which should be much smaller than T_p. Then the building aggregator only declares the first T_c elements of the *baseline* $P_t^{*f,\mathrm{ag}}$, *lower bound* $\underline{P}_t^{f,\mathrm{ag}}$, and *upper bound* $\overline{P}_t^{f,\mathrm{ag}}$ of aggregated HVAC fan power consumption profiles obtained from the previous step. The reason for only declaring a subset of computed power profiles is to reduce the negative effects of imperfect predictions of disturbance during the process.

4) In the next T_c time steps, the utility is allowed to send any power signal P_t^{reg} to building aggregator as long as $\underline{P}_t^{f,\mathrm{ag}} \le P_t^{reg} \le \overline{P}_t^{f,\mathrm{ag}}$, this signal may be sent as frequently as every few minutes or seconds.

5) The building aggregator has to obey the signal by scheduling the received power regulating signal to each building according to the proportions calculated in step 2. The power allocated to building *i* at time *t* will be

$$P_t^{i,reg} = \alpha_t^{i,\mathrm{up}} \times (P_t^{reg} - P_t^{*f,ag}), \text{ if } P_t^{reg} \ge P_t^{*f,ag} \tag{7.20}$$

$$P_t^{i,reg} = \alpha_t^{i,down} \times (P_t^{*f,ag} - P_t^{reg}), \text{ if } P_t^{reg} \le P_t^{*f,ag} \tag{7.21}$$

Tracking the power regulation signal by HVAC fan may lead the buildings to a worse state or consuming more power after T_c time steps. The utility has to offer proper incentives that can directly influence the reserve amount if it values the flexibility provided by buildings. Under the BAG contract, the buildings will be charged by the utility for their corresponding baseline power consumption at β_t^e, regardless of the actual allocated power that differs from the baseline. Then the utility rewards the aggregator and building group for the offered

flexibility at rate β_t^{up} and β_t^{down}, a fraction of the reward will be the profits of aggregator, and the rest of it will be divided for each building according to each own proportion of the provided aggregated flexibility. Therefore, the buildings, aggregator, and utility are all aware of how much each needs to pay or can earn from the beginning of the contract.

7.2.3 Robust Optimal MPC Control for Flexibility Determination

The key of the contract is to compute the *baseline* $\vec{u}^*$, *lower bound* $\vec{u}^{lb}$, and *upper bound* $\vec{u}^{ub}$ of input vector sequence of the aggregated system in step 2 mentioned before. At time *t*, the following robust optimal control problem is solved.

$$\min_{\vec{u}_t,\ \vec{\varphi}_t^{up},\ \vec{\varphi}_t^{down}} \max_{\vec{w}_t} \quad \sum_{k=0}^{T_p-1} (C_{t+k}^{hvac,ag} - R_{t+k}^{ag}) \tag{7.22}$$

$$C_{t+k}^{hvac,ag} = \sum_{i=1}^{N} (\beta_{t+k}^{e} \cdot P_{t+k}^{*f,i} + \beta^{ne,\mathrm{h}} \cdot P_{t+k}^{*h,i} + \beta^{ne,c} \cdot P_{t+k}^{*c,i}), \forall k = 0,...,T_p - 1 \tag{7.23}$$

$$R_{t+k}^{ag} = \beta_{t+k}^{down} \cdot P_{t+k}^{f,down} + \beta_{t+k}^{up} \cdot P_{t+k}^{f,up}, \forall k = 0,...,T_p - 1 \tag{7.24}$$

$$x_{t+k+1} = Ax_{t+k} + B(u_{t+k} + w_{t+k}) + Ed_{t+k}, \forall k = 0,...,T_p - 1 \tag{7.25}$$

$$y_{t+k} = Cx_{t+k}, \forall k = 1,...,T_p \tag{7.26}$$

$$\forall w_{t+k} \text{ s.t. : } \varphi_{t+k}^{down} \le w_{t+k} \le \varphi_{t+k}^{up}, \forall k = 0,...,T_p - 1 \tag{7.27}$$

$$\varphi_{t+k}^{down} \le 0, \forall k = 0,...,T_p - 1 \tag{7.28}$$

$$\varphi_{t+k}^{up} \ge 0, \forall k = 0,...,T_p - 1 \tag{7.29}$$

$$\underline{u}_{t+k} \le u_{t+k} \le \overline{u}_{t+k}, \forall k = 0,...,T_p - 1 \tag{7.30}$$

$$\underline{T}_{t+k} \le y_{t+k} \le \overline{T}_{t+k}, \forall k = 1,...,T_p \tag{7.31}$$

In this study, we only investigate the potential of providing flexible electrical power consumption via the control of HVAC supply fan (about 15% of electricity consumption in a large CB). Although we assume the heating/cooling coils are using non-electric energy, their costs still need to be considered since the control variable (airflow) affects their consumption.

Problem (7.22)-(7.31) is implemented in a receding horizon manner; it is firstly robustified by the inner maximization problem which finds the cost and constraints for the worst scenario. Then by incorporating future energy prices, reward rates, outside weather condition, comfort temperature ranges etc., $\vec{u}^{*}_{t+k}, \vec{\varphi}^{down}_{t+k}, \vec{\varphi}^{up}_{t+k}, \forall k = 0,...,T_p - 1$ are obtained by solving the outer minimization for a prediction horizon (T_P time steps) while no constraints are violated for any values of uncertainty variable *w* satisfying (7.27). With the obtained solutions, the aggregator computes the *baseline* $P^{*f,i}_{t+k}$, *lower bound* $\underline{P}^{f,ag}_{t+k}$, and *upper bound* $\overline{P}^{f,ag}_{t+k}$ of aggregated HVAC fan power for T_p time steps $(\text{i.e. } k = 0,...,T_p - 1)$ using (7.6)-(7.9), but only declares the first T_c elements $(\text{i.e. } k = 0,...,T_c - 1)$ to the utility. After T_c time steps, the aggregator receives the new building states caused by the power regulation signal sent by the utility and the new predictions of disturbances from buildings, then sets up and solves a new MPC problem for the time steps $k = T_c, T_c + 1,..., T_c + T_p - 1$, again declares the first T_c elements, i.e. $k = T_c, T_c + 1,..., 2T_c - 1$, and the horizon is receded to repeat this process until the interested time period is covered. In essence, the utility can control the HVAC supply fan power of a group of buildings for the next T_c time steps by sending flexibility signals to trigger this control algorithm.

7.2.4 Simulation and Results Discussion

7.2.4.1 Simulation Set-up and Base Case

The BAG contract framework and control algorithm proposed in Section 7.2.2 and Section 7.2.3 are implemented on the building model introduced in Chapter 6, with a sampling time of 1 hour, a prediction horizon of 24 hours and a simulation length to 24 hours. Yalmip toolbox [195] is used to set up the MPC control problem in Matlab, the non-linear optimization problem in the formulated

MPC problem is solved by Ipopt solver [196] on a laptop with an Intel Core i7-4600U CPU 2.69 GHz processor and 8 GB random access memory.

Owing to the weather condition at the location of the considered building, only the heating mode of HVAC is needed. However, the proposed method also applies to cooling mode. Due to space limitation, only three buildings are simulated to interact with a building aggregator and the utility under the BAG contract, but the proposed method certainly applies to the cases of more than three buildings. We take the building model parameters (e.g. thermal capacitances and R-values) from [167] for real Building 1 (BD1), and these parameters are increased and decreased by 20% to represent the hypothetical Building 2 (BD2) and Building 3 (BD3), respectively. For comparison purpose, Fig. 7.14 depicts the temperature and HVAC fan power of BD1 using original control method, which simply opens the airflow valve and unwisely lets SF run at nearly rated power driving the heated air to enter the building from 5:00 to 18:00. The measured supply air temperature and outdoor air temperature are shown in Fig. 7.13, assuming they are all the same for three buildings. The day-ahead price data on a winter day retrieved from PJM [180] is used as the electricity price, the regulation market clearing price data on the same day retrieved from PJM [180] is used to construct the downward flexibility reward rate (DFR) and upward flexibility reward rate (UFR), as shown in Fig. 7.15. The comfort temperature ranges for working hours (8:00-18:00) for BD1, BD2, and BD3 are [20°C, 22°C], [21°C, 21.5°C], and [21°C, 22°C], respectively, whereas the acceptable temperature ranges for non-working hours for BD1, BD2, and BD3 are [19°C, 23°C], [20.5°C, 22°C], and [21°C, 22°C], respectively. These temperature bounds are plotted as dash lines.

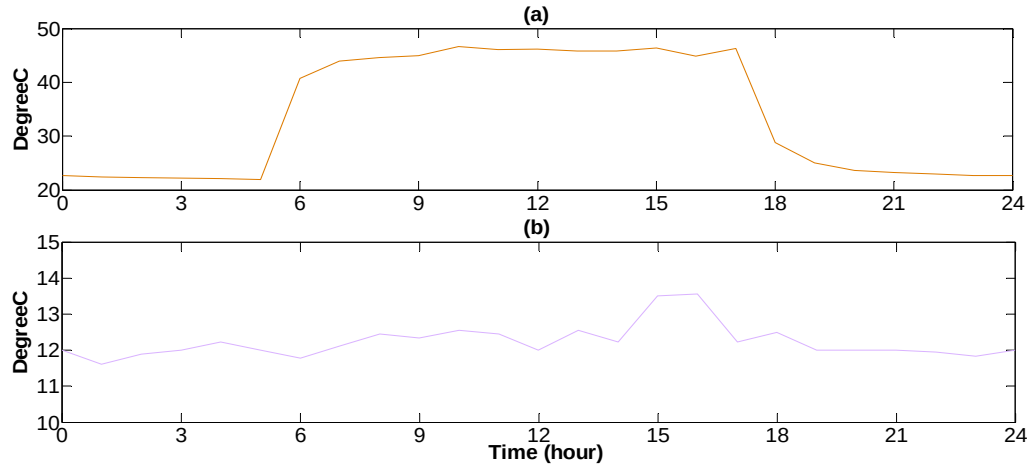

Fig. 7.13 (a) Supply air temperature of air handling unit; (b) Outdoor air temperature

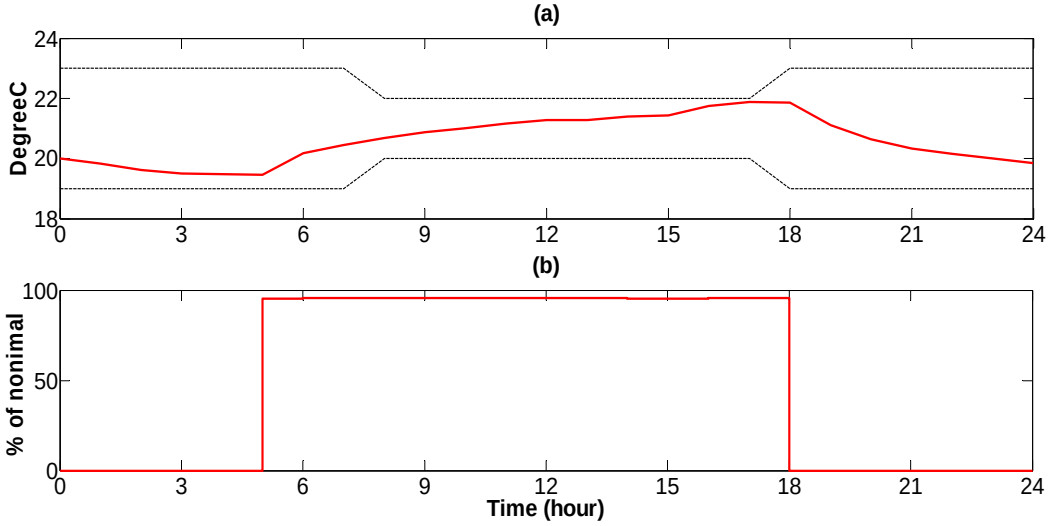

Fig. 7.14 (a) measured indoor temperature using the original controller; (b) HVAC fan power consumption using the original controller

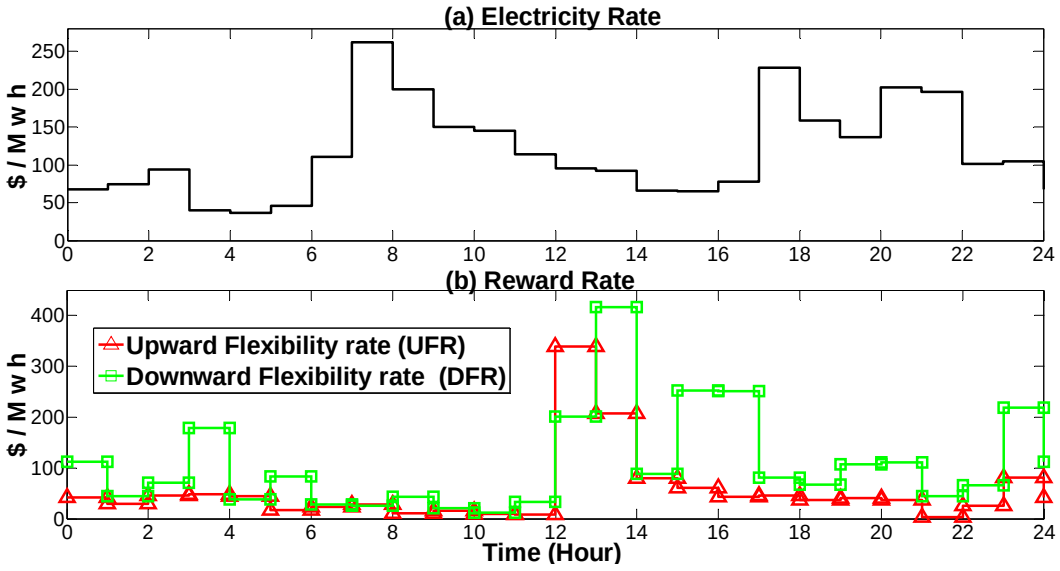

Fig. 7.15 Electricity price and flexibility reward rates for simulation

7.2.4.2 Simulation of Reserve Determination Stage

By solving problem (7.22)-(7.31), the results of implementation of step 1 and step 2 of BAG contract are presented in Fig. 7.16. Up to this stage, the utility has not played any role yet and the temperature plots in Fig. 7.16(a), Fig. 7.16(c), and Fig. 7.16(e) are caused by their corresponding baseline power consumption of HVAC fan. Whenever the DFR is much higher than UFR, such as the time interval of 0:00-1:00, 3:00-4:00, 5:00-6:00, 13:00-14:00, 16:00-17:00 etc. shown in Fig. 7.15(b), the proposed algorithm will try to maximize the reward for providing DF by setting the baseline power to (or near) the feasible upper limit as indicated in Fig. 7.16(b), Fig. 7.16(d), and Fig. 7.16(f), provided that the electricity rate is not too high in these period. Whenever the UFR is much higher than DFR such as 12:00-13:00 in Fig. 7.15(b), the baseline power will be set to (or near) the feasible lower limit as indicated in Fig. 7.16(b), Fig. 7.16(d), and Fig. 7.16(f). When both DFR and UFR are low (e.g. 6:00-12:00), the aggregator will set the baseline power to (or near) the feasible lower limits to reduce electricity costs, without caring the flexibility too much.

It should be noticed that, although the DFR is about twice higher than UFR at 19:00-21:00 from Fig. 7.15(b), the baseline power of BD1 and BD2 are not set at the upper limit in Fig. 7.16(b) and Fig. 7.16(d) because of the high electricity rate in these periods. The DFR is not high enough and it is not worthy to pay more for baseline power in order to increase the reward for providing DF, instead, the baseline power is set to an optimal point where BD1 and BD2 can still be rewarded for providing some amount of DF, while not paying too much for baseline power. Unlike BD1 and BD2, Fig. 7.16(f) shows that the baseline power of BD3 is set near the feasible upper limit at 19:00-21:00 to maximize the DF reward of BD3 because BD3's temperature bounds at these periods are much narrower than those of BD1 and BD2 and the reward can compensate the increase of payment due to the increase of baseline power. Besides, due to the smaller values of thermal resistances in BD3, heat flow from BD3 to ambient is easier, so it consumes more HVAC power than BD1 and BD2 to maintain its comfort level.

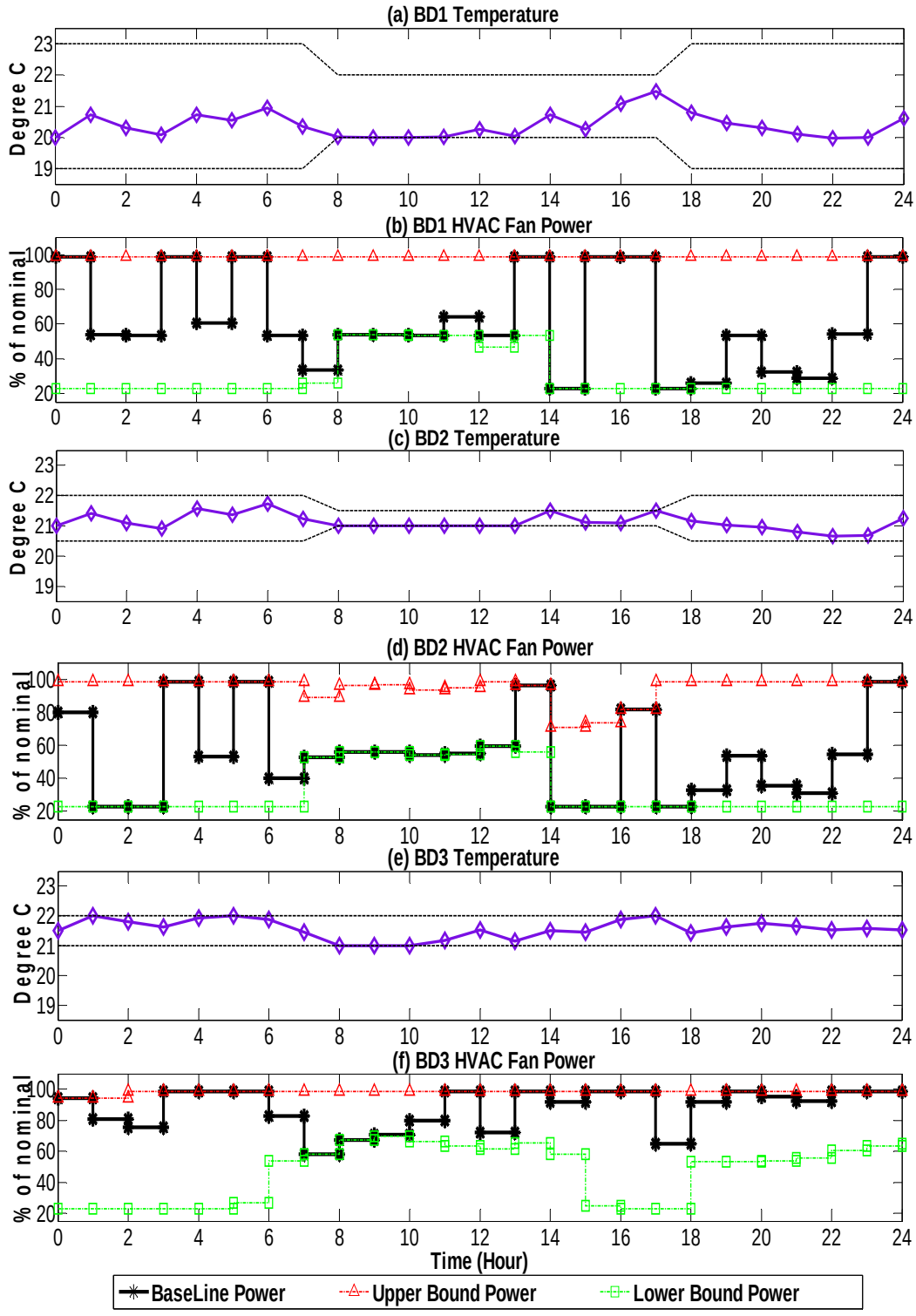

Fig. 7.16 Results of Reserve Determination Stage

7.2.4.3 Simulation of Real-time Scheduling Stage

We set the BAG contract period T_c to 1 hour in this section, which means, at each time step, the aggregator only declares the first entry of the calculated baseline, upper bound, and lower bound of aggregated HVAC fan power to the utility and allows the utility to send back the ancillary signal to control the aggregated power during the contract period. Minutely and hourly ancillary signal is randomly generated to represent the intermittent RESs or sudden loss of generation. What we observe and discuss in Fig. 7.16 also applies to Fig. 7.17 and Fig. 7.18. The temperature plots in Fig. 7.17 and Fig. 7.18 are caused by the regulation signal from the utility. The temperature variation in Fig. 7.17 is quite small because the random minutely ancillary signal fluctuates up and down very quickly, while the temperature variation in Fig. 7.18 is more obvious because the random ancillary signal lasts for a longer time (1 hour). It can be observed that higher flexibility (flexibility = upper bound power – lower bound power) is offered when the building temperature is far from the temperature limits, whereas the flexibility drops as the building temperature approaches the temperature limits or the reward rates are not high enough. These results show that, by means of proper incentives, it is feasible to provide upward and downward flexibility of HVAC power consumption to the grid by the aggregator when most needed, without violating any system constraints, provided that the ancillary signal is within the feasible bounds computed by the proposed algorithm.

The total computational time spent in the Ipopt solver is 10.735 seconds for reserve determination stage in Section 7.2.3.1, 11.182 seconds for the case with minutely ancillary signal and 10.994 seconds for the case with hourly ancillary signal, respectively. The reason why the computational time is similar for three cases is that each case has solved the min-max optimization problem for 24 times, and this means each min-max optimization problem only requires an average of about 0.46 seconds computational time. By ignoring the time spent in data

collection and data transmission, receiving regulation signals in different frequency only leads to different states of the aggregated building system for the optimization problem at next time step, consequently a slightly different computational time.

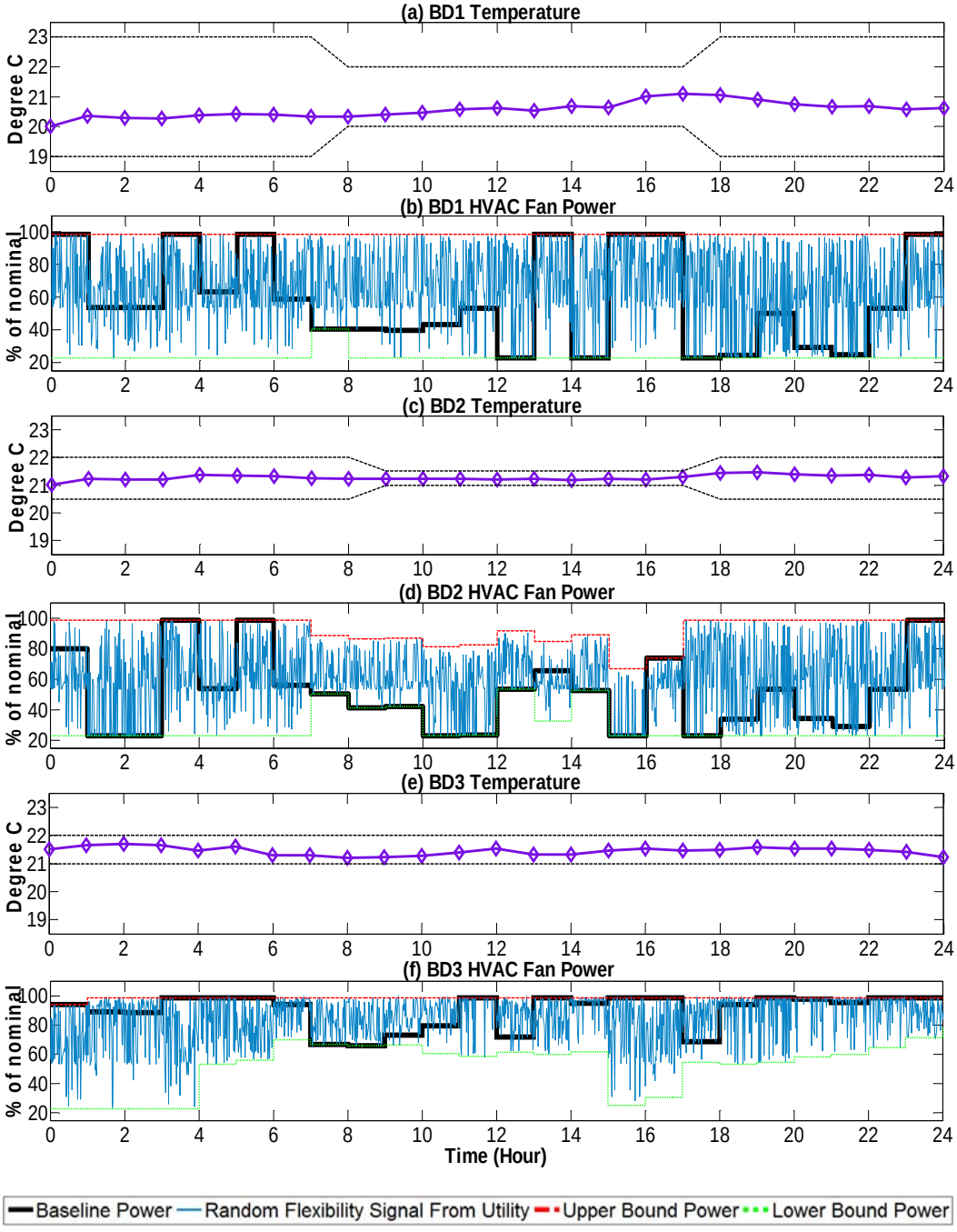

Fig. 7.17 Results of Reserve Scheduling Stage with minutely ancillary signal

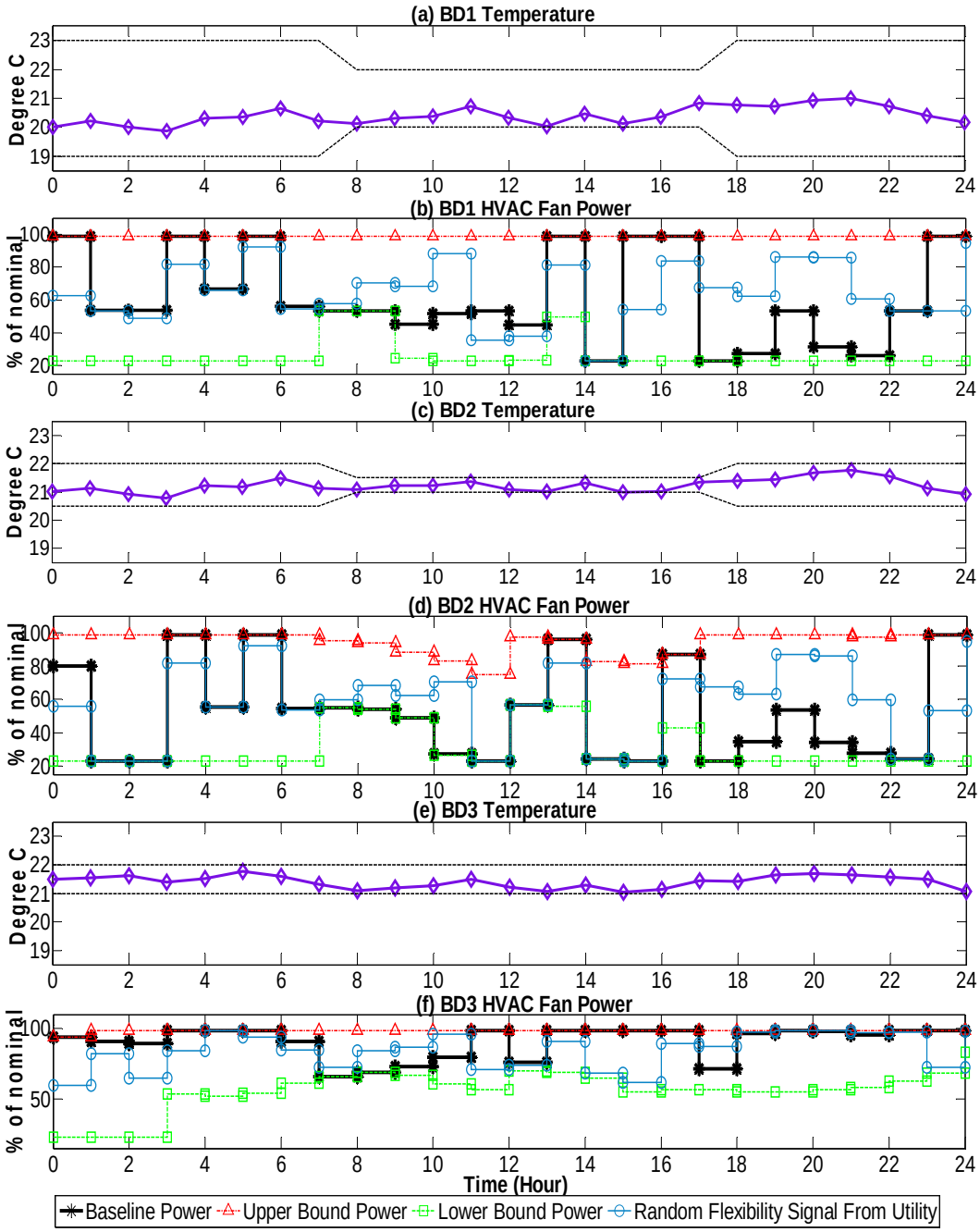

Fig. 7.18 Results of Reserve Scheduling Stage with hourly ancillary signal

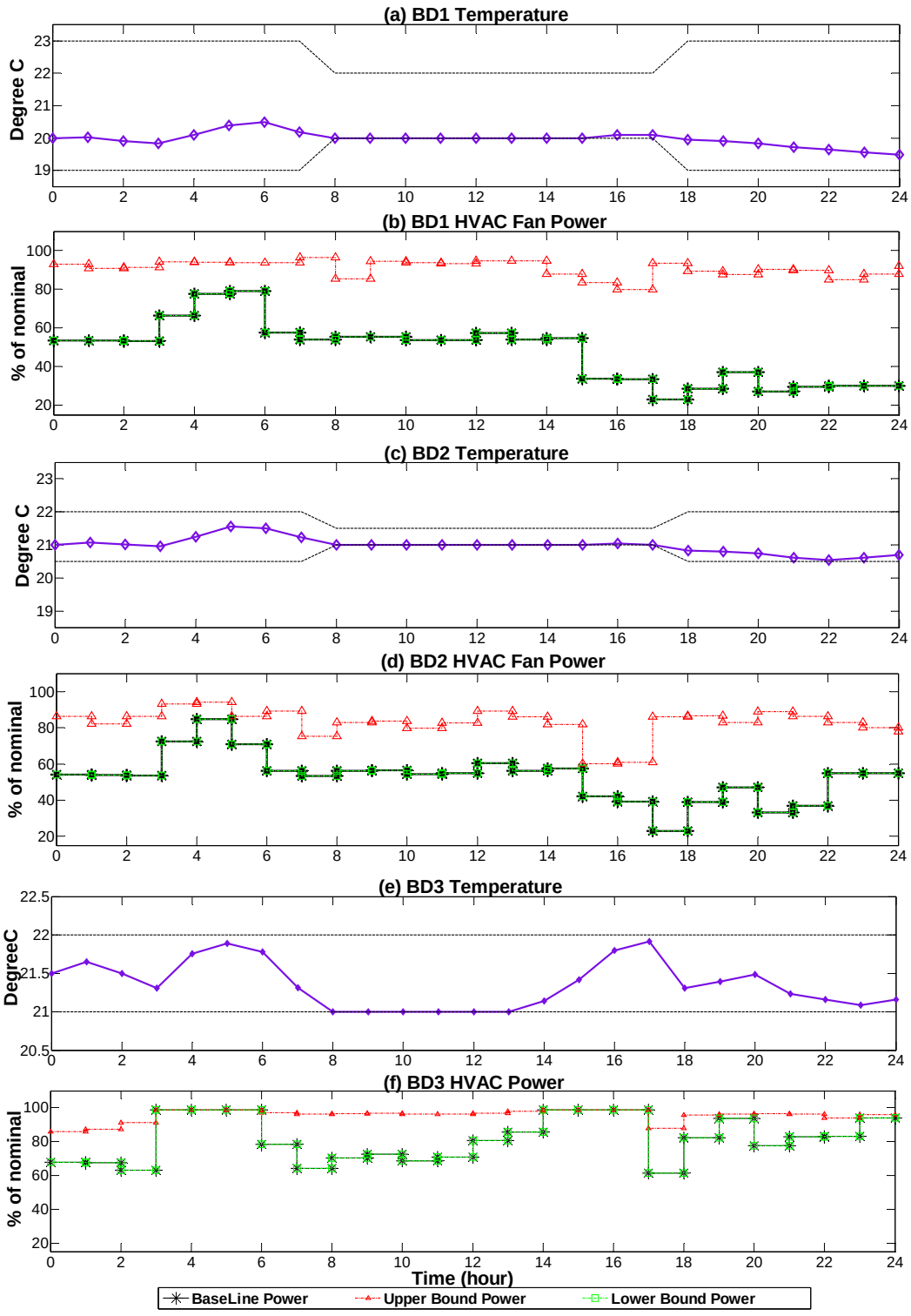

Fig. 7.19 Results of Reserve Determination Stage without reward rates.

7.2.4.4 Simulation with No Reward Incentives

To demonstrate the importance of reward incentives, we set UFR and DFR to zero while the electricity price remains the same as in Fig. 7.15(a), then problem (7.22)-(7.31) is solved. The results are shown in Fig. 7.19, which is simply the load shifting DR using thermal capacitance of buildings as mentioned in literature [186]-[188]. As expected, there is no DF because the algorithm merely minimizes the energy cost of the buildings by consuming more at low price periods (e.g. preheating effects at 3:00-6:00), while using just enough energy to satisfy the comfort constraints when electricity price is high. Fig. 7.20(b) depicts the declared flexibility of aggregator in simulation of Section 7.2.3.1, which obviously provides much more flexibility than the case with no reward incentives as shown in Fig. 7.20(a).

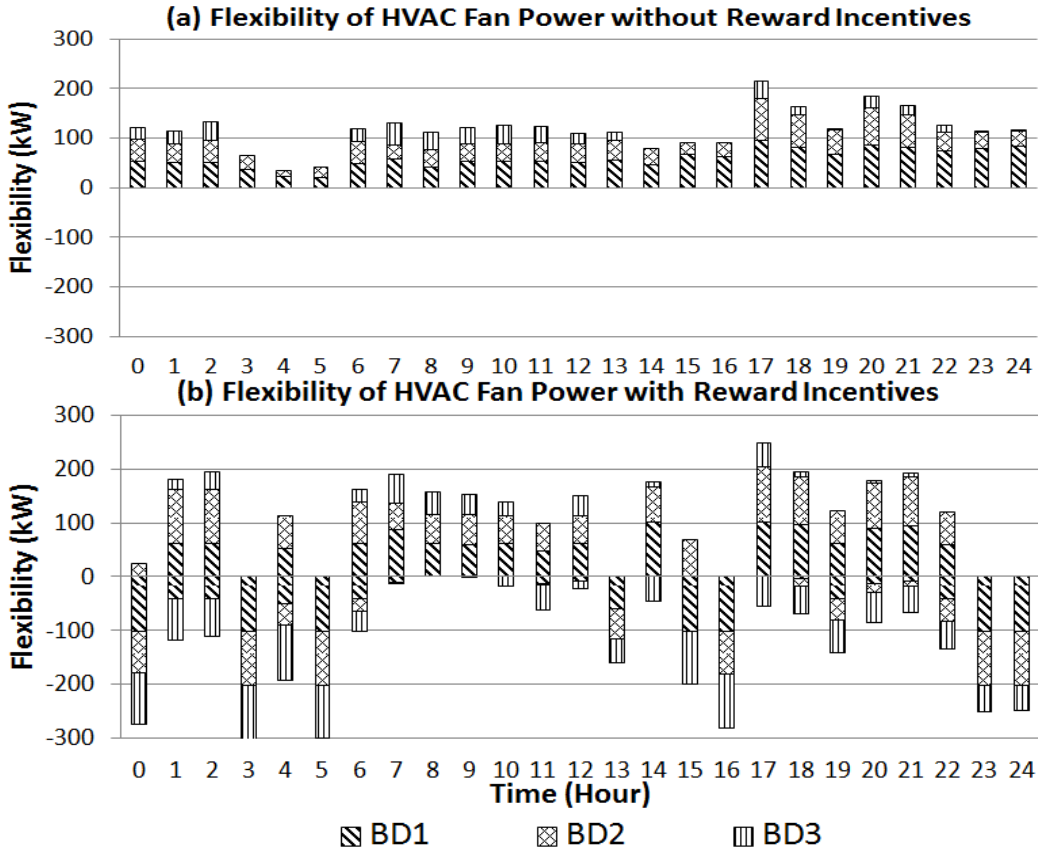

Fig. 7.20 Comparison of declared flexibility with and without reward incentives.

The provided UF and DF using our proposed approach is expected to able to reduce the variability of intermittent RES and play an important role in enabling deep penetration of RES by storing the excessive RES as thermal energy in building mass and releasing it during the shortage of RES.

7.3 Chapter Summary

This chapter proposes an economic MPC algorithm based on the thermodynamic model of buildings introduced in Chapter 6 to effectively and optimally modulate the power consumption of commercial building HVAC system in response to varying electricity price and ambient weather to minimize the electricity costs, significantly reduce the peak demand and increase energy saving and efficiency, while respecting the comfort level. Then an optimal building aggregator that can aggregate the HVAC loads to declare the power flexibility to the utility for providing fast and large-scale regulating power to the smart grid is developed under a novel contract framework between buildings, building aggregator and utility, which can maximize and reward the flexible power reserve provided by buildings. The innovative characteristics of the proposed building aggregator lie in the ability of predicting the potential total reserve amount of HVAC loads in the target building group in a defined contract time and the ability of allocating the high frequency regulation power received from the utility to each participating building while maintaining comfort levels. This chapter paves the way for commercial buildings to participate in more advanced DSM schemes.

Chapter 8

Conclusion

8.1 Summary

In order to increase the utilization of renewable energy sources and to reduce the need of generator-provided ancillary services and inefficient peaking generation, electricity consumers are progressively transforming into active participants in power system operations. This thesis focuses on applying appropriate load models to utilize flexible load response to manage power consumption in response to various supply conditions, such as high market price, peak demand, overloading, regulation signal, etc. Thus, lower grid operating costs, increased system reliability and improved energy efficiency can be achieved.

An hourly electric load of a building based on radial basis function neural network is proposed and high accuracy is demonstrated in the model validation using real building data under various weather conditions in Chapter 3. Compared with the other methods in the literature, it is simple to implement, without tedious trial-and-error parameterizing procedures. And it only needs ambient weather data and historical demand data which is easy to obtain.

A load modelling aggregation methodology is introduced in Chapter 4 to develop an aggregate load model that is able to represent the temporal variations due to the time-varying load composition caused by consumer behavior or DSM actions, as a comparison to the existing load models which typical are represented by only one set of coefficients in the load model for each loading condition, i.e. time-invariant load model coefficients. Although the residential and commercial load sectors in UK are used as examples to illustrate the

aggregation process, the method can certainly be applied to other regions as long as similar statistics on load decomposition are available.

Chapter 5 then demonstrates the importance of applying the developed aggregate load models with time-varying model coefficients to some applications in distribution system analysis. As the proportions of various load types in the aggregate load profiles are available, a general methodology is presented to model the devised DSM scenarios to assess the corresponding impacts on the network performances. An example of simple DSM scenario which disconnects/re-connects the 'wet' load is used for demonstration. Next, a CVR optimization problem based on the time-varying exponential load models is formulated to investigate the effects of varying model coefficients in load models on the CVR dispatches. The significantly different CVR dispatches and power flow results obtained from different load models further demonstrate the importance of accurate load modelling in the VVO analysis. Besides, a DSM-based OPF problem is formulated to determine the optimal location for DSM deployment and the corresponding minimum amount of load required to participate in this DSM scheme to relieve an upstream network contingency. The effective reserves provided by various types of DMLs can also be calculated using the time sequential version of this OPF problem based on the developed load models.

The loads considered in Chapter 4 participate in DSM actions by simply being disconnected, however, some other loads require more consideration during the control process of DSM implementation, such as the TCLs. Chapter 6 in this thesis focuses on leveraging the inherent flexibility of the power consumption of HVAC systems and encouraging more HVAC loads to participate in AS market. A mathematical R-C thermodynamic model of building is introduced to accurately capture the temperature dynamics inside the building to maintain the temperature within the limits.

Then in Chapter 7, an economic MPC controller is proposed to effectively and optimally modify the power consumption of commercial building HVAC system to reduce the peak load and increase energy efficiency by minimizing the electricity costs. Finally, a novel contract framework between buildings, building aggregator and utility that can maximize and reward the flexible power reserve provided by aggregate HVAC loads is proposed together with an optimal building aggregator that can aggregate the HVAC loads to declare the power flexibility to the utility for providing fast and large-scale regulating power, and it is then able to dispatch the load according to the power regulation signal from utility in the real-time scheduling stage.

8.2 Future Work

This section summaries some important areas that can be improved in the future.

The battery chargers of electric vehicles are expected to become a prevalent and significant load within the LV network in the future. Due to the large rated power, even a modest EVs penetration level will contribute a considerable portion to the aggregate demand, so an accurate generic model of the EV chargers should be developed and aggregated into the aggregate load model for use in power system analysis.

The DSM-based OPF formulation in Section 5.3 is used to disconnect the 'wet' load to relieve an upstream overloading contingency, more DSM actions can be devised for simulations and it can also be extended to accommodate the variable and intermittent output of DGs. Probabilistic simulations by examining the combined impacts of various DSM actions with different types of DGs can be carried out in detail to evaluate and quantify the potential values of DSM implementation at various locations within the system.

In the mathematical R-C thermodynamic model of building, a perfect disturbance prediction (e.g. weather conditions, internal heat gains etc.) is assumed, but the uncertainty in model parameters and disturbance predictions needs to be handled in real situations.

The economic MPC controllers in Section 7.1 and Section 7.2 are designed in response to the time-varying electricity prices, in the future, they can be extended to consider the time-varying intermittent renewable energy and investigate the potential of using this flexibility to increase the penetration and utilization of renewable energy.

In Section 7.2, the flexibility declared by the building aggregator is significant only if the reward rate is attractive, but higher reward rate results in less utility profits, so a proper reward structure that is financially and operationally beneficial to both the grid and the participating building needs to be developed in the future.

Reference

[1] DECC, “2050 pathways analysis,” Department of Energy and Climate Change, Tech. Rep., 2010.

[2] NERC, “Potential reliability impacts of emerging flexible resources,” North American Electric Reliability Corporation, Tech. Rep., 2010.

[3] E. Lannoye, D. Flynn, and M. O’Malley, “Evaluation of power system flexibility,” *IEEE Trans. Power Syst.*, vol. 27, no. 2, pp. 922–931, Jan. 2012.

[4] National Grid, “Operating the electricity networks in 2020,” National Grid, 2011.

[5] Parsons Brincknerhoff Power, “Future network architectures,” Department for Business Enterprise and Regulatory Reform, Tech. Rep., 2008.

[6] ENTSO-E, “Ten year network development plan,” European Network of Transmission System Operators for Electricity, Tech. Rep., 2010.

[7] A. Keane, L. F. Ochoa, C. L. T. Borges, G. W. Ault, A. D. Alarcon-Rodriguez, R. A. F. Currie, F. Pilo, C. Dent, and G. P. Harrison, "State-of-the-art techniques and challenges ahead for distributed generation planning and optimization," *IEEE Trans. Power Syst.*, vol. 28, no. 2, pp. 1493–1502, Sep. 2013.

[8] Tao Hong, "Short Term Electric Load Forecasting," Ph.D. dissertation, North Carolina State University, 2010.

[9] National Grid, "Operating the electricity networks in 2020," National Grid, 2011.

[10] B. A. De Souza and A. M. F. de Almeida, "Multiobjective optimization and

fuzzy logic applied to planning of the volt/var problem in distributions systems," *IEEE Trans. Power Syst.*, vol. 25, no. 3, pp. 1274–1281, Aug. 2010..

[11] J.-Y. Park, S.-R. Nam, and J.-K. Park, "Control of a ULTC considering the dispatch schedule of capacitors in a distribution system, " *IEEE Trans. Power Syst.*, vol. 22, no. 2, pp. 755–761, May 2007.

[12] G. W. Kim and K. Y. Lee, "Coordination control of ULTC transformer and STATCOM based on an artificial neural network, " *IEEE Trans. Power Syst.*, vol. 20, no. 2, pp. 580–586, May 2005.

[13] R.-H. Liang and C.-K. Cheng, "Dispatch of main transformer ULTC and capacitors in a distribution system, " *IEEE Trans. Power Del.*, vol. 16, no. 4, pp. 625–630, Oct. 2001.

[14] M. Singh, V. Khadkikar, A. Chandra, and R. K. Varma, "Grid interconnection of renewable energy sources at the distribution level with power-quality improvement features, " *IEEE Trans. Power Del.*, vol. 26, no. 1, pp. 307–315, Jan. 2011.

[15] F. A. Viawan and D. Karlsson, "Voltage and reactive power control in systems with synchronous machine-based distributed generation," *IEEE Trans. Power Del.*, vol. 23, no. 2, pp. 1079–1087, Apr. 2008.

[16] T. Senjyu, Y. Miyazato, A. Yona, N. Urasaki, and T. Funabashi, "Optimal distribution voltage control and coordination with distributed generation," *IEEE Trans. Power Del.*, vol. 23, no. 2, pp. 1236–1242, Apr. 2008.

[17] Y. P. Agalgaonkar, B. C. Pal, and R. A. Jabr, "Distribution voltage control considering the impact of PV generation on tap changers and autonomous regulators, " *IEEE Trans. Power Syst.*, vol. 29, no. 1, pp. 182–192, Jan. 2014.

[18] Y.-Y. Hong and Y.-F. Luo, "Optimal VAR control considering wind farms using probabilistic load-flow and gray-based genetic algorithms," *IEEE Trans.*

Power Del., vol. 24, no. 3, pp. 1441–1449, Jul. 2009.

[19] Z. Wang, J. Wang, B. Chen, M. Begovic and Y. He, "MPC-Based Voltage/Var Optimization for Distribution Circuits With Distributed Generators and Exponential Load Models," *IEEE Trans. Smart Grid.,* vol. 5, no. 5, pp. 2412-2420, Aug. 2014.

[20] C. Cresswell, "Steady state load models for power system analysis," Ph.D. dissertation, The University of Edinburgh, 2009.

[21] A. Collin, J. Acosta, I. Hernando-Gil, and S. Djoki´c, "An 11 kV steady state residential aggregate load model. Part 1: Aggregation methodology," *in PowerTech, 2011 IEEE Trondheim, Norway*, 2011.

[22] A. Collin, J. Acosta, I. Hernando-Gil, and S. Djoki´c, "An 11 kV steady state residential aggregate load model. Part 2: Microgeneration and demand-side management," *in PowerTech, 2011 IEEE Trondheim, Norway*, 2011.

[23] A. Collin, I. Hernando-Gil, J. L. Acosta, I. S. Ilie, and S. Djoki´c, "Realising the potential of smart grids in LV networks (Part 1)," *in ISGT Europe Conf. Manchester, UK, 2011*.

[24] A. Collin, I. Hernando-Gil, J. L. Acosta, I. S. Ilie, and S. Djoki´c, "Realising the potential of smart grids in LV networks (Part 2)," *in ISGT Europe Conf. Manchester, UK, 2011*.

[25] IEA DSM, "Integration of demand side management, distributed generation, renewable energy sources and energy storage," http://www.ieadsm.org/, International Energy Agency, 2008.

[26] IEA DSM, "Assessment and development of network driven demand side management measures," http://www.ieadsm.org/, International Energy Agency, 2008.

[27] D. Loughran and J. Kulick, “Demand side management and energy efficiency

in the United States," *The Energy Journal*, vol. 25, no. 1, pp. 19–26, 2004.

[28] M. Paulus and F. Borggrefe, "The potential of demand-side management in energy-intensive industries for electricity markets in Germany," *Applied Energy*, vol. 88, no. 2, pp. 432–441, 2011.

[29] D. Pudjianto, C. Ramsay, and G. Strbac, "Virtual power plant and system integration of distributed energy resources," *IET Renewable Power Generation*, vol. 1, no. 1, pp. 10 –16, 2007.

[30] N. Ruiz, I. Cobelo, and J. Oyarzabal, "A direct load control model for virtual power plant management," *IEEE Trans. Power Syst.*, vol. 24, pp. 959 –966, Mar. 2009.

[31] G. Sheble, "Demand is very elastic," IEEE Power and Energy Magazine, vol. 9, no. 2, pp. 14-20, Feb. 2011.

[32] M. Albadi and E. El-Saadany, "Demand response in electricity markets: An overview," *in IEEE Power Engineering Society General Meeting, Tampa, FL*, 2007.

[33] C. Alvarez, A. Gabaldon, and A. Molina, "Assessment and simulation of the responsive demand potential in end-user facilities: application to a university customer," *IEEE Trans. Power Syst.*, vol. 19, no. 2, pp. 1223 – 1231, May 2004.

[34] F. Boshell and O. Veloza, "Review of developed demand side management programs including different concepts and their results," *in IEEE PES Transmission and Distribution Conference and Exposition: Latin America, Bogota, Colombia*, 2008.

[35] M. Fotuhi-Firuzabad and R. Billinton, "Impact of load management on composite system reliability evaluation short-term operating benefits," *IEEE Trans. Power Syst.*, vol. 15, no. 2, pp. 858 –864, Aug. 2000.

[36] V. Stanojevic, V. Silva, D. Pudjianto, G. Strbac, P. Lang, and D. Macleman, "Application of storage and demand side management to optimise existing network capacity," *in 20th International Conference and Exhibition on Electricity Distribution (CIRED), Prague, Czech Republic*, 2009.

[37] R. Stewart, "Demand side management in support of the grid," *in IEEE Power Energy Society General Meeting, Calgary, Canada*, 2009.

[38] A. Brooks, E. Lu, D. Reicher, C. Spirakis, and B. Weihl, "Demand dispatch," IEEE Power and Energy Magazine, vol. 8, pp. 20 –29, 2010.

[39] A. Papavasiliou and S. Oren, "Coupling wind generators with deferrable loads," *in IEEE Energy 2030 Conference, Atlanta, GA*, 2008.

[40] Energy Saving Trust, "Location, location, location: Domestic small-scale wind field trial report," UK Department of Trade and Industry, Tech. Rep., 2009.

[41] B. J. Kirby, "Spinning reserve from responsive loads," United States, Department of Energy, Tech. Rep., 2003.

[42] B. Hayes, "Distributed Generation and Demand Side Management: Applications to Transmission System Operation," Ph.D. dissertation, The University of Edinburgh, 2013.

[43] P. Kundur, *Power System Stability and Control*. New York: McGraw-Hill, 1994.

[44] H. Willis, *Spatial Electric Load Forecasting*. CRC Press, 2002.

[45] W. Price, K. Wirgau, A. Murdoch, J. Mitsche, E. Vaahedi, and M. El-Kady, "Load modeling for power flow and transient stability computer studies," *IEEE Trans. Power Syst.*, vol. 3, no. 1, pp. 180 –187, Aug. 1988.

[46] W. Xu, E. Vaahedi, Y. Mansour and J. Tamby, "Voltage stability load parameter determination from field tests on BC Hydro's system," IEEE Trans. Power Syst., vol. 12, no. 3, pp. 1290-1297, Aug. 1997.

[47] L. Korunovic, D. Stojanovic and J. V. Milanovic, ”Identification of static load characteristics based on measurements in medium-voltage distribution Network,” *IET Generation, Transmission & Distribution*, vol. 2, no. 2, pp. 227-234, Mar. 2008.

[48] A. Collin, “Advanced load modelling for power system studies,” Ph.D. dissertation, The University of Edinburgh, 2013.

[49] J. Momoh, R. Adapa, andM. El-Hawary, “A review of selected optimal power flow literature to 1993 (parts 1&2),” *IEEE Trans. Power Syst.*, vol. 14, pp. 96–111, 1999.

[50] G. Harrison and R.Wallace, “Optimal power flow evaluation of distribution network capacity for the connection of distributed generation,” *IET Generation, Transmission, Distribution*, vol. 152, pp. 115–122, 2005.

[51] A. Keane and M. O’Malley, “Optimal allocation of embedded generation on distribution networks,” *IEEE Trans. Power Syst.*, vol. 20, pp. 1640–1646, 2005.

[52] L. Ochoa, C. Dent, and G. Harrison, “Distribution network capacity assessment: Variable DG and active networks,” *IEEE Trans. Power Syst.*, vol. 25, pp. 87–95, 2010.

[53] T. Boehme, G. Harrison, and A. Wallace, “Assessment of distribution network limits for non-firm connection of renewable generation,” *IET Renew. Power Gen.*, vol. 4, no. 1, pp. 64–74, 2010.

[54] A. Keane, L. Ochoa, E. Vittal, C. Dent, and G. Harrison, “Enhanced utilization of voltage control resources with distributed generation,” *IEEE Trans. Power Syst.*, vol. 26, pp. 252–260, 2011.

[55] M. Dolan, E. Davidson, I. Kockar, G. Ault, and S. McArthur, “Distribution power flow management utilizing an online optimal power flow technique,” *IEEE Trans. Power Syst.*, vol. 27, pp. 790–799, 2012.

[56] S. Gill, I. Kockar, and G. Ault, "Dynamic optimal power flow for active distribution networks," *IEEE Trans. Power Syst.*, vol. 29, pp. 1–11, 2014.

[57] L. Hadju, J. Peschon, W. Tinney, and D. Piercy, "Optimum load-shedding policy for power systems," *IEEE Trans. Power App. Syst.*, vol. PAS-87, pp. 784–795, 1968.

[58] D. Subramanian, "Optimum load-shedding through programming techniques," *IEEE Trans. Power App. Syst.*, vol. PAS-90, pp. 89–95, 1971.

[59] S. Majumdar, D. Chattopadhyay, and J. Parikh, "Interruptible load management using optimal power flow analysis," *IEEE Trans. Power Syst.*, vol. 11, no. 2, pp. 715–720, 1996.

[60] C. Affonso, L. C. P. Da Silva, F. G. M. Lima, and S. Soares, "MW and MVAr management on supply and demand side for meeting voltage stability margin criteria," *IEEE Trans. Power Syst.*, vol. 19, no. 3, pp. 1538–1545, 2004.

[61] M. Rider, C. Castro, V. Paucar, and A. Garcia, "Higher order interiorpoint method for minimising load-shedding in a competitive electric power market," *IET Gen., Transm., Distrib.*, vol. 151, pp. 433–440, 2004.

[62] E. Aponte and J. Nelson, "Time optimal load shedding for distributed power systems," *IEEE Trans. Power Syst.*, vol. 21, no. 1, pp. 269–277, 2006.

[63] T. Fernandes, J. Lenzi, and M. Mikilita, "Load shedding strategies using optimal load flow with relaxation of restrictions," *IEEE Trans. Power Syst.*, vol. 23, pp. 712–718, 2008.

[64] P. Wang, Y. Ding, and L. Goel, "Reliability assessment of restructured power systems using optimal load shedding technique," *IET Gen., Transm., Distrib.*, vol. 3, pp. 628–640, 2009.

[65] W. Uturbey and A. Costa, "Dynamic optimal power flow approach to account for consumer response in short term hydrothermal coordination studies," *IET*

Gen., Transm., Distrib., vol. 1, pp. 414–421, 2007.

[66] A. Gabash and P. Li, "Active-reactive optimal power flow in distribution networks with embedded generation and battery storage," *IEEE Trans. Power Syst.*, vol. 27, pp. 2026–2035, 2012.

[67] Z. Chen, L. Wu, and Y. Fu, "Real-time price-based demand response management for residential appliances via stochastic optimization and robust optimization," *IEEE Trans. Smart Grid*, vol. 3, no. 4, pp. 1822–1831, 2012.

[68] K. Schneider and T. Weaver, "Volt-VAR optimization on American Electric Power feeders in Northeast Columbus," *in IEEE PES T&D*, 2012, pp. 1-8.

[69] I. Roytelman, B. K. Wee, R. L. Lugtu, T. M. Kulas, and T. Brossart, "Pilot project to estimate the centralized volt/VAR control effectiveness," *IEEE Trans. Power Syst*., vol. 13, no. 3, pp. 864-869, Aug. 1998.

[70] N. S. Markushevich, I. C. Herejk, and R. E. Nielsen, "Functional requirements and cost-benefit study for distribution automation at B.C. Hydro," *IEEE Trans. Power Syst.*, vol. 9, no. 2, pp. 772-781, May 1994.

[71] N. Markushevich and W. Luan, "Achieving greater VVO benefits through AMI implementation," *in IEEE PES GM*, 2011, pp. 1-7.

[72] M. E. Baran and M. Y. Hsu, "Volt/VAR control at distribution substations," *IEEE Trans. Power Syst.*, vol. 14, no. 1, pp. 312-318, Feb. 1999.

[73] Y. Liu, P. Zhang, and X. Qiu, "Optimal volt/VAR control in distribution systems," *Int. J. Elect. Power & Energy Syst.*, vol. 24, no. 4, pp. 271-276, 2002.

[74] B. A. de Souza and A. M. F. de Almeida, "Multiobjective optimization and fuzzy logic applied to planning of the volt/VAR problem in distributions systems," *IEEE Trans. Power Syst*., vol. 25, no. 3, pp. 1274-1281, Aug. 2010.

[75] G. Ramakrishna and N. D. Rao, "Adaptive neuro-fuzzy inference system for volt/VAR control in distribution systems," *Elect. Power Syst. Res.*, vol. 49, no.

2, pp. 87-97, 1999.

[76] B. Milosevic and M. Begovic, "Capacitor placement for conservative voltage reduction on distribution feeders," *IEEE Trans. Power Del.*, vol. 19, no. 3, pp. 1360-1367, Jul. 2004.

[77] K. P. Schneider, F. K. Tuffner, J. C. Fuller, and R. Singh, "Evaluation of conservation voltage reduction (CVR) on a national level," US Department of Energy, Tech. Rep., Jul. 2010.

[78] He Hao, Borhan M. Sanandaji, Kameshwar Poolla, and Tyrone L. Vincent, "Aggregate flexibility of thermostatically controlled loads," *IEEE Trans. Power Syst.*, vol. 30, no. 1, pp. 189-198, Jun. 2015.

[79] D. S. Callaway and I. A. Hiskens, "Achieving controllability of electric loads," *Proceedings of the IEEE*, vol. 99, no. 1, pp.184-199, Nov. 2011.

[80] S. Koch, J.L. Mathieu, and D.S. Callaway, "Modeling and control of aggregated heterogeneous thermostatically controlled loads for ancillary services," *In Proc. PSCC*, pages 1-7, 2011.

[81] J. Kondoh, N. Lu, and D. J. Hammerstrom, "An evaluation of the water heater load potential for providing regulation service," *IEEE Trans. Power Syst.*, vol. 26, no. 3, pp. 1309–1316, Aug. 2011.

[82] D. Wang, S. Parkinson, W. Miao, H. Jia, C. Crawford, and N. Djilali, "Online voltage security assessment considering comfort-constrained demand response control of distributed heat pump systems," *Appl. Energy*, vol. 96, pp. 104–114, Aug. 2012.

[83] Y. Ma, F. Borrelli, B. Hencey, B. Coffey, S. Bengea, and P. Haves, "Model predictive control for the operation of building cooling systems," *In American Control Conference (ACC) 2010*, pp. 5106-5111.

[84] M. Maasoumy and A. Sangiovanni-Vincentelli, "Total and peak energy

consumption minimization of building HVAC systems using model predictive control," *IEEE Design and Test of Computers*, vol. 29, no.4, pp. 26–35, Aug. 2012.

[85] F. Oldewurtel, A. Parisio, C. N. Jones, D. Gyalistras, M. Gwerder, V. Stauch, B. Lehmann, and M. Morari, "Use of Model Predictive Control and Weather Forecasts for Energy Effcient Building Climate Control," *Energy and Buildings*, vol. 45, pp. 15-27, Feb. 2012.

[86] S. Klein, J. Duffie, and W. Beckman, "TRNSYS - A Transient Simulation Program," ASHRAE Trans., vol. 82, pt. 1, pp. 623–633, 1976.

[87] *DOE-2 Engineering Manual*, Version 2.1C, Lawrence Berkeley Laboratory, Berkeley, CA, 1982.

[88] D. B. Crawley, L. K. Lawrie, F. C. Winkelmann, W. F. Buhl, Y. J. Huang, C. O. Pedersen, R. K. Strand, R. J. Liesen, D. E. Fisher, M. J. Witte, and J. Glazer, "EnergyPlus: Creating a New-generation Building Energy Simulation Program," *Energy and Buildings*, vol. 33, no. 4, pp. 319–331, Apr. 2001.

[89] R. C. Sonderegger, "Diagnostic tests determining the thermal response of a house," *ASHRAE Trans.*, vol. 84, pt. 1, pp. 691–702, Feb. 1978.

[90] J. A. Crabb, N. Murdoch, and J. M. Penman, "A simplified thermal response model," *Building Serv. Eng. Res. Technol.*, vol. 8, no. 1, pp. 13–19, Feb. 1987.

[91] T. A. Reddy, L. K. Norford, and W. Kempton, "Shaving residential air-conditioner peaks by intelligent use of the building thermal mass," *Energy*, vol. 16, no. 7, pp. 1001–1010, Jul. 1991.

[92] K. A. Antonopoulos and E. Koronaki, "Apparent and effective thermal capacitance of buildings," *Energy*, vol. 23, no. 3, pp. 183–192, Mar. 1998.

[93] K. A. Antonopoulos and E. Koronaki, "Envelope and indoor thermal capacitance of buildings," *Appl. Thermal Eng.*, vol. 19, no. 7, pp. 743–756, Jul.

1999.

[94] S. Wang and X. Xu, “Parameter estimation of internal thermal mass of building dynamic models using genetic algorithm,” *Energy Convers. Manage.*, vol. 47, no. 13, pp. 1927–1941, Aug. 2006.

[95] G. Fraisse, C. Viardot, O. Lafabrie, and G. Achard, “Development of a simplified and accurate building model based on electrical analogy,” *Energy and Buildings*, vol. 34, no. 10, pp. 1017–1031, Nov. 2002.

[96] M. M. Gouda, S. Danaher, and C. P. Underwood, “Building thermal model reduction using nonlinear constrained optimization,” *Building and Environment*, vol. 37, no. 12, pp. 1255–1265, Dec. 2002.

[97] X. Xu and S. Wang, “Optimal simplified thermal models of building envelope based on frequency domain regression using genetic algorithm,” *Energy and Buildings*, vol. 39, no. 5, pp. 525–536, May 2007.

[98] R. Yao, B. Li and K. Steemers, "Energy policy and standard for built environment in China," *Renewable Energy*, vol. 30, pp. 1973-1988, 2005.

[99] “Buildings energy data book.” [Online]. Available: http://buildingsdatabook.eren.doe.gov/default.aspx.

[100] I. Fernandez, C. Borges, and Y. Penya, "Efficient building load forecasting," *in Proc. 2011 IEEE International Conference on Emerging Technologies and Factory Automation (ETFA)*, pp. 1-8.

[101] G. M. Masters, *Renewable and Efficient Electric Power Systems*, Hoboken New Jersey: Wiley, 2004.

[102] L. Baizhan, Y. Runming and DJ. Croome, "Air-conditioning in China," *Building Research and Information*, vol. 23, pp. 309-316, 1995.

[103] Y. Iwasaki, S. Kobayashi, A. Nagaiwa, "Development of district heating and cooling plant operation support system," *ASHRAE Trans*, vol. 104, pp. 5-12,

1998.

[104] Y. Jiang, "Current building energy consumption in China and effective energy efficiency measures," *HV&AC*, vol. 35, pp. 30-40, 2005 [in Chinese].

[105] Y. Jiang, "Current trend of building energy use and major conservation issues in China," Green Build, vol. 7, pp. 10-15, 2006 [in Chinese].

[106] H. Alfares and M. Nazeeruddin, "Electric load forecasting: literature survey and classification of methods," *International Journal of Systems Science*, vol. 33, no.1, pp. 23-34, 2002.

[107] V. Hinojosa and A. Hoese, "Short-term load forecasting using fuzzy inductive reasoning and evolutionary algorithms," *IEEE Trans. Power Syst.*, vol. 25, no. 1, pp. 565–574, 2010.

[108] S. Tzafestas and E. Tzafestas, "Computational intelligence techniques for short-term electric load forecasting," *Journal of Intelligent and Robotic Systems*, vol. 31, pp. 7–68, 2001.

[109] E. Feinberg and D. Genethliou, "Load forecasting," *Applied Mathematics for Power Systems*, chapter 12, pp. 269-285, 2005.

[110] S.W. Wang, X.H. Xu, "Simplified building model for transient thermal performance estimation using GA-based parameter identification," *International Journal of Thermal Sciences*, vol. 45, pp. 419–432, April 2006.

[111] T. Haida and S. Muto, "Regression based peak load forecasting using a transformation technique," *IEEE Trans. Power Syst.*, vol. 9, pp. 1788-1794, 1994.

[112] O. Hyde and P. F. Hodnett, "An adaptable automated procedure for short-term electricity load forecasting," *IEEE Trans. Power Syst.*, vol. 12, pp. 84-94, 1997.

[113] S. Ruzic, A. Vuckovic, and N. Nikolic, "Weather sensitive method for short term load forecasting in Electric Power Utility of Serbia," *IEEE Trans. Power*

Syst., vol. 18, pp. 1581-1586, 2003.

[114] D. Infield and D. Hill, "Optimal smoothing for trend removal in short term electricity demand forecasting," *IEEE Trans. Power Syst.*, vol. 13, no. 3, pp. 1115–1120, 1998.

[115] G. Mbamalu and M. El-Hawary, "Load forecasting via sub optimal seasonal auto regressive models and iteratively reweighted least squares estimation," *IEEE Trans. Power Syst.*, vol. 8, no. 1, pp. 343–348, 1993.

[116] M. Hagan and S. Behr, "The time series approach to short term load forecasting," *IEEE Trans. Power Syst.*, vol. 2, no. 3, pp. 785–791, 1987.

[117] H. Yang and C. Huang, "A new short-term load forecasting approach using self-organizing fuzzy ARMAX models," *IEEE Trans. Power Syst.*, vol. 13, no. 1, pp. 217–225, 1998.

[118] A. Jain and B. Satish, "Clustering based short term load forecasting using support vector machines," *in Proc. 2009 IEEE Bucharest PowerTech*, pp. 1–8.

[119] C. Bo-Juen, C. Ming-Wei, and L. Chih-Jen, "Load forecasting using support vector machines: a study on EUNITE competition 2001," *IEEE Trans. Power Syst.*, vol. 19, no. 4, pp. 1821–1830, 2004.

[120] K. Ho, Y. Hsu, C. Chen, T. Lee, C. Liang, T. Lai, and K. Chen, "Short-term load forecasting of Taiwan power system using a knowledge-based expert system," *IEEE Trans. Power Syst.*, vol. 5, no. 4, pp. 1214–1221, 1990.

[121] H. Mori and H. Kobayashi, "Application of a fuzzy neural network combined with a chaos genetic algorithm and simulated annealing to short-term load forecasting," *IEEE Trans. Evolutionary Computing*, vol. 10, no. 3, pp. 330–340, 2006.

[122] K.-B. Song, Y.-S. Baek, D. H. Hong, and G. Jang, "Short-term load forecasting for the holidays using fuzzy linear regression method," *IEEE Trans. Power*

Syst., vol. 20, pp. 96-101, 2005.

[123] K.-B. Song, S.-K. Ha, J.-W. Park, D.-J. Kweon, and K.-H. Kim, "Hybrid load forecasting method with analysis of temperature sensitivities," *IEEE Trans. Power Syst.*, vol. 21, pp. 869-876, 2006.

[124] S. E. Papadakis, J. B. Theocharis, S. J. Kiartzis, and A. G. Bakirtzis, "A novel approach to short-term load forecasting using fuzzy neural networks," *IEEE Trans. Power Syst.*, vol. 13, no. 2, pp. 480–492, 1998.

[125] P. Gonzalez and J. Zamarreno, "Prediction of hourly energy consumption in buildings based on a feedback artificial neural network," *Energy and Buildings*, vol. 37, no. 6, pp. 595–601, 2005.

[126] B. Ekici and U. Aksoy, "Prediction of building energy consumption by using artificial neural networks," *Advances in Engineering Software*, vol. 40, no. 5, pp. 356 – 362, 2009.

[127] A. D. Papalexopoulos, H. Shangyou, and P. Tie-Mao, "An implementation of a neural network based load forecasting model for the EMS," *IEEE Trans. Power Syst.*, vol. 9, pp. 1956-1962, 1994.

[128] A. Khotanzad, Z. Enwang, and H. Elragal, "A neuro-fuzzy approach to short-term load forecasting in a price-sensitive environment," *IEEE Trans. Power Syst.*, vol. 17, pp. 1273-1282, 2002.

[129] A. Jain and B. Satish, "Clustering based short term load forecasting using artificial neural network," *in Proc. 2009 IEEE PES Power Systems Conference Exposition (PSCE)*, pp. 1-7.

[130] P. D. Wasserman, *Advanced methods in neural computing*, Van Nostrand Reinhold, New York: Wiley, 1993.

[131] S. Haykin, *Neural networks: a comprehensive foundation*, 2nd ed, Prentice Hall, New Jersey, 1999.

[132] M. Ohlsson, C. Peterson, H. Pi, T. Rognvaldsson, B. Soderberg, "Predicting System Loads with Artificial Neural Networks-Methods and Results from the Great Energy Predictor Shootout," Tech. Rep. LU T 93-24, Sep. 1993.

[133] R. Dodier, G. Henze, "Statistical Analysis of Neural Network as applied to Building Energy Prediction. Energy Systems Laboratory," Tech. Rep. ESL-PA-96/07.

[134] "Meteorological Bureau of Shenzhen" [Online]. Available: http://www.szmb.gov.cn/.

[135] S. Chen, X. Hong and C.J. Harris, "Orthogonal forward selection for constructing the radial basis function network with tunable nodes," *in Proc. 2005 international conference on Advances in Intelligent Computing (ICIC'05)*, vol. 1, pp. 777-786.

[136] IEEE Task Force on Load Representation for Dynamic Performance,"Standard load models for power flow and dynamic performance simulation," *IEEE Trans. Power Delivery*, vol. 10, no. 3, pp. 1302-1313, Aug. 1995.

[137] D. J. Hill, "Nonlinear dynamic load models with recovery for voltage stability studies," *IEEE Trans. Power Delivery*, vol. 8, no. 1, pp. 166-176, Feb. 1993.

[138] IEEE Task Force on Load Representation for Dynamic Performance, "Load representation for dynamic performance analysis," *IEEE Trans. Power Delivery*, vol. 8, no. 2, pp. 472-482, May 1993.

[139] IEEE Task Force on Load Representation for Dynamic Performance, "Bibliography on load models for power flow and dynamic performance simulation," *IEEE Trans. Power Syst.*, vol. 10, no. 1, pp. 523-538, Feb. 1995.

[140] K. Yamashita, S. Martinaz Villanueva and J. V. Milanovic, "Initial results of international survey on industrial practice on power system load modelling conducted by CIGRE WG C4.605," *CIGRE Int. Symp., Bologna, Italy*, Sep.

2011.

[141] D. Singh, R. K. Misra and D. Singh, ”Effect of load models in distributed generation planning,” *IEEE Trans. Power Syst.*, vol. 22, no. 4, pp. 2204-2212, Nov. 2007.

[142] A. Collin, G. Tsagarakis, A. Kiprakis and S. McLaughlin, " Development of Low-Voltage Load Models for the Residential Load Sector," *IEEE Trans. Power Syst.,* vol. 29, no. 5, pp. 2180-2188, Feb. 2014.

[143] L. Korunovic, D. Stojanovic and J. V. Milanovic, "Identification of static load characteristics based on measurements in medium-voltage distribution Network," *IET Generation, Transmission & Distribution*, vol. 2, no. 2, pp. 227-234, Mar. 2008.

[144] Electrical Power Research Institute (EPRI), "Advanced load modeling - Entergy pilot study," Tech. Rep. 1011391, Dec. 2004.

[145] C. Noren and J. Pyrko, "Typical load shapes for Swedish schools and hotels," *Energy and Buildings*, vol. 28, no. 2, pp. 145-157, 1998.

[146] H. Akbari, J. Eto, S. Konopacki, A. Afzal, K. Heinemeier, and L. Rainer, "Integrated estimation of commercial sector end-use load shapes and energy use intensifies in the PG&E Service Area," Energy and Environment Division, Univ. of California, Rep. LBL-34263, Dec. 1993. [Online]. Available: http://emp.lbl.gov/sites/all/files/lbnl-34263.pdf.

[147] R. E. Brown and J. G. Koomey, "Electricity use in California: Past trends and present usage patterns," *Energy Policy*, vol. 31, no. 9, pp. 849-864, Jul. 2003.

[148] Building Research Establishment, "The impact of changing energy use patterns in buildings on peak electricity demand in the UK," Tech, Rep. 243752, Oct. 2008.

[149] Electrical Power Research Institute (EPRI), "Advanced load modeling,” Tech.

Rep. 1007318, Sept. 2002.

[150] Electrical Power Research Institute (EPRI), "Measurement-based load modeling," Rep. 1014492, Sep. 2006.

[151] Dept. of Energy and Climate Change (DECC), "Energy consumption in the UK 2011," UK government, London, UK, Jul. 2012. [Online]. Available: https://www.gov.uk/government/publications/energy-consumption-in-the-uk.

[152] Dept. for Environment, Food and Rural Affairs, "BNDL01: Domestic lighting government standards evidence base 2009: Key inputs," UK Government, London, UK, Jun. 2010.

[153] Schneider Electric, "Adjustable Frequency Controllers", Tech. Rep. SC100 R5-95. [Online]. Available: http://static.schneiderelectric.us/

[154] S. Z. Djokic, A. J. Collin and C. E. Cresswell, "The Future of Residential Lighting: Shift from Incandescent to CFL to LED light sources," presented at the *Illuminating Engineering Society of North America Annual Conf.* 2009, Seattle, WA, Nov. 15-17.

[155] A. J. Collin, C. E. Cresswell and S. Z. Djokic, "Harmonic Cancellation of Modern Switch-Mode Power Supply Load," presented at *14th IEEE International Conference on Harmonics and Quality of Power, ICHQP*, Bergamo, Italy, Sept. 26 – 29, 2010.

[156] C. Cresswell and S. Djokic, "Representation of directly connected and drive-controlled induction motors. Part 1: Single-phase load models," presented at *18th Int. Conf. on Elect. Machines*, Vilamoura, Portugal, Sept. 6-9 Sept, 2008.

[157] C. Cresswell and S. Djokic, "Representation of directly connected and drive-controlled induction motors. Part 2: Three-phase load models," presented at *18th Int. Conf. on Elect. Machines*, Vilamoura, Portugal, Sept. 6-9 Sept, 2008.

[158] C. E. Cresswell and S. Z. Djokic, "The analysis of the occurrence of high in-

rush currents in dc power supplies," in *Proc. 4th IET Conf. Power Electronics, Machines & Drives*, York, UK, 2008, pp. 441-445.

[159] P. Trichakis, P. C. Taylor, P. F. Lyons and R. Hair, "Predicting the technical impacts of high levels of small-scale embedded generators on low-voltage networks," *IET Renewable Power Generation*, vol. 2, no. 4, pp. 249 - 262, Dec. 2008.

[160] C. Pout, F. MacKenzie, and E. Olluqui, "The impact of changing energy patterns in buildings on peak electricity demand in the UK," Department of Energy and Climate Change, Tech. Rep., 2008.

[161] Market Transformation Programme, "BCNL01: Commercial lighting government standards evidence base 2009: Key inputs," Department of Environment, Food and Rural Affairs, Tech. Rep., 2010.

[162] M. E. Baran and F. F. Wu, "Network reconfiguration in distribution systems for loss reduction and load balancing," *IEEE Trans. Power Del.*, vol. 4, no. 2, pp. 1401–1407, Apr. 1989.

[163] Ting Wu, Weijie Mai, Mingwen Qin, Chunxue Zhang and C. Y. Chung, "Optimal Operation of Combined Cooling Heat and Power Microgrid with PEVs", *in Proc. IEEE PowerTech*, Eindhoven, Jun. 2015, Page 1-6.

[164] T. O. Ting, K. P. Wong, C. Y. Chung, "Hybrid constrained genetic algorithm/particle swarm optimization load flow algorithm", *IET Generation, Transmission and Distribution*, vol. 2, no. 6, pp. 800-812, Nov. 2008.

[165] G. Harrison and R.Wallace, "Optimal power flow evaluation of distribution network capacity for the connection of distributed generation," *IET Renewable Power Generation*, vol. 152, pp. 115–122, 2005.

[166] SP Distribution Long Term Development Statement, Scottish Power Distribution, 2011.

[167] M. Maasoumy, "Controlling Energy-Efficient Buildings in the Context of Smart Grid: A Cyber Physical System Approach," Elect. Eng. Dept., Univ. California, Berkeley, Tech. Rep. UCB/EECS-2013-244, Dec. 28, 2013.

[168] A. Kelman, Y. Ma and F. Borrelli, "Analysis of local optima in predictive control for energy efficient buildings," *Journal of Building Performance Simulation*, vol. 6, no. 3, pp. 236–255, Apr. 2012.

[169] H. Hao, A. Kowli, Y. Lin, P. Barooah, and S. Meyn, "Ancillary service for the grid via control of commercial building HVAC systems," in *Proc. 2013 Amer. Control Conf. (ACC)*, pp. 467–472.

[170] Weijie Mai and C. Y. Chung, "Economic MPC of Aggregating Commercial Buildings for Providing Flexible Power Reserve", *IEEE Trans. Power Syst.*, Vol. 30, No. 5, pp. 2685-2694, Sep. 2015.

[171] A. Standard. 90.1-1989. American Society of Heating, Refrigerating, and Air-Conditioning Engineers, 1989.

[172] J. E. Braun, K. W. Montgomery, and N. Chaturvedi, "Evaluating the Performance of Building Thermal Mass Control Strategies," *HVAC&R Research*, vol. 7, no. 4, pp. 403–428, 2001.

[173] C. D. Corbin, G. P. Henze, and P. T. May-Ostendorp, "A model predictive control optimization environment for real-time commercial building application," *Journal of Building Performance Simulation*, vol. 6, no. 3, pp. 159–174, 2013.

[174] S. Kiliccote, M. A. Piette, E. Koch, and D. Hennage, "Utilizing Automated Demand Response in Commercial Buildings As Non-Spinning Reserve Product for Ancillary Services Markets," *in 50th IEEE Conference on Decision and Control and European Control Conference*, 2011, pp. 4354–4360.

[175] J. D. Kueck, B. J. Kirby, M. R. Ally, and K. Rice, "Using Air Conditioning

Load Response for Spinning Reserve," 2009.

[176] J. A. Short, D. G. Infield, and L. L. Freris, "Stabilization of Grid Frequency Through Dynamic Demand Control," *IEEE Trans. on Power Syst.*, vol. 22, no. 3, pp. 1284–1293, 2007.

[177] P. Zhao, G. P. Henze, S. Plamp, and V. J. Cushing, "Evaluation of commercial building HVAC systems as frequency regulation providers," *Energy Build*, vol. 67, pp. 225–235, Dec. 2013.

[178] B. Arguello-Serrano and M. Velez-Reyes. Nonlinear control of a heating, ventilating, and air conditioningsystem with thermal load estimation. *IEEE Transactions on Control Systems Technology*, vol. 7, no. 1, pp. 56-63, 1999.

[179] Y. Ma, A. Kelman, A. Daly and F. Borrelli, "Predictive Control for Energy Efficient Buildings with Thermal Storage: Modeling, Stimulation, and Experiments," *IEEE Control Systems*, vol. 32, no. 1, pp. 44–64, Feb. 2012.

[180] PJM Markets & Operations. [Online]. Available: http://www.pjm.com/markets-and-operations.aspx.

[181] Y. Makarov, C. Loutan, J. Ma, and P. de Mello, "Operational impacts of wind generation on California power systems," *IEEE Trans. Power Syst.*, vol. 24, no. 2, pp. 1039–1050, May. 2009.

[182] H. Yu, C. Y. Chung, K. P. Wong, and J. H. Zhang, "A chance constrained transmission network expansion planning method with consideration of load and wind farm uncertainties," *IEEE Trans. Power Syst.*, vol. 24, no. 3, pp. 1568–1576, Aug. 2009.

[183] H. M. Yang, C. Y. Chung, and J. H. Zhao, "Application of plug-in electric vehicles to frequency regulation based on distributed signal acquisition via limited communication," *IEEE Trans. Power Syst.*, vol. 28, no. 2, pp. 1017–1026, May. 2013.

[184] S. L. Andersson, A. K. Elofsson, M. D. Galus, L. Göransson, S. Karlsson, F. Johnsson, and G. Andersson, "Plug-in hybrid electric vehicles as control power: Case studies of Sweden and Germany," *Energy Policy*, vol. 38, no. 6, pp. 2751–2762, 2010.

[185] S. Han, S. Han, and K. Sezaki, "Development of an optimal vehicle-to-grid aggregator for frequency regulation," *IEEE Trans. Smart Grid*, vol. 1, no. 1, pp. 65–72, Jun. 2010.

[186] J. H. Yoon, R. Baldick, and A. Novoselac, "Dynamic Demand Response Controller Based on Real-Time Retail Price for Residential Buildings," *IEEE Trans. Smart Grid*, vol. 5, no. 1, pp. 121–129, Jan. 2014.

[187] J. Ma, S. J. Qin, B. Li, and T. Salsbury, "Economics model predictive control for building energy systems," in *Proc. IEEE PES Innov. Smart Grid Technol. (ISGT)*, 2011, pp. 1–6.

[188] F. Oldewurtel, A. Ulbig, M. Morari, and G. Andersson, "Building control and storage management with dynamic tariffs for shaping demand response," in *Proc. IEEE PES Eur. Conf. Innov. Smart Grid Technol. (ISGT)*, 2011, pp. 1–8.

[189] Y. Zong, D. Kullmann, A. Thavlov, O. Gehrke, and H. W. Bindner, "Application of Model Predictive Control for Active Load Management in a Distributed Power System With High Wind Penetration," *IEEE Trans. Smart Grid*, vol. 3, no. 2, pp. 1055–1062, Jun. 2012.

[190] Z. Zhou, F. Zhao, and J. Wang, "Agent-based electricity market simulation with demand response from commercial buildings," *IEEE Trans. Smart Grid*, vol. 2, no. 4, pp. 580–588, Dec. 2011.

[191] N. Lu, "An evaluation of the HVAC load potential for providing load balancing service," *IEEE Trans. Smart Grid*, vol. 3, no. 3, pp. 1263–1270, Sep. 2012.

[192] D. S. Callaway, "Tapping the energy storage potential in electric loads to

deliver load following and regulation, with application to wind energy," *Energy Convers. Manage*., vol. 50, no. 9, pp. 1389–1400, 2009.

[193] A. Molina-Garciá, M. Kessler, J. A. Fuentes, and E. Gómez-Lázaro, "Probabilistic characterization of thermostatically controlled loads to model the impact of demand response programs," *IEEE Trans. Power Syst.*, vol. 26, no. 1, pp. 241–251, Feb. 2011.

[194] F. Rubinstein, L. Xiaolei, and D. Watson, "Using dimmable lighting for regulation capacity and non-spinning reserves in the ancillary services market. A feasibility study," LBNL, Tech. Rep., 2010.

[195] J. Lofberg, "YALMIP: A Toolbox for Modeling and Optimization in MATLAB," in *Proc. CACSD Conf.*, Taipei, Taiwan, 2004. [Online]. Available: http://users.isy.liu.se/johanl/yalmip.

[196] A. Wachter and L. T. Biegler, "On the implementation of an interior-point filter line-search algorithm for large-scale nonlinear programming," *Mathematical programming*, vol. 106, no. 1, pp. 25–57, Apr. 2005.